

Title	低分子量成分を含んだ相溶系/非相溶系ポリマーブレンドの特異的なレオロジー特性と構造形成
Author(s)	MOONPRASITH, NANTINA
Citation	
Issue Date	2022-09
Type	Thesis or Dissertation
Text version	ETD
URL	<a href="http://hdl.handle.net/10119/18149">http://hdl.handle.net/10119/18149</a>
Rights	
Description	Supervisor:山口 政之, 先端科学技術研究科, 博士

Anomalous rheological response and structure  
development for miscible/immiscible polymer blends  
having a low molecular weight component

NANTINA MOONPRASITH

Japan Advanced Institute of Science and Technology

Doctoral Dissertation

Anomalous rheological response and structure  
development for miscible/immiscible polymer blends  
having a low molecular weight component

NANTINA MOONPRASITH

Supervisor: Masayuki Yamaguchi

Graduate School of Advanced Science and Technology

Japan Advanced Institute of Science and Technology

Materials Science

September 2022

## Abstract

### **Anomalous rheological response and structure development for miscible/immiscible polymer blends having a low molecular weight component**

Blending of two different polymers is a common and simple method for enhancing polymer characteristics. The final morphology of mixtures is the most essential aspect in determining its qualities. Miscible polymer blends and immiscible polymer blends are the two main types of polymer mixtures. Molecular weight is one of the key factors to decide the miscibility and the structure. Moreover, molecular weight and its distribution affect the properties of polymers. In this study, a role of a low-molecular-weight polymer in polymer blends including both miscible and immiscible systems is focused.

Some systems are miscible because of the influence of the mixing entropy. Recently, it was revealed that a miscible polymer blend exhibited a flow-induced segregation behavior without phase separation. In specifically, surface of an injection-molded product was enriched with a low-molecular-weight fraction. This phenomenon was revealed using binary blends of PC and PMMA, in which one of them has low molecular weight. In the study, miscible blends of PC and low-molecular-weight PMMA were used to investigate the effect of processing variables such as shear rate, residence time, and temperature on segregation behavior. A capillary rheometer with a rectangular die was utilized for extrusion, and ATR-IR was used to measure the PMMA content at surface. It was found that the PMMA segregation occurred during flow, resulting in a PMMA-rich surface. The PMMA content at surface increased at high shear rates and high temperatures. In contrast, the residence time in a die barely affected the segregation. The effect of PMMA molecular weight on separation was also investigated. The experimental results indicated that lower molecular weight PMMA was segregated significantly. Furthermore, there was no segregation seen in the extrudate of PC/PC-L ("L" in the sample code denotes that the molecular weight is low), i.e. the blend system consisting of the same polymer species with low molecular weight. These results suggest that segregation phenomena occurs in a miscible blend with a positive Flory-Huggins parameter. Furthermore, the PC/PMMA blends of high and low molecular weights with a blend ratio of 90/10 were used to study the segregation phenomena at injection-molding. It was found that products obtained by injection molding from PMMA-H/PC-L (90/10) had more PC-L content on the surface than films produced via compression molding from the same blend. Furthermore, the injection-molded products obtained from PC-H/PMMA-L (90/10) had a higher concentration of PMMA-L on the surface than the compression-molded films prepared from the same blend. Moreover, the segregation was pronounced near the gate, i.e., the region with a high shear rate.

In the case of immiscible mixtures containing a low-molecular-weight component, the influence on shear viscosity was studied. High and low molecular weights of polypropylene (PP) and polystyrene (PS) including with low molecular weight polyethylene (PE) were used in the experiment. A low viscosity dispersion deformed significantly into a fibrous shape, which increased the interface area between immiscible polymers. Because of a high interfacial tension, interfacial slippage occurred, resulting in low shear viscosity. Decrease in the shear viscosity is desired significantly at injection molding.

For a miscible blend, a low-molecular weight polymer has a high potential on segregation to the surface under pressure-driven shear flow. In an immiscible blend, it plays an important role on viscosity drop due to an enlarge interfacial area with a high interfacial tension. Although this thesis effectively defined the rheological behaviors under shear flow for polymer blends incorporating a low-molecular-weight polymer, the mechanical characteristics of these samples should be validated in future.

**Keywords:** low-molecular-weight, miscible/immiscible blend, surface segregation, viscosity decrease, interfacial tension

## Contents

<b>Chapter 1: General introduction</b> .....	1
1.1. Polymer.....	1
1.2. Molecular weight and molecular weight distribution.....	4
1.3. Chain stiffness.....	7
1.4. Entanglement molecular weight.....	9
1.5. Polymer Blends.....	10
1.6. Structure development of immiscible blends .....	12
1.7. Purpose of this research .....	19
References.....	19
<b>Chapter 2: Mechanism of shear-induced segregation</b> .....	22
2.1 Introduction.....	22
2.1.1 Bisphenol A Polycarbonate and Poly(methyl methacrylate) .....	22
2.1.2 Blends of PC and PMMA.....	24
2.1.3 Segregation in miscible polymer blends.....	28
2.2 Experimentals.....	31
2.2.1 Materials.....	31
2.2.2 Sample preparation.....	32
2.2.3 Measurements.....	33
2.3 Results and discussion.....	34
2.3.1 Miscibility of the blends.....	34
2.3.2 Surface segregation.....	39
2.4 Conclusion.....	46
References.....	46
<b>Chapter 3: Application to injection-molding</b> .....	51
3.1 Introduction.....	51

3.1.1	Polymer processing.....	51
3.1.2	Injection-molding.....	54
3.2	Experimentals.....	54
3.2.1	Materials.....	54
3.2.2	Sample preparation.....	55
3.2.3	Measurements.....	56
3.3	Results and discussion.....	57
3.3.1	Viscoelastic properties and miscibility.....	57
3.3.2	Segregation behavior at injection-molding .....	61
3.4	Conclusion.....	65
	References .....	66
<b>Chapter 4: Viscosity drop in immiscible blends.....</b>		<b>68</b>
4.1	Introduction.....	68
4.2	Experimentals.....	74
4.2.1	Materials.....	74
4.2.2	Sample preparation.....	74
4.2.3	Measurements.....	75
4.3	Results and discussion.....	76
4.4	Conclusion.....	86
	References .....	87
<b>Chapter 5: General conclusion.....</b>		<b>90</b>
<b>Achievements.....</b>		<b>94</b>
<b>Acknowledgements.....</b>		<b>96</b>

This dissertation was prepared according to the curriculum for the Collaboration Education Program organized by Japan Advanced Institute of Science and Technology and Sirindhorn International Institute of Technology, Thammasat University.

## Chapter 1: General introduction

### 1.1 Polymer

A polymer is composed of a number of repeating units called monomer. A polymer chain is like a string, which comprises more than hundreds of monomers in general. Some polymers are composed of one monomer species. Polyisoprene is an example of a natural polymer with one monomer. Polystyrene is another example of a synthetic polymer with one monomer. Some polymers are composed of two or more monomers, that are called copolymers. Most materials in living organisms such as proteins, cellulose, and nucleic acids are composed of multiple monomers.

From the viewpoint of molecular weight, there is no specific definition on “polymer”. However, various properties are different beyond a specific molecular weight, i.e., critical molecular weight ( $M_c$ ), which is around twice of average molecular weight between entanglement couplings, so-called entanglement molecular weight  $M_e$ . Beyond  $M_c$ , the intermolecular interaction, called entanglement couplings, is inevitable. The entanglement molecular weight ( $M_e$ ) is dependent upon the chemical structure of monomer. Table 1-1 shows the  $M_e$  values of various polymer species. Because the chain flexibility decides the shape of polymer chains,  $M_e$  has a relationship with the molecular characteristic that represents the chain stiffness, which will be discussed later.

Even for a polymer comprising one monomer, it is still a mixture, because they have molecular weight distribution. Therefore, the average values of molecular weight are important. As a simple example of polymer formation from small molecules, let's consider the alkane hydrocarbon series. These compounds have the general structure as shown in Figure 1-1.

Table 1-1 Entanglement molecular weight ( $M_e$ ) of several polymer species at 413K [1-4]

Polymer	$M_e$ (g/mol)
Polyethylene	828
Poly(ethylene oxide)	1624
Poly(methyl methacrylate)	10013
Polystyrene	13309
Poly(dimethyl siloxane)	12293
1,4-Polybutadiene	1815
1,4-Polyisoprene	6147
a-Polypropylene	4623

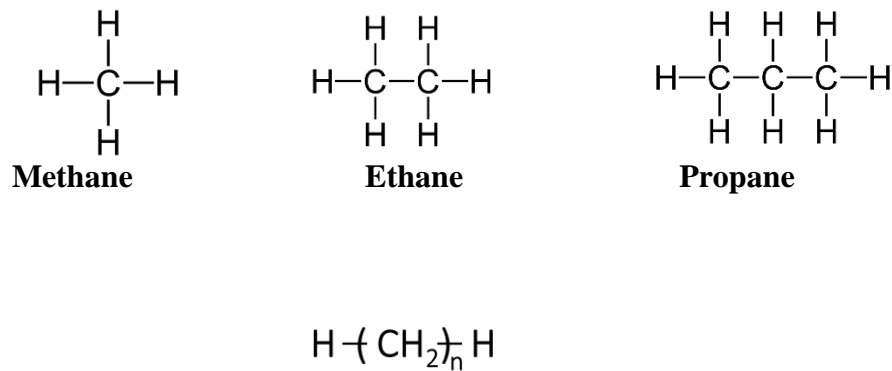


Figure 1-1 Examples of alkanes

The number of  $-\text{CH}_2-$  group  $n$  is allowed to increase up to several thousand. When is it called a polymer? The polymeric material of alkanes containing thousands of carbon atoms is known as polyethylene. For example, with an increase in the repeating unit of methylene  $-\text{CH}_2-$ , the characteristics of materials are similar to those of polyethylene as shown in Table 1-2. Eventually, the characteristics barely depend on the molecular weight. For such materials, we call “polymers”.

Table 1-2 Effect of molecular weight on the characteristics for alkanes [5]

n	Molecular Weight	Melting Point, T <sub>m</sub> (°C)	Boiling Point (°C)	State at room temp.
1	30	-183	-88.6	Gas
2	58	-135	-0.5	Gas
3	86	-94	69	Liquid
4	114	-57	126	Liquid
5	142	-30	174	Liquid
10	282	38	205	Soft solid
30	842	99	degradation	Soft solid
60	1682	104	degradation	Soft solid
100	2802	106	degradation	Brittle solid
1000	28002	110	degradation	Tough solid

A similar material to a polymer, but with short length, is called an oligomer. Therefore, the characteristics of oligomers are usually dependent upon the molecular weight. Then how to calculate the molar mass of a molecule? The size of a polymer is expressed by molar mass or molecular weight " $M$ " which is typically defined in units of dalton (Da; 1 Da = 1 g/mol). Degree of polymerization presented by " $n$ " is the number of repeat unit in a polymer, which is known as the degree of polymerization.

The molar mass of a polymer can be written as the following relationship, where the new variable  $M_0$  is the molar mass of the repeat unit:

$$M = nM_0 \quad (1.1)$$

In the case of copolymers, we define  $\overline{M}_0$  as follows, where  $x$  is the mole fraction of each monomer.

$$\overline{M}_0 = \sum_i^n x_i M_i \quad (1.2)$$

## 1.2 Molecular weight and molecular weight distribution

There are four types of average molecular weights used in common, such as the number-average molecular weight,  $M_n$ , the weight-average molecular weight,  $M_w$ , the z-average molecular weight,  $M_z$ , and the viscosity-average molecular weight,  $M_v$ . Those are defined as the followings in terms of  $N_P$  which is the number of molecules with a degree of polymerization of  $P$ .  $M_P$  is the molecular weight of a molecule with a degree of polymerization of  $P$ ,  $x_P$  is the mole fraction, and  $w_P$  is the weight fraction of a polymer with molecular weight  $M_P$ .

Mole fraction

$$x_p = \frac{N_P}{\sum N_P} = \frac{x_P}{\sum x_P} \quad (1.3)$$

Weight fraction

$$w_p = \frac{M_P N_P}{\sum M_P N_P} = \frac{x_P M_P}{\sum x_P M_P} \quad (1.4)$$

Number-average molecular weight

$$M_n = \sum M_P x_P = \frac{\sum M_P N_P}{\sum N_P} = \frac{\sum w_P}{\sum \left(\frac{w_P}{M_P}\right)} \quad (1.5)$$

Weight-average molecular weight

$$M_w = \sum M_P W_P = \frac{\sum M_P^2 N_P}{\sum M_P N_P} \quad (1.6)$$

Z-average molecular weight

$$M_z = \frac{\sum M_P^3 N_P}{\sum M_P^2 N_P} \quad (1.7)$$

Viscosity-average molecular weight

$$M_v = \left[ \frac{\sum M_P^{1+a} N_P}{\sum M_P N_P} \right]^{1/a} \quad (1.8)$$

where  $a$  is the constant value used in the Mark-Houwink-Sakurada theory;  $a = 0$  for spheres, 0.5-0.8 for random coil, 1.0 for stiff coils, and 2.0 for rods.

Therefore, the following relation is always applicable.

$$M_n \leq M_w \leq M_z \quad (1.9)$$

Figure 1-2 illustrates the molecular weight distribution. When a polymer is monodisperse, we will find that  $M_n = M_w = M_z$ .

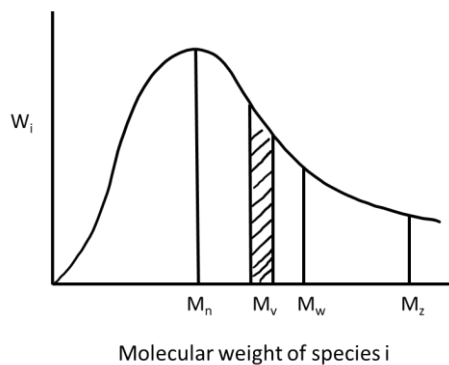


Figure 1-2 Illustration of molecular weight distribution with various average values [2]

The conventional method to determine the molecular weight and its distribution is gel permeation chromatography (GPC), although the values are relative ones with a polymer with specific molecular weight as an external standard. Recently, GPC is called size exclusion chromatography (SEC) [5,8]. For SEC,  $M_n$ ,  $M_w$ , and  $M_z$  are evaluated together by a single measurement. Figure 1-3 shows the illustration of SEC measurements [5]. The sample is injected into the column. The porous structure in a column affects the retention time to pass through the column, which depends on the molecular weight.

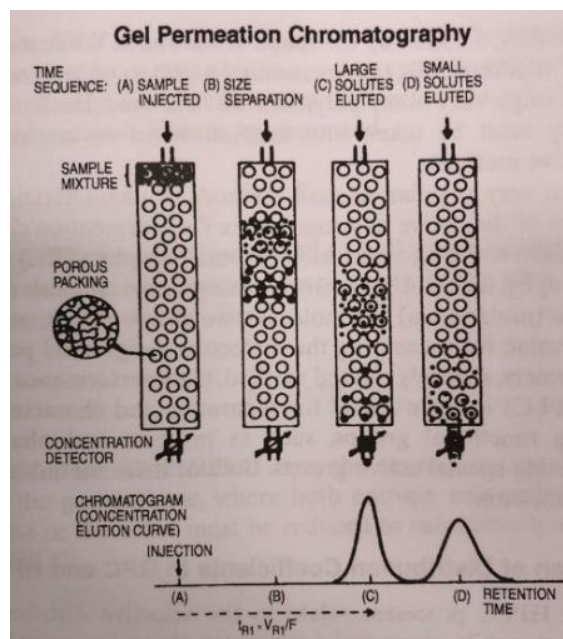


Figure 1-3 Illustration of the SEC experiment. The sample is diluted by a solvent which flows into a porous packed bed. Larger molecules flow faster, whereas smaller ones take a longer retention time to pass [5].

### 1.3 Chain stiffness

Chain stiffness refers to the rigidity of a polymer chain, since the polymer is composed of various repeating units with covalent bonds. In a molten state or in a solvent, a polymer chain exists a coil. The size of a coil is determined by the chain stiffness.

Chain stiffness decides the characteristics of polymers including  $M_e$ . Therefore, this is very important in polymer science. Various parameters are known to express the chain stiffness. One of the most important parameters must be the characteristic ratio  $C_\infty$ , defined as eq. (1.10), where  $\langle r^2 \rangle_0$  is the mean square end-to-end distance of an unperturbed chain.

$$C_\infty = \langle r^2 \rangle_0 / nl^2 \quad (1.10)$$

where  $l$  is the bond length and  $n$  is the number of bonds. In Table 1-3, the values of  $C_\infty$  are summarized. Kuhn segment length shown, in Table 1-4, and packing length (Table 1-3) are other important parameters expressing the chain stiffness. The packing length  $p$  is defined as follows

$$p = \frac{M/N_A \rho}{\langle r^2 \rangle_0 / 6} \quad (1.11)$$

where  $\rho$  is the density and  $N_A$  is the Avogadro's number.

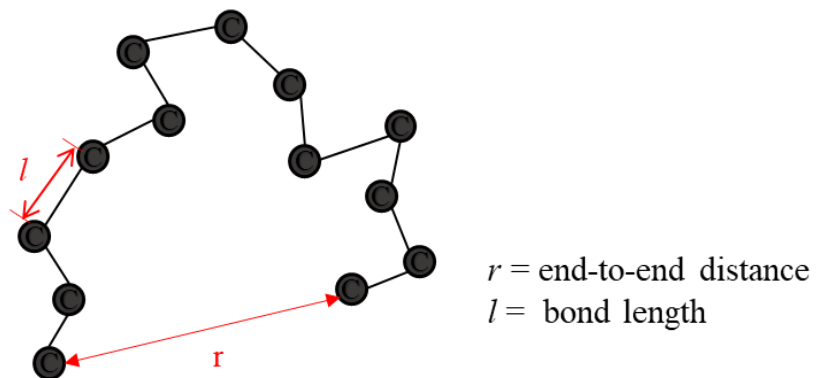


Figure 1-4 Schematic illustration of a polymer chain

Another important parameter to express the chain stiffness is the Kuhn step length, sometimes called segment length. This is given by the following relation.

$$l_k = l C_\infty \quad (1.12)$$

where  $l_k$  is the Kuhn step length.

Table 1-3 Characteristic ratio  $C_\infty$  and packing length  $p$  of several polymer species [10,11,13]

Polymer	$C_\infty$	$p$ (nm)
Polyethylene	6.80	0.169
Polystyrene	9.85	0.395
Poly(ethylene oxide)	4.10	0.191
Polybutadiene, 98% cis	4.75	0.212
cis-Polyisoprene	4.75	0.310
Polycarbonate	2.40	0.155
Poly(methyl methacrylate)	8.20	0.358

Table 1-4 Kuhn length, of some vinyl polymers [9]

Polymer	$l_k$ (nm)
Polyethylene	0.96
Poly(vinyl chloride)	1.05
Poly(methyl methacrylate)	1.36
Poly(vinyl acetate)	1.39
Polystyrene	1.67

### 1.4 Entanglement molecular weight

For a linear polymer with low molecular weight, i.e.,  $M < M_c$ , the zero-shear viscosity  $\eta_0$  of a polymer is directly proportional to molecular weight  $M$  as denoted in eq. (1.13). Beyond  $M_c$ , at which entanglement coupling is inevitable, the viscosity strongly increases with  $M$  as shown in eq. (1.14) [12-14]. The smooth crossover between these two regimes occurs at  $M_c$ .

$$\eta_0 = K \cdot M, \quad (M < M_c) \quad (1.13)$$

$$\eta_0 = K \cdot M^{3.4}, \quad (M > M_c) \quad (1.14)$$

Rheological properties, of course, depend on the molecular weight, which are significantly different below/beyond  $M_c$ . Once a polymer chain is entangled with at least two other chains, it may form a temporary three-dimensional network via entanglements [11]. The parameter  $M_e$  is typically calculated from the rubbery plateau shear modulus ( $G_N^0$ ) of a polymer as shown in eq. (1.15). This relation was proposed following the classical theory of rubber elasticity.

$$M_e = \frac{\rho RT}{G_N^0} \quad (1.15)$$

where  $R$  is the universal gas constant,  $T$  is the temperature, and  $\rho$  is the density.

Because the chain stiffness decides the shape of polymer chains,  $M_e$  has a relationship with the molecular characteristic that represents the chain stiffness. One famous example is the packing length  $p$ . The relationship between  $G_N^0$  and  $p$  is given by the following equation.

$$G_N^0 = \frac{k_B T}{1.98 p^3} \quad (1.16)$$

where  $k_B$  is the Boltzmann constant ( $1.38 \times 10^{-23}$  J/K).

Figure 1-5 shows the relationship between the packing length and measured rubbery plateau modulus for various polyolefins [15]. The slope was found to be 3 irrespective of polymer species.

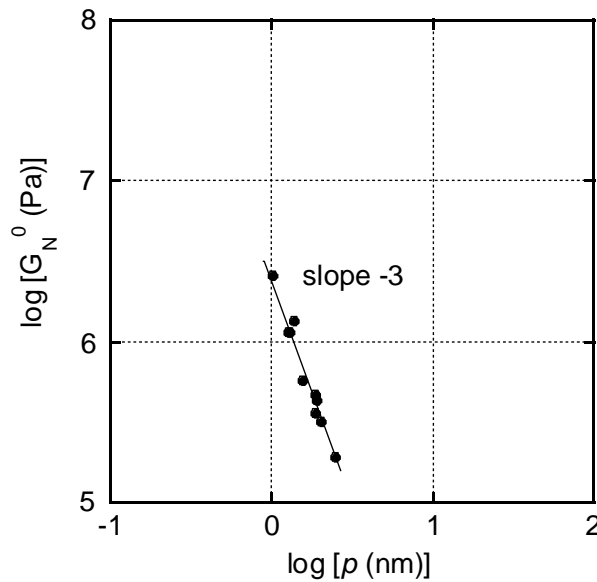


Figure 1-5 Relationship between the packing length  $p$  and measured rubbery plateau modulus  $G_N^0$  for various polyolefins [15]

## 1.5 Polymer Blends

A polymer blend is a mixture of at least two polymers. This is an easy and conventional technique to improve polymer properties. The final blend morphology is the most important factor to decide their properties. Generally, polymer blends can be divided into two categories such as miscible blends and immiscible blends.

A miscible blend has a negative value of the free energy of mixing, i.e.,  $\Delta G_m < 0$ . Molecular chains of both polymers are dissolved each other in a molecular scale, and thus the blend is homogeneous. Such a system shows only one glass transition temperature.

An immiscible blend shows a positive value of  $\Delta G_m$ . Therefore, a system shows phase separation at the equilibrium state. When a blend is modified to make a fine structure, e.g., by adding a compatibilizer, it is called a “compatible blend”. Therefore, “compatible blends” do not have strict definition from the scientific point of views.

For the miscibility of polymer blends, its molecular weight plays an important role, which is different from other materials. Flory and Huggins considered the effect of molecular weight and then described the free energy of mixing for polymer blends. This is the well known as Flory-Huggins theory. The formula is given as follows.

$$\frac{\Delta G_m}{RT(V/V_x)} = \frac{\phi_1}{\xi_1} \ln \phi_1 + \frac{\phi_2}{\xi_2} \ln \phi_2 + \phi_1 \phi_2 \chi_{12} \quad (1.17)$$

where  $V$  is the volume of the system,  $V_x$  is the volume of the segment,  $\phi_i$  and  $\xi_i$  represent the volume fraction and the number of segments per a chain of the  $i$ -th component. Furthermore,  $\chi_{12}$  is known as the Flory-Huggins interaction parameter, which expresses the contributions except for the entropy change calculated from the classical lattice model. Although the exact evaluation of the  $\chi_{12}$  value is difficult, a rough estimation can be performed from the differences in the solubility parameter  $\delta$  of each polymer as follows.

$$\chi_{12} = \frac{V_c}{RT} (\delta_1 - \delta_2)^2 \quad (1.18)$$

As seen in eq. 1.17, when a polymer has low molecular weight, it has a great possibility to be miscible with another polymer species. Therefore, low-molecular-weight compounds such as thermal stabilizer, plasticizer, and oligomer are often miscible with a polymer.

Patterson and Robard discussed the interaction parameter  $\chi_{12}$  in detail [16]. According to them,  $\chi_{12}$  is composed of two contributions such as free volume matching and interaction

between neighboring molecules. The introduction of the concept of free volume contribution successfully supports the LCST (lower critical solution temperature) behavior. When the interaction contribution is a small positive value, both UCST (upper critical solution temperature) and LCST may appear in the same system (Figure 1-6).

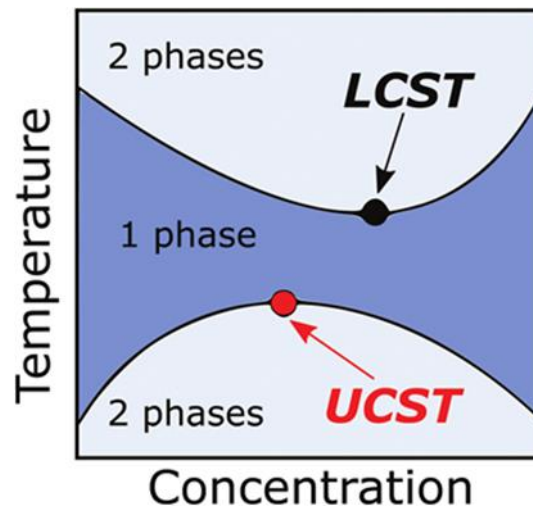


Figure 1-6 Phase diagram with upper and lower critical solution temperatures (UCST) and (LCST) [17]

### 1.6 Structure development of immiscible blends

A blend composed of chemically different polymers is often immiscible and has phase separated structure. Since the structure directly affects mechanical properties and so on, the precise control of the structure is always required for materials design. Here, the structure development of immiscible blends under flow is summarized.

Under the flow field, dispersed droplets are deformed in the continuous phase as shown in Figure 1-7. The shape of dispersion is determined by the ratio of the interfacial stress

between the two immiscible phases to hydrodynamic stress such as shear stress, which is called the capillary number  $Ca$ .

$$Ca = \frac{\sigma R_d}{\Gamma} \quad (1.19)$$

where  $\sigma$  is shear stress,  $R_d$  is the radius of the dispersed phase, and  $\Gamma$  is the interfacial tension.

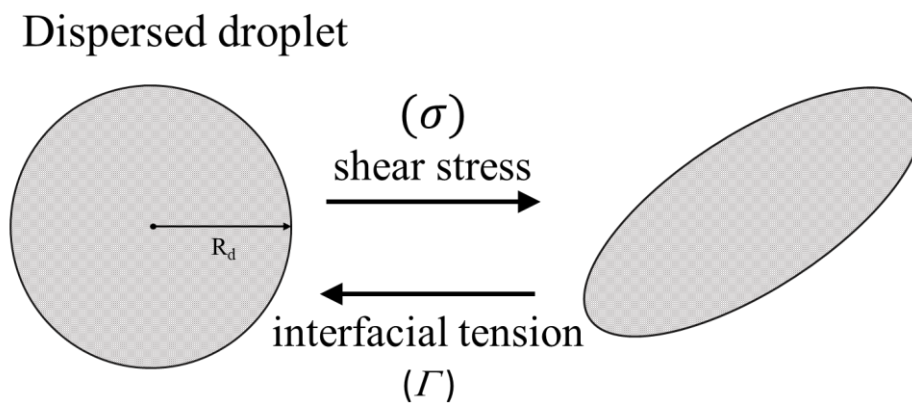


Figure 1-7 Balance of hydrodynamic force and interfacial force under flow

As increasing the shear stress, droplets are deformed greatly. Eventually, a droplet breaks up into small droplets as demonstrated in Figure 1-8 [18]. The capillary number at this point is called “critical capillary number  $Ca_{crit}$ .”

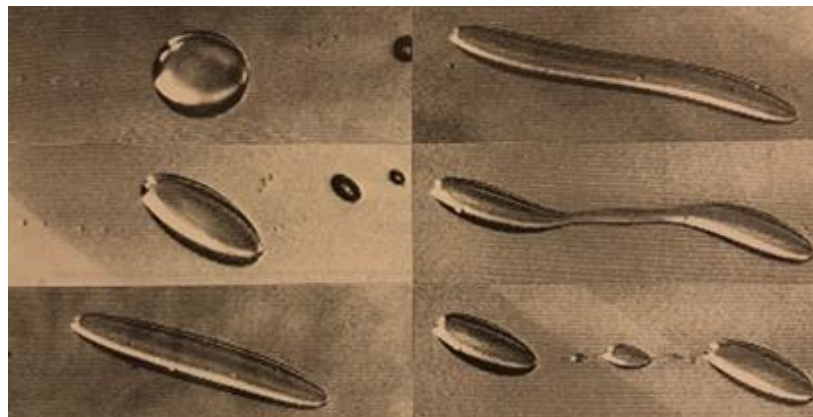


Figure 1-8 Droplet break-up under shear flow [18]

Structure growth under flow field for immiscible blends is dominated by various factors such as volume fraction, viscosity ratio of the compositions, type of flow, and interfacial tension between the phases. Briscoe et al. [19] reviewed the Taylor's work and summarized the factors to influence the strain required to break up a droplet under laminar flow. For a Newtonian fluid, the droplet deformation is controlled by two dimensionless numbers, such as viscosity ratio  $p_\eta$  and capillary number  $Ca$ .

Grace studied the variation of the critical capillary number as a function of the viscosity ratio in shear and elongational flow. The result is shown in Figure 1-9. The horizontal axis represents the viscosity ratio of a dispersion phase  $\eta_d$  to a continuous phase  $\eta_c$ , i.e.,  $p_\eta = \eta_d/\eta_c$ . The figure demonstrates that the elongational flow is more effective than shear in deforming and breaking up the droplets [20].

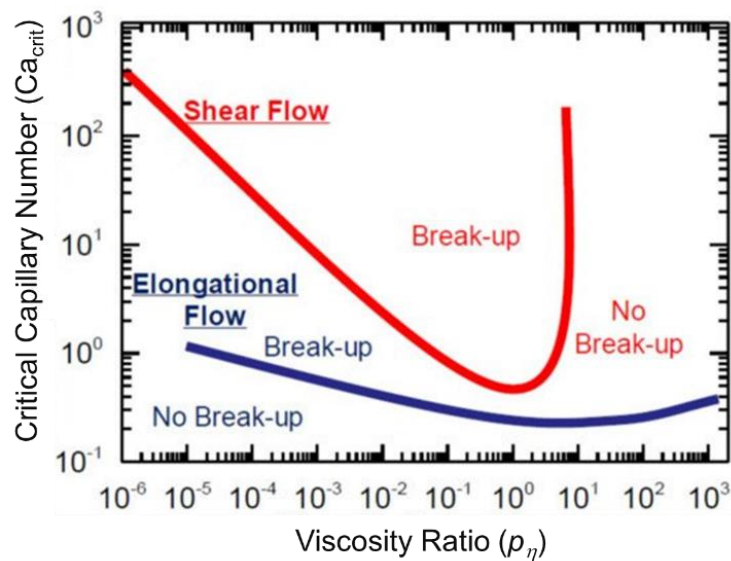


Figure 1-9 Critical capillary number  $Ca_{crit}$  as a function of the viscosity ratio  $p_\eta$  in polymer blends according to the Grace's analysis. [21]

Under shear flow, break-up of a droplet never occurs when  $\eta_d/\eta_c > 4$ . Therefore, a single-screw extruder, in which shear flow is dominated, cannot mix a high viscous dispersion. In contrast, a twin-screw extruder or an internal mixer is appropriate to mix such a system, because elongational flow occurs during mixing. From the viewpoint of viscosity ratio, fine dispersion is attained when both continuous and dispersed phases show the same viscosity, i.e.,  $\eta_p = 1$ .

When  $Ca < Ca_{crit}$ , dispersed particles deform to a flow direction to some degree without break-up. The interfacial force is balanced with the hydrodynamic force. When  $Ca > Ca_{crit}$ , break-up occurs. Once  $Ca$  is much larger than  $Ca_{crit}$ , however, affine deformation of a dispersion droplet occurs. As a result, a significantly large deformation is applicable to dispersions, which eventually deform into fibrous shape. The shape of dispersion is known to be expressed by the Taylor number  $D_{Taylor}$  defined as eq. 1.20.

$$D_{Taylor} = \frac{l_a - l_b}{l_a + l_b} \quad (1.20)$$

where  $l_a$  is the length of long axis and  $l_b$  is that of short axis, which are shown in Figure 1.10.

The Taylor number is between 0 and 1. When the dispersion is fiber,  $D_{Taylor} = 1$ . Furthermore,  $D_{Taylor} = 0$  means that the dispersion is sphere.

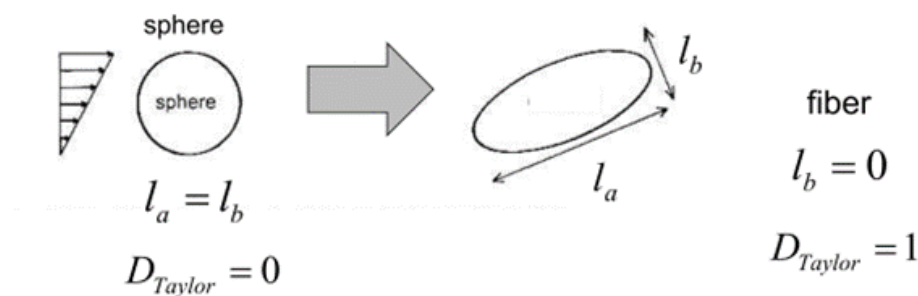


Figure 1-10 the shape of dispersion described by the Taylor number. [22]

In Figure 1-11, the Taylor number is plotted against the dimensionless time, i.e., total applied deformation, in the elongation flow and shear flow. In both cases, the viscosity of dispersion is much lower than that of continuous phase. As seen in the figures, affine deformation is detected at high  $Ca/Ca_{crit}$  condition. Therefore, the following relations are applicable.

$$D_{Taylor} = \frac{e^{3\varepsilon/2} - 1}{e^{3\varepsilon/2} + 1} \quad (1.21)$$

$$D_{Taylor} = \frac{\gamma^{3/2} - 1}{\gamma^{3/2} + 1} \quad (1.22)$$

where  $\varepsilon$  is the tensile strain.

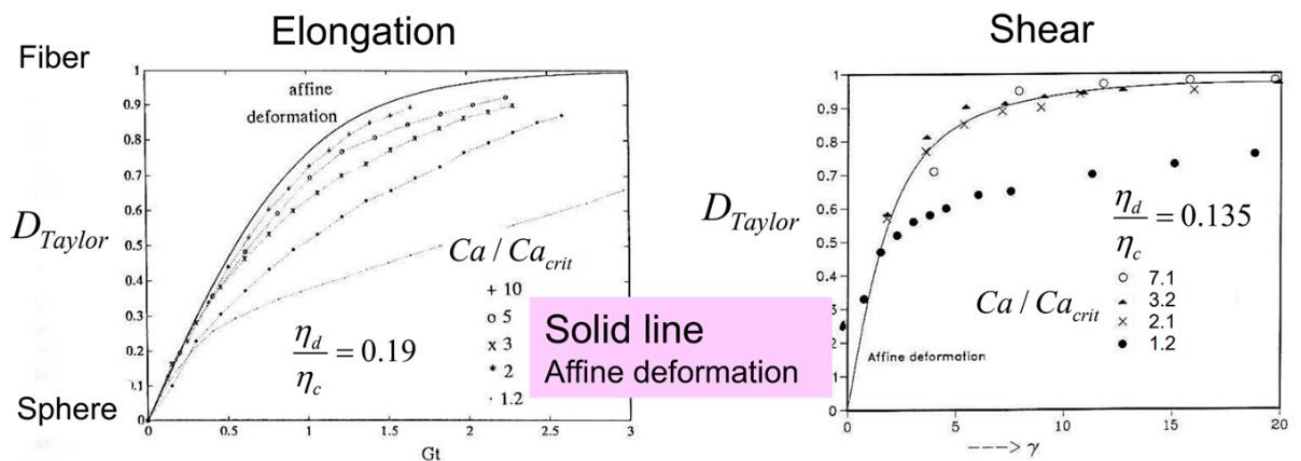


Figure 1-11 Taylor number plotted against the dimensionless time in the elongation flow and shear flow [22]. The solid lines represent the affine deformation.

After the cessation of flow, however, fluctuation takes place. This is known as Rayleigh disturbance [18]. It eventually leads to break-up of a droplet to minimize the interface in the system. Figure 1-12 illustrates the Rayleigh disturbance of a castor oil thread in Newtonian silicone oil.

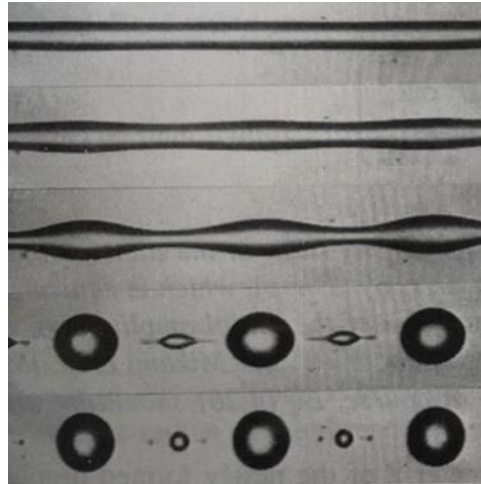


Figure 1-12 Disintegration of a castor oil thread in Newtonian silicone oil [18]

Because of the Rayleigh disturbance, the morphology of immiscible polymer blends is affected by the processing conditions. Figure 1-13 shows the structure of high-density polyethylene (HDPE)/polystyrene (PS) blends after T-die extrusion [22]. Although the same blend was extruded using the same machine, the length between the die exit and the chill roll, so called “air gap”, greatly affected the structure. When the air gap is long, the disintegration occurs, leading to small spherical droplets. In contrast, long fibrous droplets are detected after passing the short air gap, i.e., immediate solidification.

The same phenomenon is detected in an injection-molded plate for an immiscible blend composed of isotactic polypropylene and ethylene-1-hexene copolymer. As shown in Figure 1-14, the skin layer has fibrous dispersion due to an immediate solidification. In the case of core layer, however, disintegration occurs during cooling and small spherical droplets are dispersed [23].

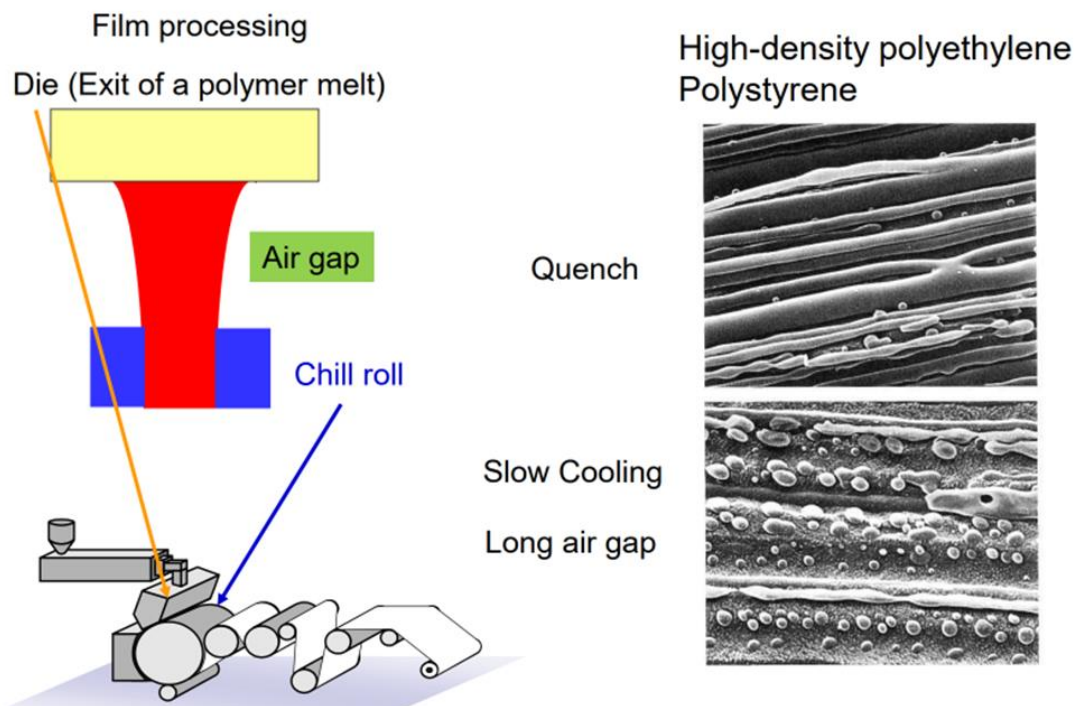


Figure 1-13 Morphology of immiscible polymer blends of HDPE/PS blends affected by the processing conditions at T-die extrusion [22]

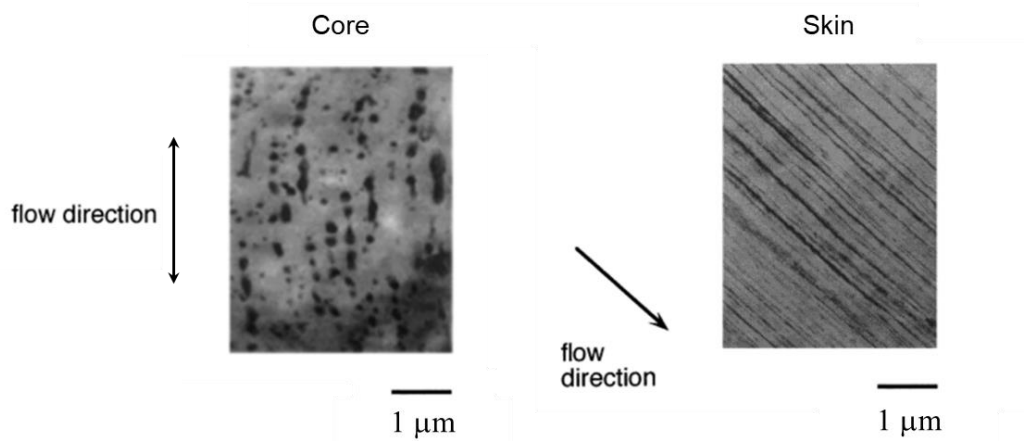


Figure 1-14 TEM images of immiscible polymer blends in an injection-molded plate at core and skin for polypropylene/ethylene-1-hexene copolymer blends [23]

## 1.7 Purpose of this research

In this thesis, low-molecular-weight materials are added in a conventional polymer. Because of the contribution of mixing entropy, some systems are miscible. Recently, flow-induced segregation behavior without phase separation was reported in a miscible polymer blend. In particular, a low-molecular-weight fraction was segregated on the surface of a product obtained by injection-molding. This is an attractive phenomenon to modify the surface properties of a polymer. In my thesis, miscible blends in which one has low molecular weight were employed to study the segregation behavior.

Furthermore, immiscible blends having a low-molecular-weight component were also employed to study the effect on shear viscosity. Dispersion with a low viscosity deforms into fibrous shape greatly, which enlarges the interfacial area between immiscible polymers. This situation may lead to the interfacial slippage, which results in the low shear viscosity. Decrease in the shear viscosity without decreasing the molecular weight is desired significantly at injection molding.

## Reference

1. L. J. Fetters, D. J. Lohse, D. Richter, T. A. Witten, and A. Zirkel, *Macromolecules* 1994, 27, 4639.
2. L. J. Fetters and D. J. Lohse, *Macromolecules* 2002, 35, 10096.
3. L. J. Fetters, D. J. Lohse, and R. H. Colby, *Physical Properties of Polymers Handbook* (J. E. Mark, editor) AIP Press, Woodbury, NY, 1996.
4. M. Rubinstein and R. H. Colby, *Polymer Physics*, Oxford University Press, Oxford, 2003.

5. L. H. Sperling, 4<sup>th</sup> ed, *Introduction to Physical Polymer Science*, John Wiley & Sons, Inc, Hoboken, 1932.
6. L. H. Peebles, *Molecular Weight Distributions in Polymers*, Wiley-Interscience, New York, 1971.
7. P. E. Slade, ed, *Polymer Molecular Weights*, Marcel Dekker, New York, 1975.
8. W. W. Yau, J. J. Kirkland, and D. D Bly, eds, *Modern Size Exclusion Chromatography*, Wiley-Interscience, New York, 1979.
9. J. Brandrup and E. H. Immergut, eds., *Polymer Handbook*, 2<sup>nd</sup> ed., Wiley-Interscience, New York, 1975.
10. R. Wool, *Polymer Interfaces*, Hanser, Munich, 1995.
11. L. J. Fetters, D. J. Lohse, and S. T. Milner, *Macromolecules* 1999, 32, 6847.
12. D. W. van Krevelen, *Properties of Polymers*, 2<sup>nd</sup> Edn, Elsevier, Amsterdam, 1976.
13. M. Doi and S. F. Edwards, *The Theory of Polymer Dynamics*, Oxford Univ. Press, New York, 1986.
14. R. Krishnamoorti, *J. Polym. Sci.: Part B: Polym. Phys.* 2002, 40, 1768.
15. J. Lohse, *Macromol. Sci. C, Polym. Rev.* 2005, 45, 289.
16. D. Patterson and A. Robard, *Macromolecules* 1978, 11, 690.
17. J. Niskanen and H. Tenhu, *Polymer Chemistry* 2017, 8, 220.
18. I. M. Zloczower and Z. Tadmor, eds, *Mixing and compounding of polymers*, Hanser Munich, 1994.
19. B. J. Briscoe, C. J. Lawrence, and W. G. P. Mietus, *Adv. Colloid Interface Sci.* 1999, 81, 1.
20. V. García-Masabet, O. Santana Pérez, J. Cailloux, T. Abt, M. Sánchez-Soto, F. Carrasco, and M. L. Maspoch, *Polymers* 2020, 12, 10.
21. H. P. Grace, *Chem. Eng. Commun.* 1982, 14, 225.

22. H. E. H. Meijer and J. M. H. Janssen, *Mixing and Compounding of Polymers*, Hanser, 1994.
23. M. Yamaguchi, K. Suzuki, and H. Miyata, *J. Polym. Sci.: B: Polym. Phys.* 1999, 37, 701.

## Chapter 2: Mechanism of shear-induced segregation

### 2.1 Introduction

#### 2.1.1 Bisphenol A Polycarbonate and Poly(methyl methacrylate)

Polycarbonates are synthesized from the reaction of a dihydroxy compound and phosgene with the elimination of hydrogen chloride. The most conventional diol is bisphenol A (BPA). Although various diols have been tested in place of BPA, only a few have been found for a commercial use. The most important polycarbonate is BPA polycarbonate, commonly referred as polycarbonate and abbreviated as PC. It has one of the largest sales among engineering thermoplastics. PC is known to show many attractive properties including high light transmittance, good thermal resistance, impact toughness as well as good dimensional stability and creep resistance [1-3]. The chemical structure of PC is shown in Figure 2-1. PC has an aromatic ring in the main chain and is used as an amorphous polymer because of its extremely slow crystallization rate at conventional processing conditions.

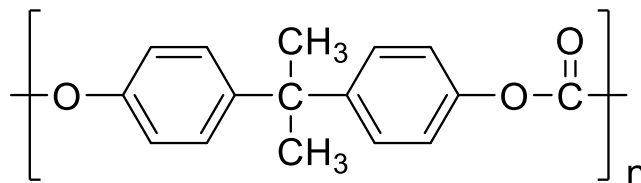


Figure 2-1 Chemical structure of PC

Since PC shows excellent transparency and impact resistance, they are used for headlamps in the automotive field. Furthermore, because of its excellent transparency and dimensional stability, it is used in optical discs such as compact disc (CD) and digital versatile disc (DVD) and dialysis machines in the medical field [4]. However, as a disadvantage, it is easily hydrolyzed by hot water with poor anti-solvent property.

Furthermore, flowability at injection-molding is not good enough because of a rapid viscous increase during cooling in a mold.

Poly(methyl methacrylate) (PMMA), shown in Figure 2-2, is produced by polymerization of methyl methacrylate (MMA) as a monomer. Most commercial grades are polymerized by free radical polymerization, yielding atactic polymers [5].

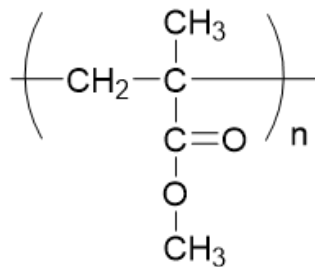


Figure 2-2 Chemical structure of PMMA

PMMA has various advantages such as excellent transparency, good weather resistance, and excellent scratch resistance. It is used in a wide range of fields, including optical materials, exteriors, and vehicles. PMMA is also used in the medical field [6]. Since it is highly safe, it can be recovered by pyrolysis after use. Therefore, it has an attracting attention as a material that is friendly to the human body and the environment. However, there are disadvantages such as low heat resistance and mechanical toughness [7].

Various properties of PC and PMMA, such as optical properties, mechanical properties, thermal property, processability, and weatherability are summarized in Table 2-1. As seen in the table, PC and PMMA exhibit quite different properties except for the transparency. Therefore, properties of one polymer can be compensated by the addition of another one. This is the reason to explore the structure control of the blend system.

Table 2-1 Comparison of PC and PMMA

	PC	PMMA
Refractive index	Large	Small
Birefringence	Large	Small
Mechanical toughness	Very good	Poor
Surface hardness (anti-scratch property)	Very poor	Very good
Heat distortion temperature	Very good	Poor
Flowability at injection	Poor	Good
Weatherability	Poor	Very good

### 2.1.2 Blends of PC and PMMA

As mentioned previous, blends of PC and PMMA may have attractive properties. However, the transparency is easily deteriorated by phase separation due to a large difference in the refractive indices. The Flory-Huggins parameter was reported to be  $0.039 \pm 0.004$  at  $250^\circ\text{C}$  [8] and  $0.035 \pm 0.010$  [9]. Although it is a positive value, the Gibbs free energy of mixing can be negative by the contribution of combinatorial mixing entropy. For example, miscible state was detected for the blends prepared by solution casting although the film preparation condition including solvent evaporation speed greatly affected the structure [10, 11]. Moreover, PC and PMMA can be miscible when one of them, at least, has low molecular weight. For the interfacial tension, therefore, small values were reported;  $1.44 \pm 0.16$  mN/m at  $240^\circ\text{C}$  [12] and  $0.6$  mN/m [13]. The blends show LCST phase diagram as exemplified in Figure 2-3 [14]. In the figure, the miscibility was evaluated by the transparency, i.e., cloud point, which was often employed for the blend system.

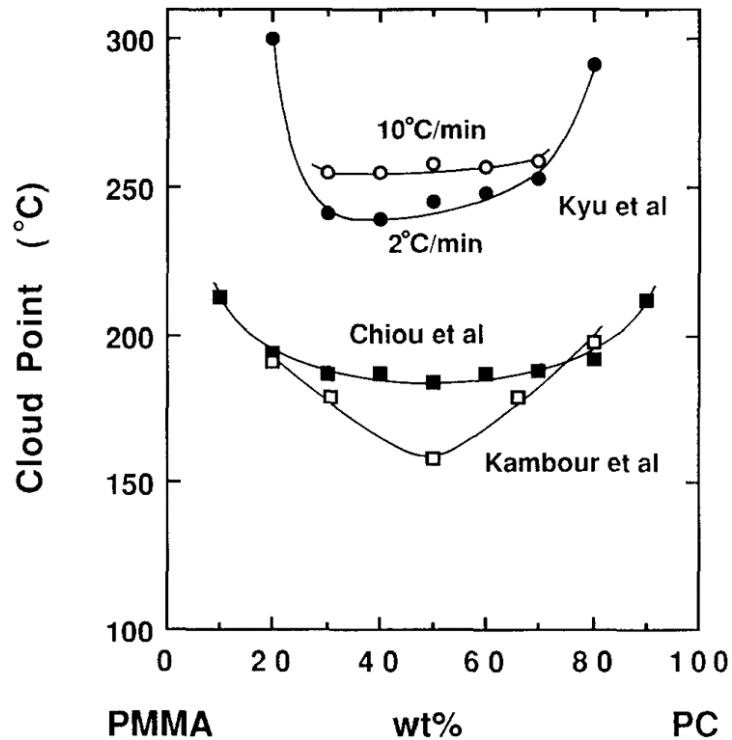


Figure 2-3 Cloud point at various blend ratios for PC/PMMA blend [14]

Recently, the miscibility of PC and PMMA was found to be affected by pressure and shear rate. Under high pressure, the specific volume decreases. As a result, the molecular interaction between PC and PMMA is enhanced, which overcomes the contribution of free volume matching [15]. Since they show a positive Flory-Huggins parameter, a high pressure leads to phase separation. In particular, beyond 200 MPa, at which shear viscosity increases 7.4 times due to reduced free volume [16], phase separation occurs even when one component has low molecular weight [17]. Moreover, shear-induced phase separation as well as phase mixing were detected for the same blend [17]. A similar result was reported for binary blends of polystyrene and poly(vinyl methyl ether) as shown in Figure 2-4 [18]. Such phenomena must be important for actual processing in industry, because PC is always processed under high pressure and high shear rate especially at injection molding.

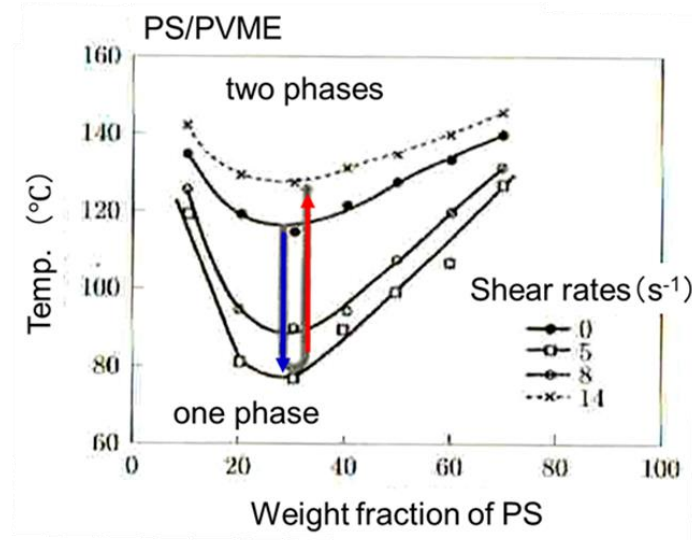


Figure 2-4 Phase diagram for binary blends of polystyrene and poly(vinyl methyl ether) under shear flow [18]

Moreover, transesterification reaction improves the miscibility of PC and PMMA. Furthermore, the reaction can be enhanced by the addition of a specific catalyst such as tin compounds [19,20,21]. According to Singh et al., tin compound enhanced the transparency of PC/PMMA (80/20) blends as shown in Figure 2-5 [21].

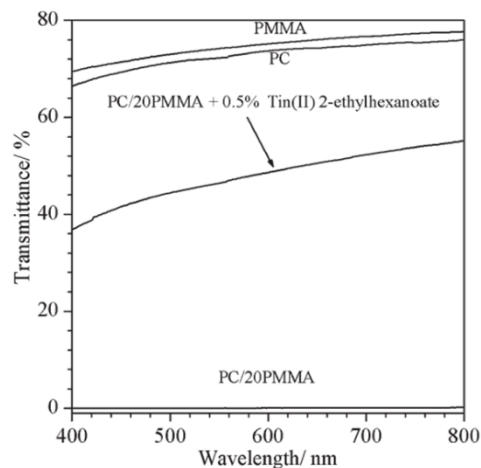


Figure 2-5 Optical transmittance of pure PC, pure PMMA, uncompatibilized PC/20PMMA, and compatibilized PC/20PMMA blend prepared using 0.5% tin(II) 2-ethylhexanoate catalyst. [21]

Bubmann et al. obtained more transparent blends using PC/PMMA (50/50) blends as illustrated in Figure 2-6 [23]. Yang et al., moreover, used ultrasonic to promote the transesterification reaction [22]. For such a reactive blend system, besides the catalyst, appropriate processing history, including temperature, duration of mixing, and flow behavior, must be set to appropriate values to control the structure.

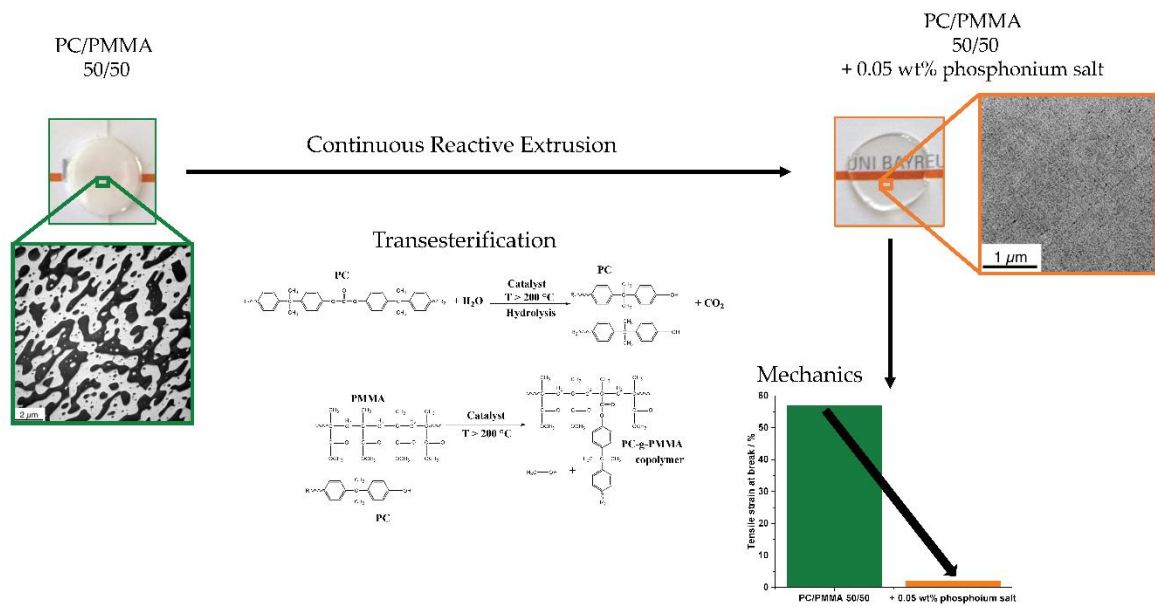


Figure 2-6 Transparent blends of PC/PMMA (50/50) by transesterification [23]

Graft and block copolymers composed of PC and PMMA, which were prepared without transesterification reaction, have been also prepared to increase the compatibility and to enhance the scratch resistance for PC. Since the transesterification always decreased the mechanical properties due to excess chain scission reaction, this method is preferred. In fact, Okamoto [24] and Jang [25] revealed the addition of PC-grafted-PMMA increased the surface hardness and scratch resistance for PC. Figure 2-7 shows the Vickers hardness of the blend and graft copolymer of PC and PMMA, reported by Okamoto [24].

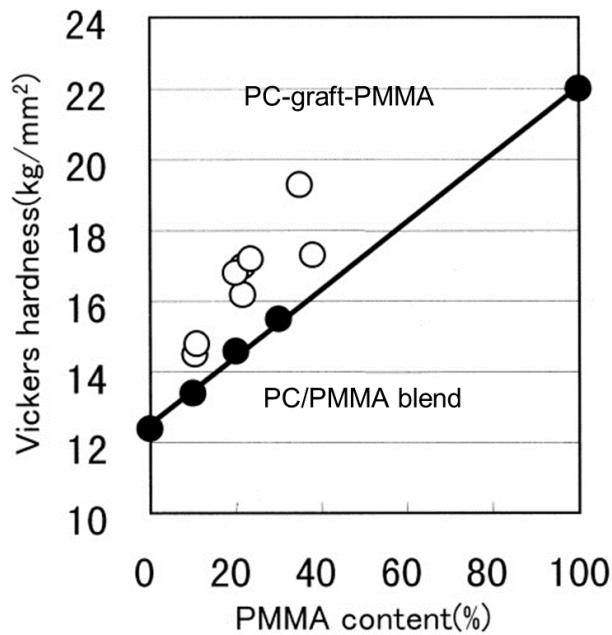


Figure 2-7 Relationship between PMMA content and Vickers hardness. ○ Graft copolymer.  
• PC/PMMA blend [24]

### 2.1.3 Segregation in miscible polymer blends

Even a polymer material has an excellent toughness and good flexibility, its surface is often required to be modified to provide various properties, such as antiscratch, antifouling, adhesive, water-repellant, and biocompatible properties. For PC, surface hardness with scratch resistance is always required because the surface is easily damaged by a harder material [1,26,27]. Therefore, surface coating, called hard coating, is performed in many applications. In contrast, PMMA shows good surface hardness with excellent antiscratch property, although the mechanical toughness is poor compared to PC. Once the concentration of PMMA is rich at surface for a miscible blend of PC and PMMA, it should be a good material having high mechanical toughness with antiscratch property. If such a material is produced without any specific facilities such as multi-layered film-processing machines and surface treatment machines, it must be significantly attractive to widen applications.

Until now, there have been several reports on the segregation phenomena. For example, a solution-cast film of a miscible blend shows surface segregation due to the difference in surface tension. A polymer with a large surface tension tends to be exposed on surface [28-31]. It was also reported that the segregation of one component in a miscible blend, which gives concentration gradient without phase-separation, occurred in the temperature gradient [32,33]. In this case, a low-molecular-weight component was localized at high temperature. A similar phenomenon occurs in miscible solvents, which is called the Soret effect [34,35]. According to Siriprumpoonthum et al. [32], on the other hand, the grading phenomenon in the temperature gradient has a relationship with the free volume fraction. They found this conclusion based on the experimental results using a polymer melt with broad molecular weight distribution. Since a large free volume is required for a low-molecular-weight component [36], their content is rich in the high temperature region. Segregation of a low-molecular-weight component at surface was also reported for other polymers [37-40], at which a large free volume ascribed to chain ends as well as the large surface tension is believed to be responsible for this phenomenon.

Sako et al. studied shear-induced segregation using binary blends composed of PC and PMMA [41]. They found that low-molecular-weight PMMA is segregated at surface during flow. Moreover, the injection-molded products showed high surface hardness compared with the compression-molded product having no segregation. This result demonstrated that surface segregation of PMMA is quite effective to enhance the surface properties even through the molecular weight of PMMA is low ( $\sim M_w = 15,000$ ) [41]. Figure 2-8 shows the surface roughness after scratching by Hoffman scratch tester under 100 g. The surface roughness was evaluated by a white light interferometer. Both arithmetic mean roughness  $R_a$  and maximum roughness  $R_z$  were found to be modified by the addition of 5 wt% PMMA,

which was more evident for the injection-molded sample. This was attributed to the surface segregation of PMMA [42]. Since some of PC products are produced by injection-molding, shear-induced segregation should be noted. However, at present, the driving force of segregation, especially under shear flow, was unknown.

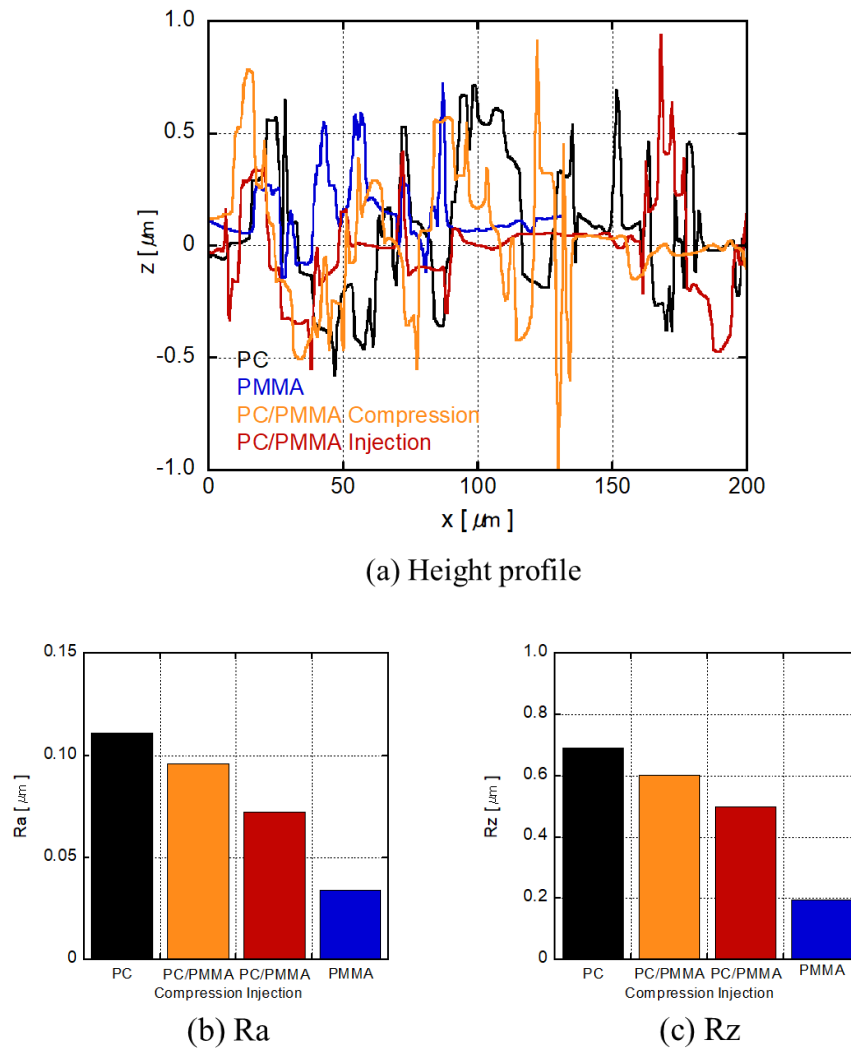


Figure 2-8 Average roughness and height profile of PC/PMMA blends using Hoffmann Scratch Tester (Load 100g) [42]

In this chapter, miscible blends of PC containing 10 wt% of PMMA samples with low molecular weight were employed with a reference blend of PC with a low-molecular-weight PC sample. The effect of the shear rate, residence time, and temperature was investigated

from the viewpoints of processing variables. Moreover, the effect of polymer species, i.e., the Flory-Huggins interaction parameter, and the molecular weight of PMMA was studied to clarify the mechanism of the shear-induced segregation.

## 2.2 Experimental

### 2.2.1 Materials

The raw materials used in this study were a commercially available BPA polycarbonate, denoted as PC in this study, (Iupilon S2000, Mitsubishi Engineering Plastics, Tokyo, Japan) and a commercially available low-molecular-weight BPA polycarbonate (Iupilon AL-071, Mitsubishi Engineering Plastics, Tokyo, Japan), denoted as PC-L. Two types of PMMA samples having low molecular weights, such as PMMA-7k and PMMA-13k, were prepared by Mitsubishi Chemical Corporation. The number- ( $M_n$ ) and weight-average ( $M_w$ ) molecular weights were evaluated by the size exclusion chromatography as polystyrene standard for PC and PC-L, and PMMA standard for PMMA-7k and PMMA-13k. The average molecular weights are summarized in Table 2-2.

Table 2-2 Molecular weights of polymers

<b>code</b>	<b><math>M_n</math></b>	<b><math>M_w</math></b>
PC	$2.8 \times 10^4$	$5.7 \times 10^4$
PC-L	$3.1 \times 10^3$	$8.7 \times 10^3$
PMMA-7k	$5.0 \times 10^3$	$7.0 \times 10^3$
PMMA-13k	$9.0 \times 10^3$	$1.3 \times 10^4$

### 2.2.2 Sample preparation

Prior to mixing, the raw materials were dried in a vacuum oven at 80°C for 4h. PC/PMMA (90/10 wt%) and PC/PC-L (90/10 wt%) blends were fabricated by melt-mixing using an internal mixer with a volume of 30 cc (Labo plastmill 10M100, Toyo Seiki Seisakusyo, Tokyo, Japan) at 250°C for 5 min. The blade rotation speed was 30 rpm. The obtained mixture was compressed into a film with 500  $\mu\text{m}$  thickness by compression-molding at 250°C. Then, the samples were immediately quenched at 5°C in another compression-molding machine.

Extrusion through a rectangular die to obtain an extrudate with flat surface was performed using a capillary rheometer (140SAS, Yasuda Seiki Seisakusyo, Nishinomiya, Japan) at various shear rates. The extrudates were cut by scissors and quenched in an ice-water bath as illustrated in Figure 2-9.

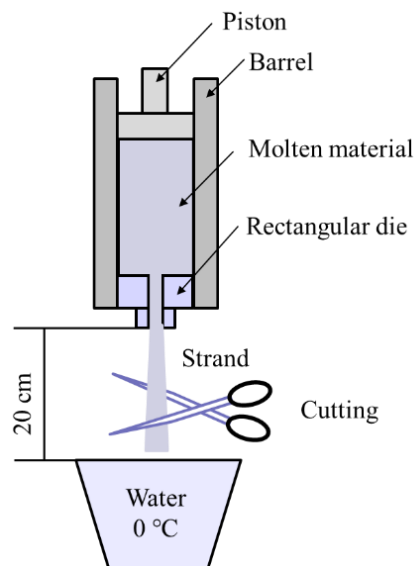


Figure 2-9 Illustration of sample collection

Two rectangular dies having different lengths  $L$ , i.e., 10 mm and 30 mm, were employed to evaluate the effect of residence time in the die. The width  $W$  and gap  $G$  of both

dies were 3 mm and 1 mm, respectively. The apparent shear rate on wall  $\dot{\gamma}$  and apparent shear viscosity on wall  $\eta$  were calculated by the following equations [43],

$$\dot{\gamma} = \frac{6Q}{G^2W} \quad (2.1)$$

$$\eta = \frac{\sigma}{\dot{\gamma}} = \frac{G^3W}{12Q} \frac{P}{L} \quad (2.2)$$

where  $Q$  is the volume flow rate,  $\sigma$  is the apparent shear stress on wall, and  $P$  is the pressure.

### 2.2.3 Measurements

Transparency of the compression-molded films with 500  $\mu\text{m}$  thickness was evaluated at 25°C by an UV-vis spectrophotometer (Lambda25, Perkin-Elmer, Waltham, MA, USA) as a function of the wavelength from 200 to 800 nm.

Temperature dependence of oscillatory tensile moduli in the solid state was measured at 10 Hz from 25 to 250°C at a heating rate of 2°C/min by a dynamic mechanical analyzer (E-4000, UBM, Muko, Japan). The specimens were cut into a rectangular shape with 5 mm in width and 20 mm in length.

Angular frequency dependence of oscillatory shear moduli in the molten state was measured by a cone-and-plate rheometer (AR2000ex, TA Instruments, New Castle, DE, USA) under a nitrogen atmosphere at 250°C. The angle of the cone was 4 and the diameter was 25 mm. The angular frequency was ranged from 0.1 to 628.3  $\text{s}^{-1}$ .

The PMMA concentration at the extrudate surface was quantified by the attenuated total reflectance Fourier-transform infrared spectra (ATR-IR) (Spectrum 100 FT-IR spectrometer, Perkin-Elmer). As characteristic absorption bands of PC and PMMA, 1770 and 1730  $\text{cm}^{-1}$ , both the stretching vibration modes of the carbonyl group, were used. Prior to the

evaluation, a calibration curve was prepared using compression-molded films. At measurements, the absorbance of  $1770\text{ cm}^{-1}$  was adjusted to be  $0.2 \pm 0.01$  under the pressure from 20 to 40 MPa. The measurements were performed 10 times for each sample and the average value was calculated.

The surface of extrudates ( $20 - 50\ \mu\text{m}$ ) were grinded by a metal file to evaluate the molecular weight by the size exclusion chromatography (SEC) (HLC-8020, Tosoh, Tokyo, Japan). The measurement was also performed using pure polymers and the blend samples prepared by compression molding as references. The sample was dissolved in chloroform with a concentration of 0.2 wt%, and the flow rate was 1 mL/min at  $40^\circ\text{C}$ .

## 2.3 Results and Discussion

### 2.3.1 Miscibility of the blends

Figure 2-11 shows the light transmittance of the compression-molded films with 500  $\mu\text{m}$  thickness. Considering that the surface reflectance  $R_s$ , which can be calculated by eq. (2.3), as around 10 % [44,45], all films including PC/PMMA-13k were found to be transparent in the visible wavelength. This was also confirmed by the photographs. These results demonstrated that the samples were in the miscible state at the mixing and processing temperature, i.e.,  $250^\circ\text{C}$ .

$$R_s = \left( \frac{1-n}{1+n} \right)^2 \quad (2.3)$$

where  $n$  is the refractive index

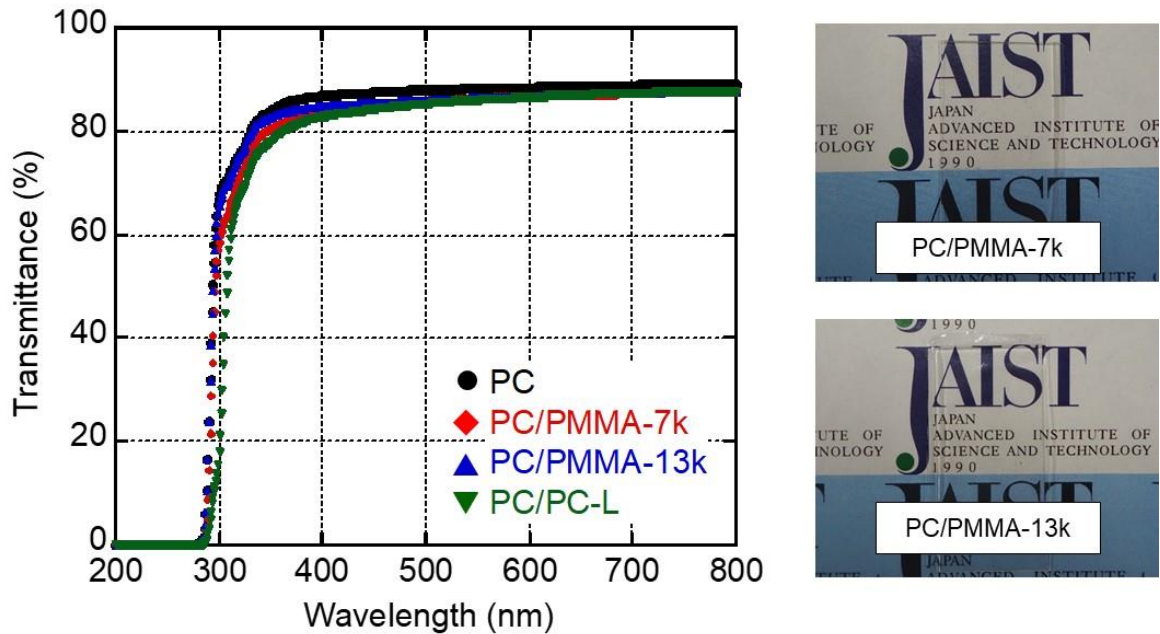


Figure 2-11 Light transmittance as a function of wavelength for the compression-molded films; (circles) PC, (diamonds) PC/PMMA-7k, (triangles) PC/PMMA-13k, and (inverted triangles) PC/PC-L. The film thickness was 0.5 mm. The photographs of PC/PMMA-7k and PC/PMMA-13k are also shown.

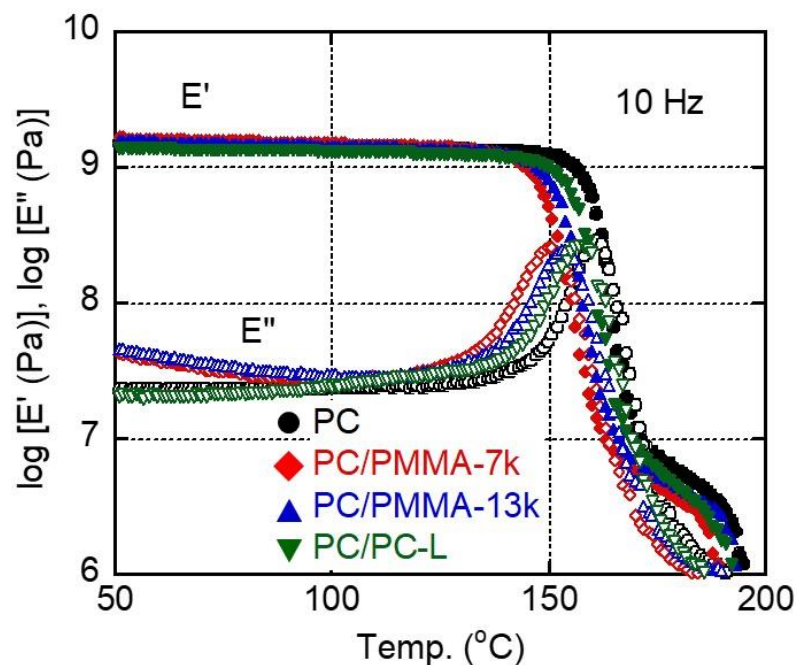


Figure 2-12 Temperature dependence of tensile storage modulus  $E'$  and loss modulus  $E''$  at 10 Hz for films prepared by compression molding; (circles) PC, (diamonds) PC/PMMA-7k, (triangles) PC/PMMA-13k, and (inverted triangles) PC/PC-L.

The temperature dependence of tensile storage modulus  $E'$  and loss modulus  $E''$  for the compression-molded films is shown in Figure 2-12. Both PC/PMMA-7k and PC/PMMA-13k showed a single peak in the  $E''$  curves, which were located at the temperatures between  $T_g$ 's of PC and PMMA. This result also supported that they were miscible. In this case,  $T_g$  of the blends must be predicted by the Fox equation (eq. (2.4)) [46]. Furthermore,  $T_g$  of PC/PC-L was found to be lower than that of pure PC. This is reasonable because PC-L has low molecular weight, leading to low  $T_g$  [47]. It is well known that  $T_g$  is affected by the molecular weight as denoted in eq. (2.5).

$$\frac{1}{T_{g \text{ blend}}} = \frac{w_A}{T_{g A}} + \frac{w_B}{T_{g B}} \quad (2.4)$$

$$T_g = T_g^0 - \frac{c}{M_n} \quad (2.5)$$

where  $w_i$  and  $T_{g i}$  are the weight fraction and  $T_g$  of  $i$ -th species, respectively,  $T_g^0$  is the  $T_g$  of a polymer having infinite molecular weight and  $c$  is the constant.

The difference in  $T_g$  between PC/PMMA-7k and PC/PMMA-13k must be also attributed to the difference in  $T_g$  of pure PMMA samples, i.e.,  $T_g$  of PMMA-7k was lower than that of PMMA-13k. In the case of the blends with PMMA, the  $E''$  values in the low temperature region were higher than those of PC and PC/PC-L. This is attributed to the  $\beta$ -relaxation mode of PMMA [48], which is the local motion of the carbonyl group.

Figure 2-13 shows the frequency dependence of oscillatory shear modulus at 250°C. As seen in the figure,  $G'$  and  $G''$  were proportional to  $\omega^2$  and  $\omega$ , respectively. Both  $G'$  and  $G''$  for the blends were lower than those of PC. Moreover, all blends did not show a shoulder in the  $G'$  curve ascribed to a long-time relaxation due to the interfacial stress of phase-separated blends [49,50]. This is the typical behavior in the rheological terminal zone for a

homogeneous polymer melt, demonstrating that both PC/PMMA-7k and PC/PMMA-13k were in the miscible state. The  $G''$  values of the blends were almost the same irrespective of the low-molecular-weight component, demonstrating that zero-shear viscosities  $\eta_0$ , defined by eq. (2.6), were not so different.

$$\eta_0 = \lim_{\omega \rightarrow 0} \frac{G''}{\omega} \quad (2.6)$$

The zero-shear viscosities of the pure components were also calculated from  $G''$  and found to be as follows; 2850 (Pa s) for PC, 0.60 (Pa s) for PMMA-7k, 5.3 (Pa s) for PMMA-13k, and 2.3 (Pa s) for PC-L at 250°C.

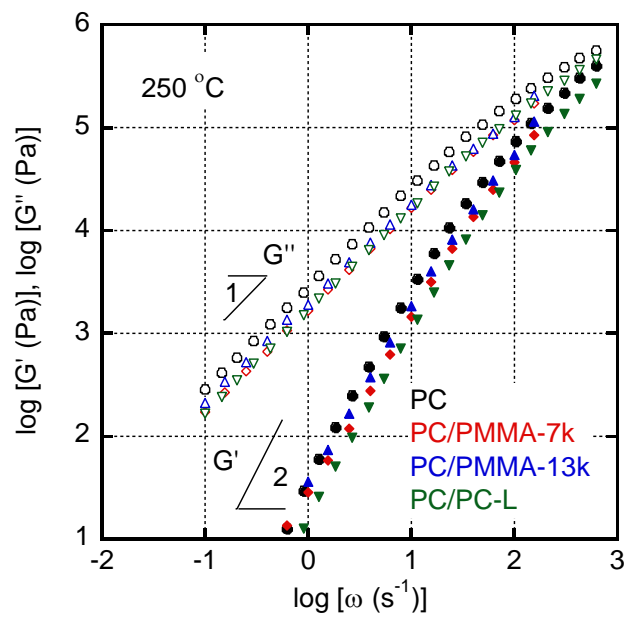


Figure 2-13 Angular frequency dependence of (open symbols) shear storage modulus  $G'$  and (closed symbols) loss modulus  $G''$  for (circles) PC, (diamonds) PC/PMMA-7k, (triangles) PC/PMMA-13k, and (inverted triangles) PC/PC-L at 250°C.

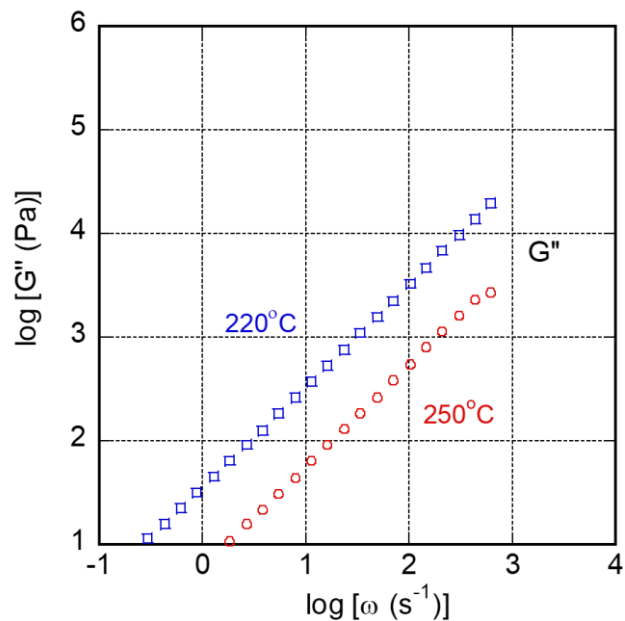


Figure 2-14 Angular frequency dependence of shear loss modulus  $G''$  for PC-L at (square)  $220^\circ\text{C}$  and (circle)  $250^\circ\text{C}$ .

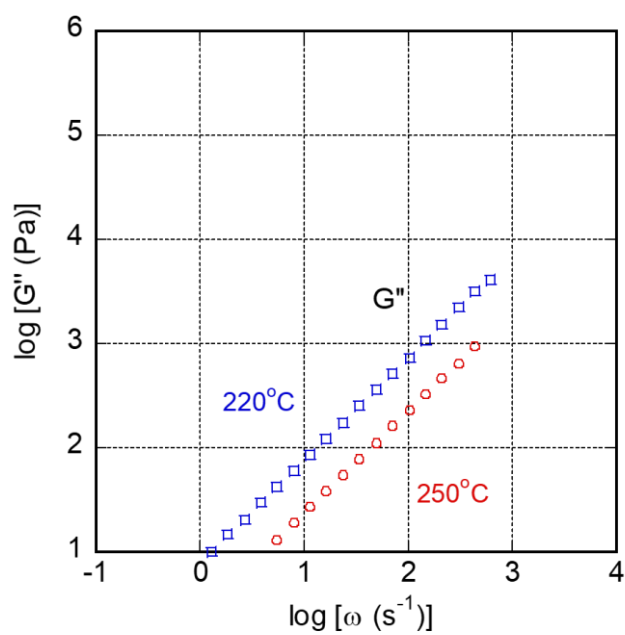


Figure 2-15 Angular frequency dependence of shear loss modulus  $G''$  for PMMA-13k at (square)  $220^\circ\text{C}$  and (circle)  $250^\circ\text{C}$ .

### 2.3.2 Surface segregation

For the ATR-IR measurements to characterize the PMMA content on the extrudates, the rectangular die was used, which provided flat surface at least at 250°C.

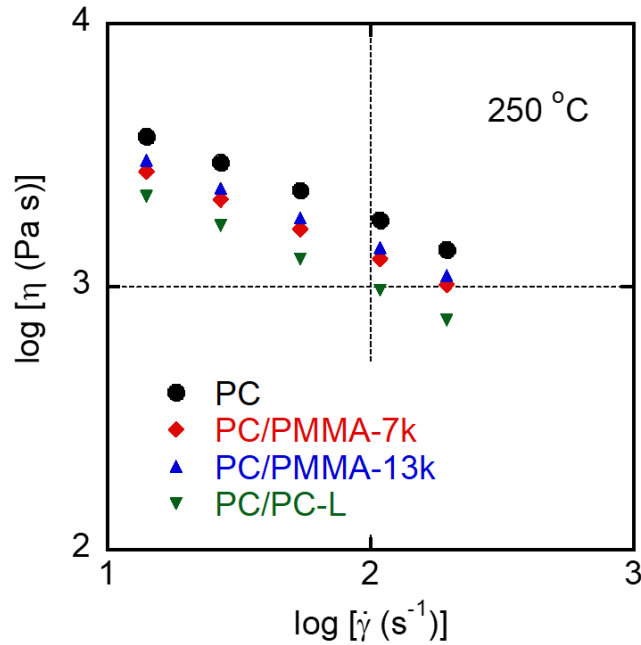


Figure 2-16 Steady-state shear viscosity  $\eta$  plotted against shear rate  $\dot{\gamma}$  at 250°C for (circles) PC, (diamonds) PC/PMMA-7k, (triangles) PC/PMMA-13k, and (invert triangles) PC/PC-L.

Figure 2-16 shows the flow curves, i.e., shear viscosity  $\eta$  plotted against shear rate  $\dot{\gamma}$ , evaluated using the rectangular die with  $L = 10$  mm. As predicted, the addition of PMMA samples and PC-L decreased the shear viscosity.

Figure 2-17 compares ATR-IR spectra of the strands extruded at  $194 \text{ s}^{-1}$  and those of the compression-molded films. The vertical axis was normalized by the absorbance ascribed to PC. The penetration depth of infrared light,  $d_p$ , varies depending on the wavelength  $\lambda$ , which is expressed as,

$$d_p = \frac{\lambda/n_1}{2\pi\sqrt{\sin^2\theta - (n_2/n_1)^2}} \quad (2.7)$$

where  $\theta$  is an angle of incidence and  $n_1$  and  $n_2$  are the refractive indices of the ATR crystal and sample, respectively.

According to eq. (2.7), the penetration depth at the present experiment was about 1.4  $\mu\text{m}$ .

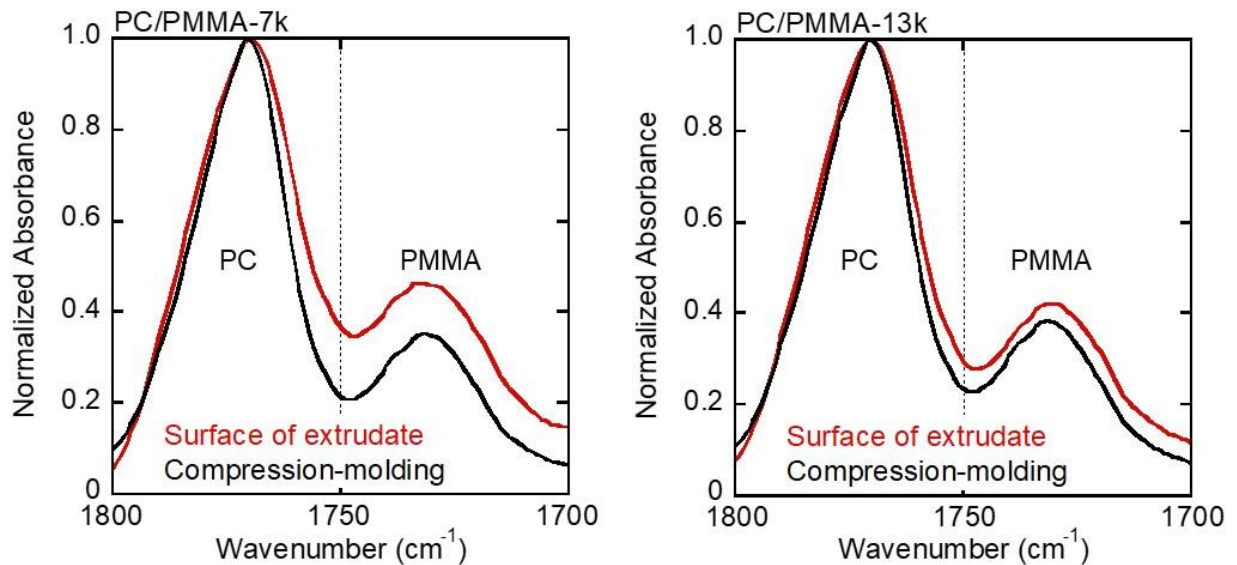


Figure 2-17 Normalized ATR-IR spectra of the extrudate at  $194 \text{ s}^{-1}$  and compression-molded film for (left) PC/PMMA-7k and (right) PC/PMMA-13k.

As seen in the figure, the absorbance ascribed to PMMA at the extrudate surface was stronger than that of the compression-molded film for both blends. Furthermore, the difference was pronounced for PC/PMMA-7k as compared with PC/PMMA-13k. Similar measurements were performed for the samples extruded at various shear rates. Based on the calibration curve, which was obtained using compression-molded films, the PMMA content at surface was plotted against the shear rate as shown in Figure 2-18. The PMMA contents at extrudates' surface were always higher than 10%, demonstrating that the surface segregation occurred at any conditions.

The figure suggested that the PMMA content increased with increasing shear rate. Moreover, the contents at PC/PMMA-7k surfaces were higher than those at PC/PMMA-13k, demonstrating that marked segregation occurred for a blend having PMMA with low molecular weight.

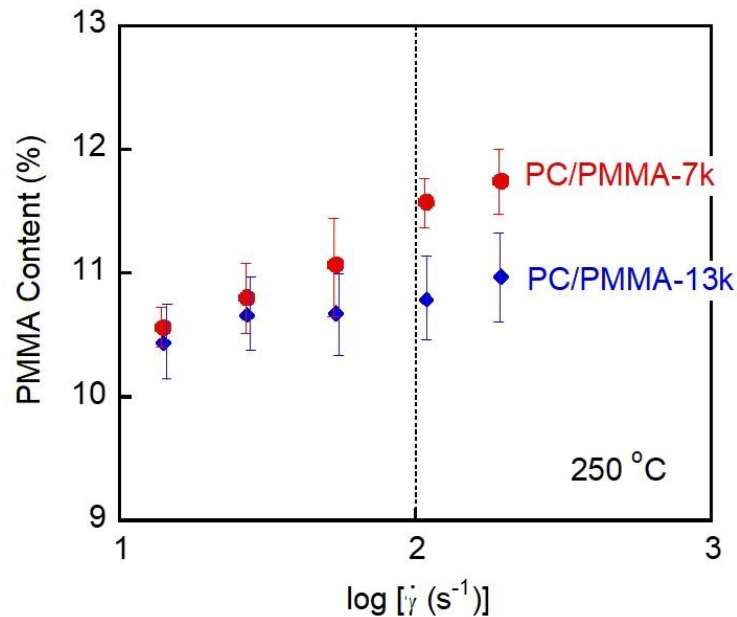


Figure 2-18 PMMA contents at surface of extrudates plotted against the shear rate  $\dot{\gamma}$  at 250°C for (circles) PC/PMMA-7k and (diamonds) PC/PMMA-13k.

The PMMA contents at surface were evaluated using a long die to discuss the effect of the residence time in a die land. It was found from Figure 2-19 that both dies provided the same extent of the segregation considering the experimental error, indicating that the segregation did not progress more even using a long die. It is generally known that a flow velocity near die surface is very slow, leading to a long residence time. A prolonged residence time at surface, even through a short die, may be responsible for this result, i.e., no difference in the PMMA content.

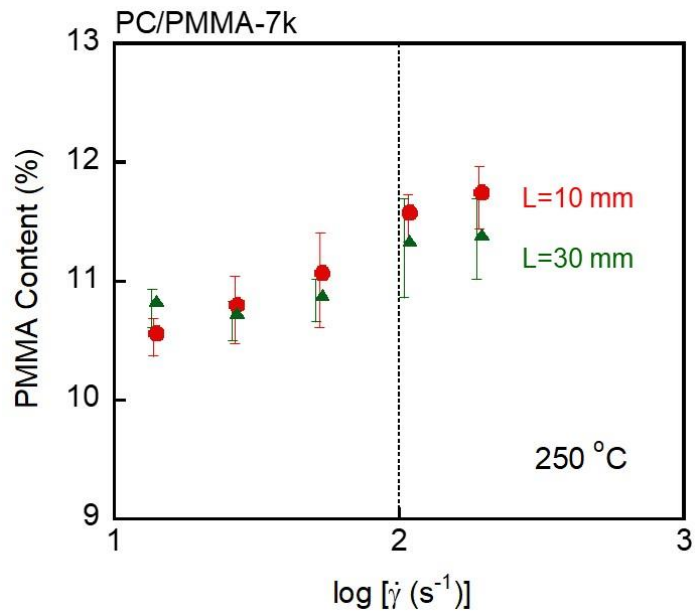


Figure 2-19 PMMA contents on the strand surface plotted against the shear rate  $\dot{\gamma}$  at 250°C for PC/PMMA-7k extruded through the rectangular dies with the length of (circles) 10 mm and (triangles) 30 mm.

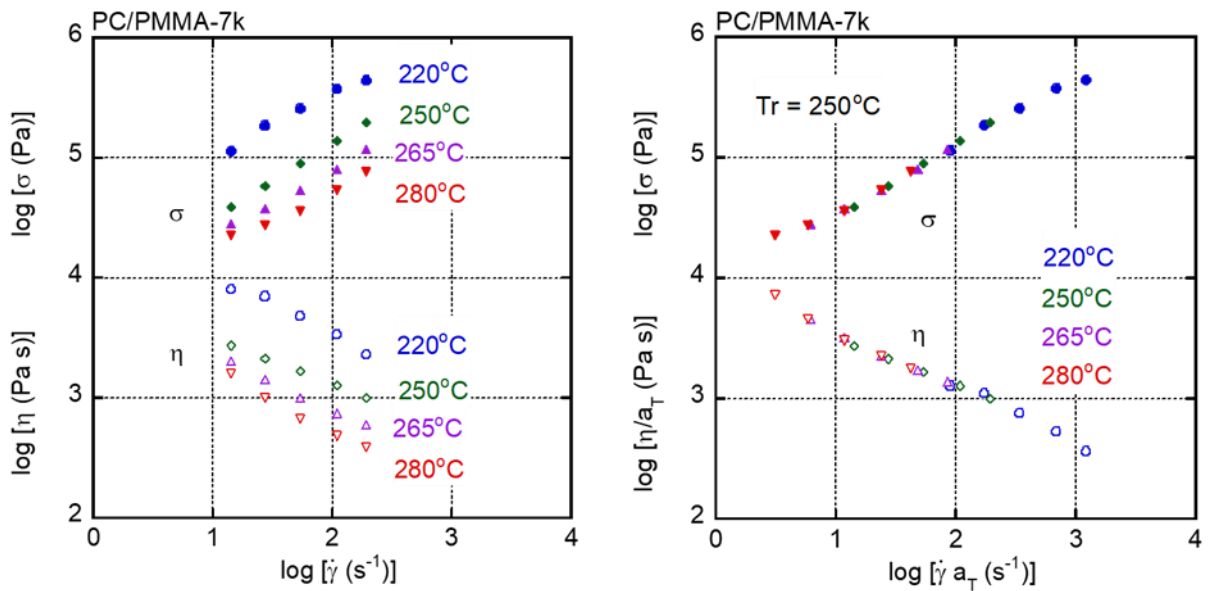


Figure 2-20 Shear stress  $\sigma$  and shear viscosity  $\eta$  plotted against shear rate  $\dot{\gamma}$  at (circles) 220°C, (diamonds) 250°C, (triangles) 265°C, and (inverted triangles) 280°C for PC/PMMA-7k. The measurements were performed using the rectangular die with  $L=10$  mm.

The extrusion was performed at various temperatures using PC/PMMA-7k. The flow curves are shown in Figure 2-20 with the master curve at 250°C as a reference temperature  $T_r$ . Neither Bagley nor Rabinowitsch corrections were performed. The time-temperature superposition principle was applicable in this temperature range. All of the extrudates were found to be transparent, suggesting that they were miscible. The ATR-IR measurements were not performed for the extrudates at 265°C and 280°C because of the distorted surface due to their low viscosities.

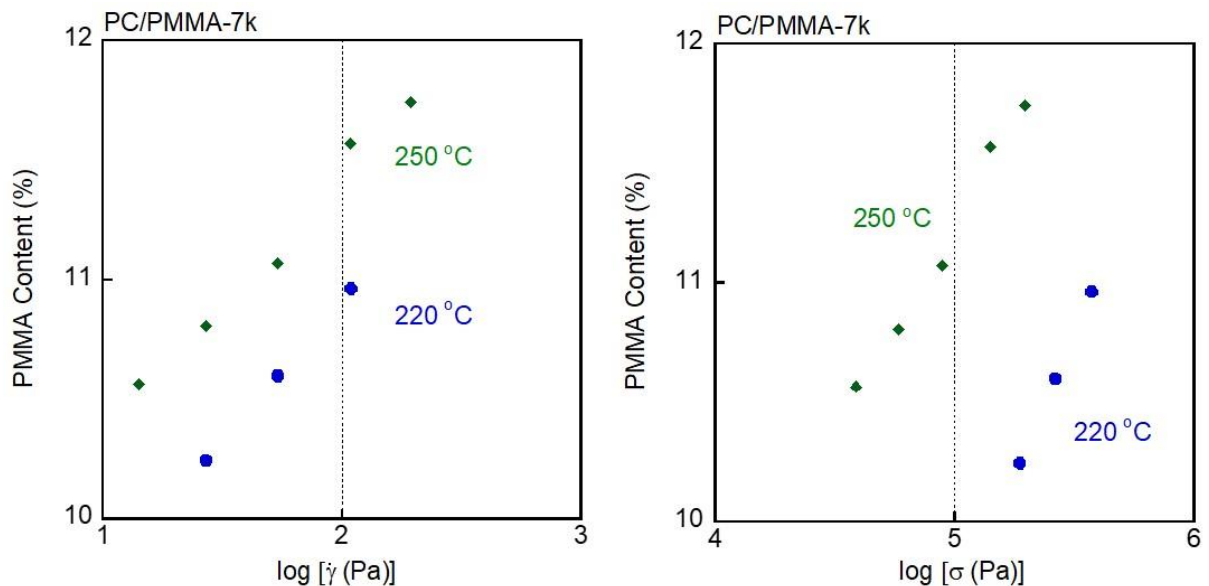


Figure 2-21 Relationship between (left) shear rate  $\dot{\gamma}$  and (right) shear stress  $\sigma$  and the PMMA content at the surface of extrudates for PC/PMMA-7k. The extrusion was performed at (circles) 220°C and (diamonds) 250°C.

The PMMA contents at extrudates' surface for PC/PMMA-7k are plotted as a function of shear rate  $\dot{\gamma}$  and shear stress  $\sigma$  in Figure 2-21. It was interesting to note that the time-temperature superposition principle was not applicable to the segregation phenomenon. Furthermore, the figures demonstrated that neither shear rate nor shear stress decide the

degree of segregation. The segregation became pronounced at high temperature, although the applied shear stress is low.

The segregation phenomenon was also evaluated using PC/PC-L. For the blend, however, ATR-IR spectra do not provide the information on the PC-L content at surface. Therefore, the molecular weight and its distribution were evaluated by collecting the surface region of the sample extruded at  $194 \text{ s}^{-1}$ . As a comparison, the PC/PC-L sample prepared by compression molding was also employed with the individual pure components.

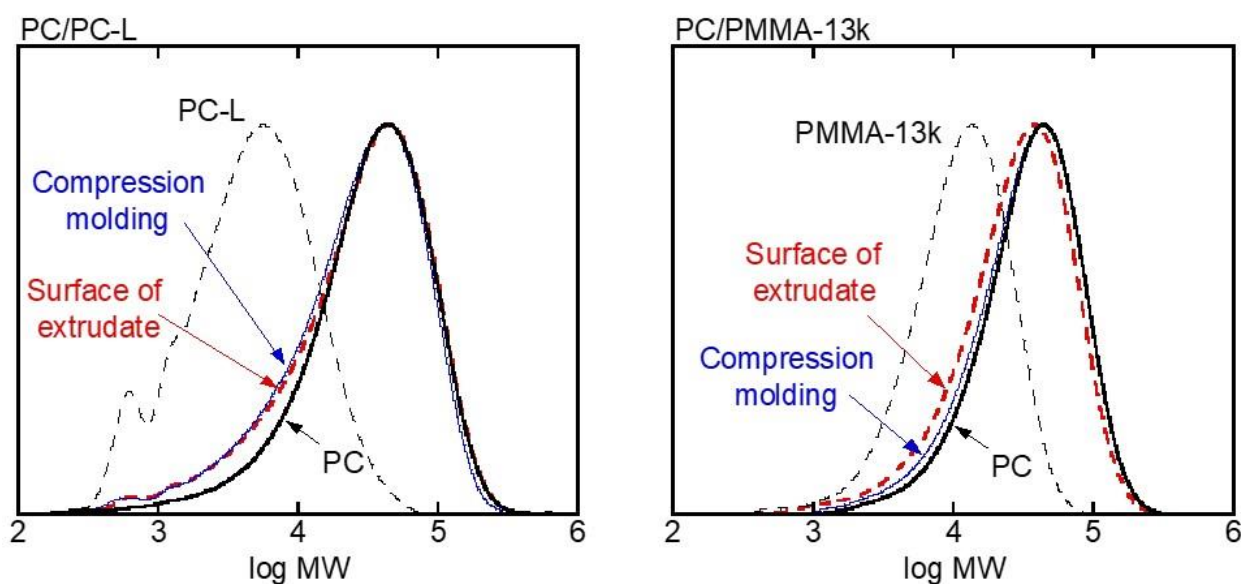


Figure 2-22 SEC curves for (left) PC/PC-L and (right) PC/PMMA-13k: (bold dotted lines) surface of extrudates at  $194 \text{ s}^{-1}$  (thin solid line) compression-molded films. In the figure, pure PC as solid lines and PC-L or PMMA-13k as thin dotted lines were also plotted.

Figure 2-22 shows the size exclusion chromatography (SEC) curves. As seen in the figure, in which the horizontal axis represents the molecular weight as a polystyrene standard, the surface at a PC/PMMA-13k extrudate has more low-molecular-weight fraction than the compression-molded film. In contrast, the SEC curves of PC/PC-L were almost the same

irrespective of the processing methods, indicating that the surface segregation of PC-L was not prominent in an extrudate.

When the low-molecular-weight fraction is localized at the surface region by a pressure-driven shear flow, shear stress should decrease. Therefore, the total stress for the flow will decrease, which may be a driving force of the surface segregation [51,52]. However, the present result indicated that segregation phenomenon was pronounced for PC/PMMA-13k compared to PC/PC-L, although PC-L showed lower shear viscosity. Furthermore, Figure 2-21 demonstrated that segregation occurred at high temperature, i.e., near LCST, although shear stress became low at the high temperature. These results indicated that the surface segregation was not originated from the reduction of the hydrodynamic force. Considering that segregation became prominent at the high temperature for PC/PMMA-7k, it may have a relation with the shear-induced demixing [53-58]. Although phase separation was not detected in this study, the driving force of segregation behavior would be the decrease in the Gibbs energy of mixing owing to the decrease in the mixing entropy and/or increase in the Flory-Huggins parameter [53-58].

As mentioned in the introduction of this chapter, the surface segregation of PMMA can increase the surface hardness and antiscratch property of PC even though the molecular weight of PMMA was low. However, the critical molecular weight to enhance the surface properties many exist because a polymer with very low molecular weight is usually significantly brittle. In near future, such molecular weight should be clarified because the surface segregation is more significant for PMMA with lower molecular weight, although PMMA with  $M_w = 15000$  is good enough to improve the scratch resistance as introduced previously.

Finally, surface segregation phenomena will be widely applicable to various processing operations. Considering shear rate applied at processing operations, injection-molding is one of the most appropriate processing methods. In the following chapter, the segregation behavior was studied using injection-molded products.

## 2.4 Conclusion

The blend composition at the surface of extrudates was studied using miscible blends of PC containing another polymer having low viscosity. The extrudate was found to have more PMMA at surface, which was detected by the ATR-IR spectra and SEC curves. The segregation behavior was pronounced when the molecular weight of PMMA was low. The residence time in the die did not play an important role. Moreover, the segregation was pronounced at high temperature, i.e., near LCST. Finally, the segregation was not detected for the extrudate of PC/PC-L, i.e., the blend system with the same polymer species. These results suggested that the segregation phenomenon occurs in a miscible blend with a positive Flory-Huggins parameter.

## References

1. M. Okamoto, *J. Appl. Polym. Sci.* 2002, 83, 2774.
2. H. Schnell, *Chemistry and Physics of Polycarbonate*, Interscience Publishers, New York, 1964.
3. D. Freitag, G. Fengler, and L. Morbitzer, *Angew. Chem. Int. Ed. Eng.* 1991, 30, 1598.
4. W. S. Higley, P. A. Cantor, and B. S. Fisher, *Thin Polycarbonate Membranes for Use in Hemodialysis*, United States Patent 4,069,151, Jan. 17, 1978.
5. <http://polymer-database.com>

6. S. I. Salih, J. K. Oleiwi, and A. S. Mohamed, *ARPN J. Eng. Appl. Sci.* 2018, 13, 8889.
7. R. K. Alla, S. Sajjan, V. R. Alluri, K. Ginjupalli, and N. Upadhya, *J. Biomater. Nanobiotechnol.* 2013, 4, 91.
8. W. N. Kim and C. M. Burns, *Macromolecules* 1987, 20, 1876.
9. J. Kolarik, F. Lednicky, B. Pukanszky, and M. Pegoraro, *Polym. Eng. Sci.* 1992, 32, 886.
10. M. Dixit, V. Mathur, S. Gupta, M. Baboo, K. Sharma, and N. S. Saxena, *Phase Transitions*, 2009, 82, 866.
11. J. S. Chiou, J. W. Barlow, and D. R. Paul, *J. Polym. Sci.: Part B: Polym. Phys.* 1978, 25, 1459.
12. C. J. Carriere and A. Cohen, *J. Rheol.*, 1991, 35, 205.
13. Eds. J. Brandrup, E. H. Immergut, and E. D. Grulke 4<sup>th</sup> Edn, *Polymer Handbook* Wiley, New York, 1999.
14. M. Nishimoto, H. Keskkula, and D. R. Paul, *Polymer* 1991, 32, 272.
15. D. Patterson & A. Robard, *Macromolecules* 1978, 11, 690.
16. M. Fernández, M. E. Muñoz, A. Santamaría, S. Syrjäälä, and J. Aho, *Polym. Test.* 2009, 28, 109.
17. M. Yamaguchi, K. Nakamura, T. Kimura, N. Moonprasith, T. Kida, K. Tsubouchi, T. Narita, and T. Hiraoka, *Materials* 2022, 15, 2783.
18. S. Madbouly, M. Ohmomo, T. Ougizawa, and T. Inoue, *Polymer* 1999, 40, 1465.
19. X. Shuting, H. Yajiang, Y. Qi, and L. Guangxian, *Ind. Eng. Chem. Res.* 2014, 53, 14, 5916.
20. T. Bubmann, A. Seidel, and V. Altstädt, *Polymer* 2019, 11, 2070.
21. A. K. Singh, R. Prakash, and D. Pandey, *RSC Adv.* 2012, 2, 10316.

22. M. Yang, L. Wei, J. Li, and S. Guo, *Polym. Eng. Sci.* 2018, 58, 1508.
23. T. Bubmann, A. Seidel, and V. Altstädt, *Polymer* 2019, 11, 2070
24. M. Okamoto, *J. Appl. Polym. Sci.* 2001, 80, 2670.
25. H. Jang, F. Ahmed, H. Joo, T. Ryu, H. Yang, S. Yoon, W. Kim, and H. S. Jeon, *J. Nanosci. Nanotechnol.* 2017, 17, 7381.
26. S. Scholtyssek, V. Seydewitz, R. Adhikari, F. Pfeifer, G. H. Michler, and H. W. Siesler, *J. Appl. Polym. Sci.* 2013, 127, 4262.
27. I. F. Francke, M. Berrebi, B. Lavedrine, and O. Fichet, *Materials Today* 2019, 21, 100582.
28. Y. Kano and S. Akiyama, *Polymer* 1996, 37, 4497.
29. V. S. Minnikanti, Z. Qian, and L. A. Archer, *J. Chem. Phys.* 2007, 126, 144905.
30. K. Tanaka, A. Takahara, and T. Kajiyama, *Acta Polym.* 1995, 46, 476.
31. T. F. Schaub, G. J. Kellogg, A. M. Mayes, R. Kulasekere, J. F. Ankner, and H. Kaiser, *Macromolecules* 1996, 29, 3982.
32. M. Siriprumpoonthum, N. Mieda, S. Nobukawa, and M. Yamaguchi, *J. Polym. Res.* 2011, 18, 2449.
33. T. Sako, S. Nobukawa, and M. Yamaguchi, *Polym. J.* 2015, 47, 576.
34. P. Polyakov, E. Rossinsky, and S. Wiegand, *J. Phys. Chem. B* 2009, 113, 13308.
35. Y. T. Maeda, A. Buguin, and A. Libchaber, *Phys. Rev. Lett.* 2011, 107, 038301.
36. H. Morita, K. Tanaka, T. Kajiyama, T. Nishi, and M. Doi, *Macromolecules* 2006, 39, 6233.
37. J. L. Keddie, R. A. L. Jones, and R. A. Coury, *Europhys. Lett.* 1994, 27, 59.
38. K. Tanaka, A. Takahara, and T. Kajiyama, *Macromolecules* 1997, 30, 6626.

39. J. Suwa, M. Kakiage, T. Yamanobe, T. Komoto, and H. Uehara, *Langmuir* 2007, 23, 5882.
40. N. W. Matsen and P. Mahmoudi, *Eur. Phys. J. E* 2014, 37, 79.
41. T. Sako, A. Ito, and M. Yamaguchi, *J. Polym. Res.* 2017, 24, 89.
42. T. Sako, Ph.D. Thesis, Japan advanced institute of science and technology, Ishikawa, 2018.
43. Z. Tadmor and C. G. Gogos, *Principles of Polymer Processing*, 2<sup>nd</sup> ed., Wiley, Hoboken, NJ 2006.
44. S. Takahashi, H. Okada, S. Nobukawa, and M. Yamaguchi, *Eur. Polym. J.* 2012, 48, 974.
45. N. Kuhakongkiat, M. Sugiyama, M. Guesnier, F. A. Azaman, K. Yoshida, and M. Yamaguchi, *J. Appl. Polym. Sci.* 2017, 135, 45927.
46. T. G. Fox and P. J. Ferry, *J. Appl. Phys.* 1950, 21, 581.
47. T. G. Fox, *Bull. Am. Phys. Soc.* 1956, 1, 123.
48. A. Miyagawa, V. Ayerdurai, S. Nobukawa, and M. Yamaguchi, *J. Polym. Sci., Part B, Polym. Phys. Ed.* 2016, 54, 2388.
49. J. F. Palierne, *Rheol. Acta* 1990, 29, 204.
50. T. Yokohara and M. Yamaguchi, *Eur. Polym. J.* 2008, 44, 677.
51. J. Seemork, M. Siriprumpoonthum, Y. Lee, S. Nobukawa, and M. Yamaguchi, *Adv. Polym. Technol.* 2015, 34, 21477.
52. J. Seemork, T. Sako, B. M. A. Mohd Amran, and M. Yamaguchi, *J. Rheol.* 2017, 61, 1.
53. T. Ougisawa and T. Inoue, *Morphology of Polymer Blends*, in: L. A. Utracki and C. A. Wilkie (Eds.), *Polymer Blends Handbook*, 2<sup>nd</sup> ed., Hanser, Munich, Germany 2014.

54. S. Mani, M. F. Malone, H. H. Winter, J. L. Halary, and L. Monnerie, *Macromolecules* 1991, 24, 5451.
55. L. A. Hindawi, J. S. Higgins, and R. A. Weiss, *Polymer* 1992, 33, 2522.
56. A. Onuki, *Intern. J. Thermophys.* 1995, 16, 381.
57. W. Soontaranun, J. S. Higgins, and T. D. Papathanasiou, *Fluid Phase Equilib.* 1996, 121, 273.
58. R. G. Larson, *Rheol. Acta* 1992, 31, 497.

## **Chapter 3: Application to injection-molding**

### **3.1 Introduction**

#### **3.1.1 Polymer processing**

Polymer processing is commonly defined as the “activity performance on polymeric materials to increase their usefulness” [1]. It involves not only shaping but sometime also synthesis, transformation, compounding, functionalization, and stabilization of polymer materials. The combination of these operations determines final properties and performance of polymeric products. Most of polymers are processed under molten state. Therefore, the control of rheological behaviors is one of key factors for polymer processing operations. Of course, thermal properties are also important to decide processability at various processing operations. Among various operations, main ones for thermoplastics are extrusion and injection-molding. Because of their good cost-performance, applicability to extrusion and/or injection-molding decides the application of thermoplastic. For example, most automobile parts of thermoplastics are currently produced by injection-molding.

#### **3.1.2 Injection-molding**

Injection-molding is a manufacturing process by injecting a molten material into a mold. This process needs high pressure to fill a fluid material into a specific mold cavity to provide a desired shape. The materials are heated up before injection to give flowability. The screw delivers the raw material forward, with homogenising thermal and viscous distributions in a polymer. Then a molten resin is stocked in the top of the barrel, and pushed by forward moving of a screw to fill a molten resin into a mold to cool. During filling in a mold, shear flow is generated. A typical injection-molding machine is shown in Figure 3-1.

A molten polymer injected from a nozzle of a screw cylinder goes into a mold from a sprue. Then after passing through a runner, it goes into a cavity from a gate. Figure 3-2 shows the schematic illustration inside of a mold. Inside of a cavity, a polymer melt flows by laminar flow as shown in Figure 3-3.

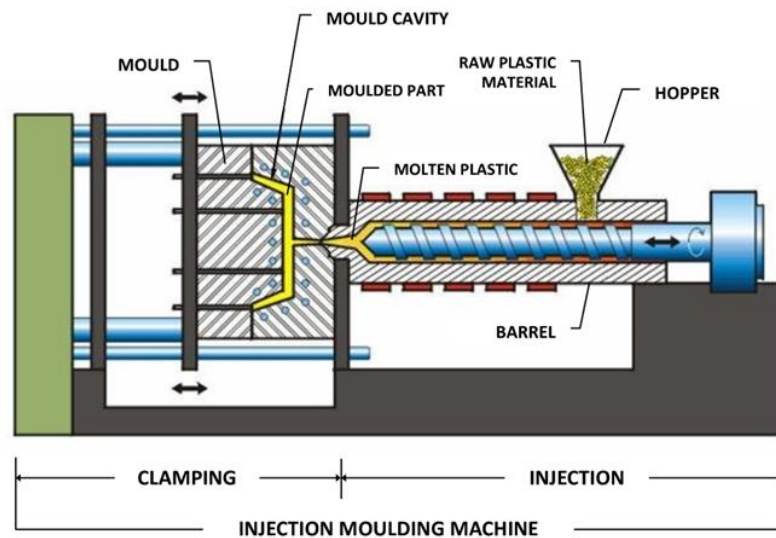


Figure 3-1 Injection-molding machine [2]

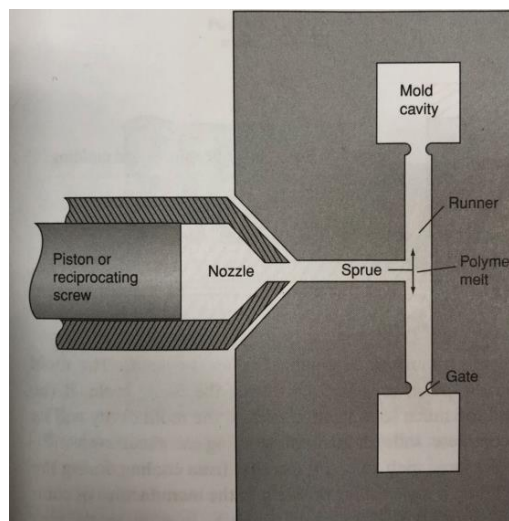


Figure 3-2 Illustration of inside of a mold [3]

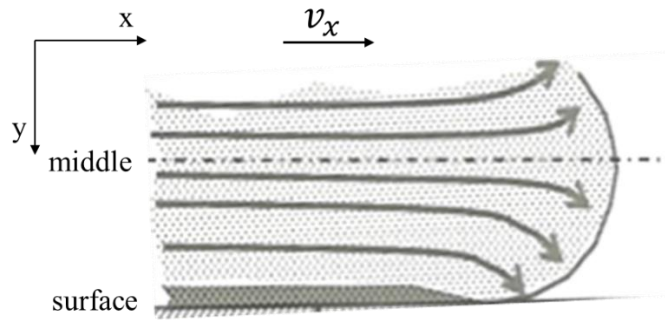


Figure 3-3 Flow velocity distribution of molten resin in a mold [4]

From this figure, not only shear but elongation flow also occurs at the top of a molten resin. Besides this area, shear flow dominates. The highest shear rate, i.e.,  $dv_x/dy$ , is applied near the wall surface of a mold. Furthermore, in the vicinity of the mold wall surface, the molten resin is quenched, which results in high molecular orientation. Therefore, different structures such as orientation of the molecular chain and shape of the dispersed phase are formed, depending upon the location of a product, i.e., distance from the mold surface.

The flow velocity profile of a molten material is illustrated in Figure 3-4. The highest velocity occurs at center of a mold and the lowest velocity is at mold surface. Since the shear rate is given by the velocity gradient, it is the highest at the surface. For residence time, which is proportional to  $v^{-1}$ , it is the longest at surface.

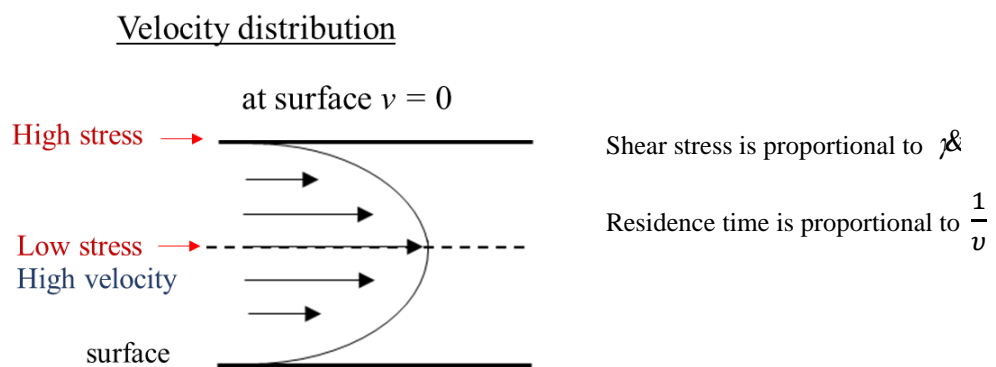


Figure 3-4 Schematic illustration of velocity profile in a mold

As mentioned in the introduction of chapter 2, even in the miscible system of PC and PMMA with low molecular weight, the low-molecular-weight component tends to be located at the surface of the blend sample. This is pronounced at high shear rates. Therefore, injection-molding process would be an ideal processing operation to obtain a gradient product, because a high shear rate is expected in a mold. In Figure 3-5, applied shear rates at various processing operations were denoted. Furthermore, it can be regarded as a novel method to modify the surface properties of a product.

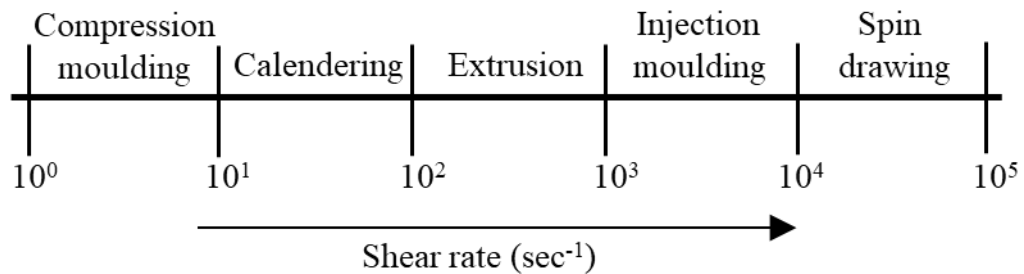


Figure 3-5 Shear rates at various processing operations [5]

In this study, therefore, the segregation behavior at surface using injection-molded products composed of PC and PMMA, in which one of them has low molecular weight, was studied.

## 3.2 Experimental

### 3.2.1 Materials

Commercialized biphenol A polycarbonate samples, denoted as PC-H (Panlite L-1225Y, Teijin, Japan) and PC-L (Iupilon AL-071, Mitsubishi Engineering-Plastics, Japan), were used as raw materials. Two types of PMMA with different molecular weights, prepared by Mitsubishi Chemical, were also employed for this study. A high-molecular-weight PMMA

was represented as PMMA-H and a low-molecular-weight PMMA was denoted as PMMA-L. The samples were used as obtained. The number- ( $M_n$ ) and weight-average ( $M_w$ ) molecular weights were determined by the size exclusion chromatography (HLC-8020, Tosoh, Tokyo, Japan) as polystyrene standard. The molecular weights of polymers were summarized in Table 3-1 [6-9].

Table 3-1 Molecular weights of polymers

Sample code	$M_n$	$M_w$
PC-H	28000	46000
PC-L	3100	8700
PMMA-H	58000	120000
PMMA-L	8900	15000

### 3.2.2 Sample preparation

Vacuum drying was performed at 80°C for 4 hours. The melt-mixing of samples was carried out using a 15 mm diameter co-rotating twin-screw extruder (ULT15TWnano, Technovel, Osaka, Japan) at 250°C. The screw rotation speed was 30 rpm. Both PC-H/PMMA-L and PMMA-H/PC-L were obtained as the blend ratios of 90/10 and 80/20 wt%. Moreover, PC-H/PMMA-H (90/10) and PMMA-H/PC-H (90/10) were obtained using the same procedure for comparison.

The compression-molding was carried out at 250°C under 10 MPa. Then they were quenched at 25°C to obtain films with 500  $\mu\text{m}$  thickness. Injection-molding was performed by an injection-molding machine (HM7, Nissei Plastic Industrial). The temperature at nozzle/barrel and mold were controlled at 250°C and 70°C, respectively. The obtained bar having the following dimensions were produced; the length of 70 mm, the width of 10 mm, and the thickness of 2 mm. A square-shaped gate with 1.5 mm x 1.5 mm was employed.

### 3.2.3 Measurements

Transparency of the compression-molded films with 500 mm thickness was evaluated at 25°C using a UV-vis spectrophotometer (Lambda25, Perkin-Elmer) at the wavelength 589 nm.

Temperature dependence of oscillatory tensile moduli in the solid state was measured at 10 Hz from 30 to 180°C at 2°C/min using a dynamic mechanical analyzer (E-4000, UBM). The specimens were cut to rectangular shape with 5 mm in width and 20 mm in length.

Angular frequency dependence of oscillatory shear moduli was measured in a molten state using a cone-and-plate rheometer (AR2000ex, TA Instrument) under a nitrogen atmosphere at 250°C. The angle of the cone was 4° and the diameter was 25 mm. The angular frequency was ranged from 0.1 to 628.3 s<sup>-1</sup>.

The blend composition at surface of the injection-molded bars was characterized by the attenuated total reflectance Fourier-transform infrared (ATR-IR) spectra (Spectrum 100 FT-IR spectrometer, Perkin-Elmer) at 25°C. KRS-5 was used as an ATR crystal. The absorbance of 1770 cm<sup>-1</sup> was adjusted to be 0.2 ± 0.01 under the pressure from 20 to 40 MPa. Each sample was tested 10 times and the average value was calculated. The measurement points of an injection-molded bar were denoted in Figure 3-6. The gate position was also indicated.

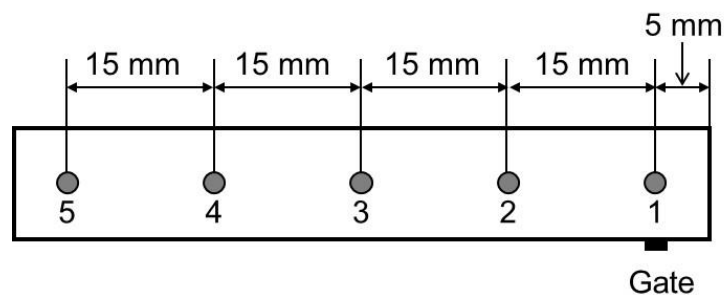


Figure 3-6 Measurement points of ATR-IR spectra.

### 3.3 Results and Discussion

#### 3.3.1 Viscoelastic properties and miscibility

The compression-molding films with 500  $\mu\text{m}$  thickness are shown in Figure 3-7. It was found that the films containing a low-molecular-weight component up to 20 wt% were transparent. Considering the huge difference in the refractive index between PC and PMMA, once they are immiscible then light scattering will take place [10]. Therefore, these films obtained by compression-molding at 250°C are in the miscible state.

Furthermore, the UV-vis spectrophotometer was employed to characterize the film clarity. The light transmittances of the films containing PC-L or PMMA-L (86-89%) were 86-89%. They were almost identical to those of pure PC-H (86%) and PMMA-H (89%). The values were represented in the pictures. Because approximately 10% of the incident light was reflected at both surfaces as mentioned in the previous chapter, light scattering barely occurred inside of the films. In comparison, PC-H/PMMA-H (90/10) and PMMA-H/PC-H (90/10) were opaque as a result of light scattering from the phase-separated structure.

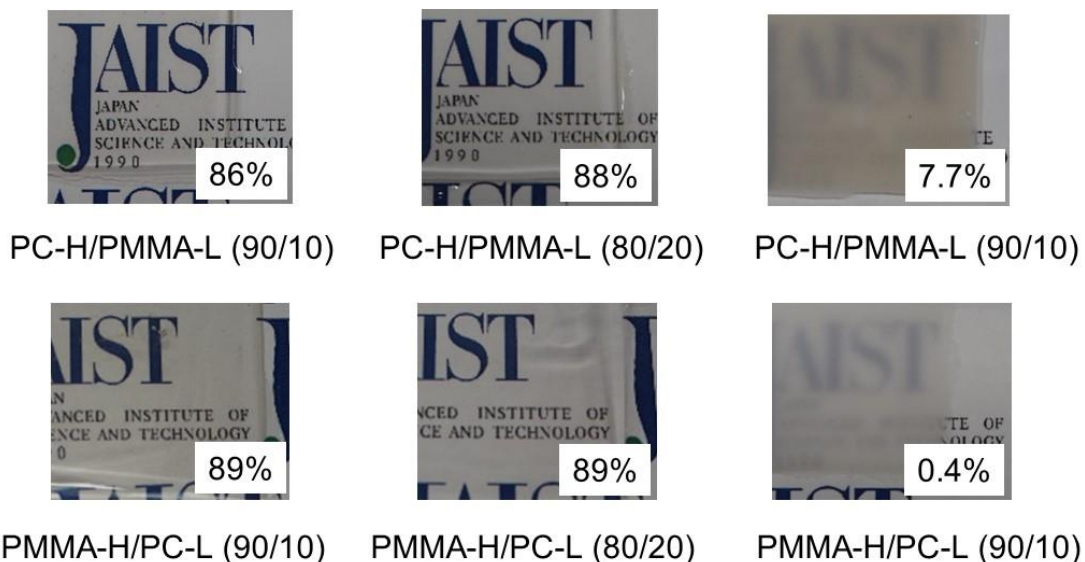


Figure 3-7 Pictures of films obtained by compression-molding. The numerals in the figure denote the light transmittance at 589 nm.

Dynamic mechanical analysis was employed to characterize the miscibility between PC and PMMA, because the glass-to-rubber transition is clearly identified in the system as shown in Chapter 2. Figure 3-8 shows the temperature dependence of tensile storage modulus  $E'$  and loss modulus  $E''$  for PC-H, PC-H/PMMA-L (90/10), and PC-H/PMMA-L (80/20). The compression-molded films were employed for this investigation. The  $E''$  curve showed a single peak ascribed to glass transition temperature  $T_g$ , suggesting that the systems were miscible. It was in accordance with Figure 3-7. With increasing the PMMA-L amount, the peak temperature, i.e.,  $T_g$ , decreased. Furthermore,  $E'$  values in the glassy region increased by the addition of PMMA-L, suggesting that PMMA-L acted as an antiplasticizer for PC-H. Numerous materials are known to serve as an antiplasticizer for PC, and they reduce thermal expansion and alter the birefringence. [7,9,11-13]. The modulus enhancement in the glassy region would be also attractive for PC [7,14,15]. Moreover,  $E''$  values in the glassy region were as enhanced with the PMMA-L content. This would be ascribed to  $\beta$ -dispersion of PMMA [8].

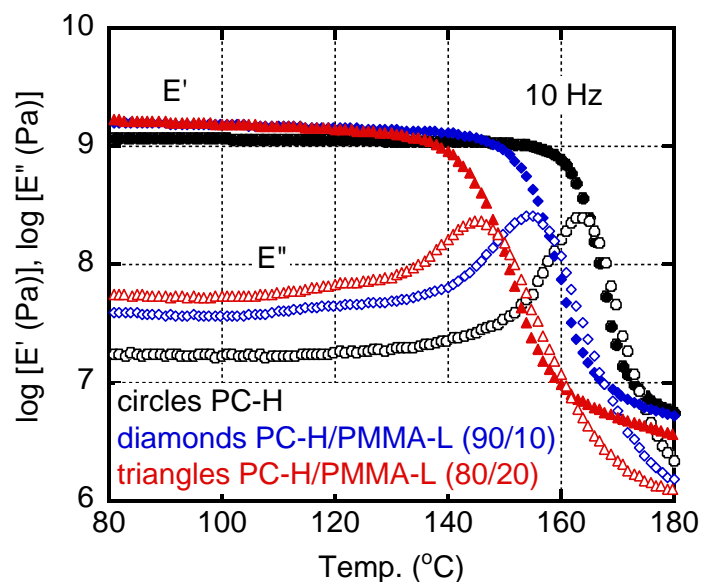


Figure 3-8 Dynamic mechanical properties at 10 Hz; (circles) PC-H, (diamonds) PC-H/PMMA-L (90/10), and (triangles) PC-H/PMMA-L (80/20).

The dynamic tensile moduli  $E'$  and  $E''$  for PMMA-H, PMMA-H/PC-L (90/10), and PMMA-H/PC-L (80/20) were displayed in Figure 3-9. There was a single peak in the  $E''$  curve for each blend, suggesting only one  $T_g$ . This means that they are miscible systems. The peaks of PMMA-H/PC-L blends were located at a lower temperature than that of pure PMMA-H. This is ascribed to low  $T_g$  of PC-L. As mentioned in the previous chapter,  $T_g$  is a function of molecular weight [16]. Due to very low-molecular-weight of the current sample, PC-L,  $T_g$  is significantly lower than that of ordinary PC samples. Moreover,  $E'$  values in the glassy region decreased with increasing the PC-L content. This phenomenon was opposite to the trend of PC-H/PMMA-L blends, i.e., antiplasticized system. Beyond  $T_g$ ,  $E'$  of the blends decreased rapidly, because PC-L played a role of a plasticizer for PMMA-H.

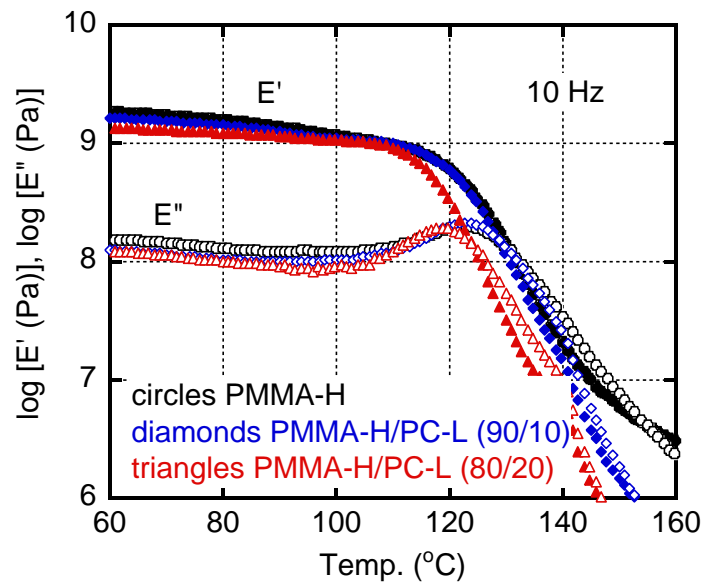


Figure 3-9 Dynamic mechanical properties at 10 Hz of; (circles) PMMA-H, (diamonds) PMMA-H/PC-L (90/10), and (triangles) PMMA-H/PC-L (80/20).

Moreover, the viscoelastic properties in the molten state, i.e., 250°C, were also investigated to examine the miscibility. The oscillatory shear storage modulus  $G'$  and loss modulus  $G''$  is plotted against the angular frequency  $\omega$  in Figure 3-10. Rheological terminal zone was detected for all samples. It should be remarked that both  $G'$  and  $G''$  values for the mixtures were lower than those for pure PC-H and PMMA-H. Furthermore, the slope of  $G'$  curves in the logarithm plot is approximated to 2 without showing a shoulder, implying that they were miscible in the molten state at 250°C.

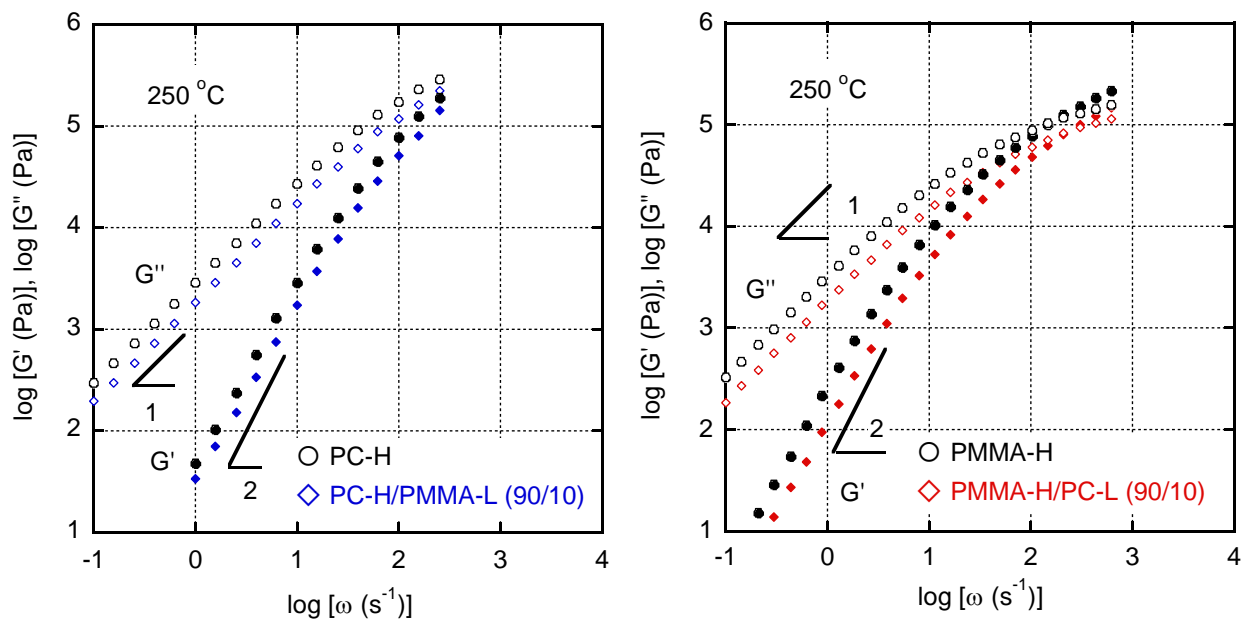


Figure 3-10 Angular frequency  $\omega$  dependence of oscillatory shear storage modulus  $G'$  and loss modulus  $G''$  at 250°C for (left) PC-H and PC-H/PMMA-L (90/10) and (right) PMMA-H and PMMA-H/PC-L (90/10).

Because the  $G''$  slopes were almost 1, the zero-shear viscosities  $\eta_0$  at 250°C were calculated using eq. (3.1),

$$\eta_0 = \lim_{\omega \rightarrow 0} \frac{G''}{\omega} \quad (3.1)$$

The  $\eta_0$  was 3000 (Pa s) for PC-H at 250°C, which was higher than  $\eta_0$  of PC-H/PMMA-L (90/10) (1950 Pa s). Therefore, 10 wt% of PMMA-L decreased  $\eta_0$  about 35 %. In the case of PMMA-H,  $\eta_0$  was found to be 3100 (Pa s), whereas that of PMMA-H/PC-L (90/10) was 1950 (Pa s), i.e., 37% decrease in  $\eta_0$ .

The  $\eta_0$  values of PMMA-L and PC-L were also evaluated and found to be 3.4 (Pa s) for PMMA-L, 2.5 (Pa s) for PC-L, although their results were not shown in the figures. PC-L and PMMA-L played as plasticizers at this temperature, leading to the decrease in the entanglement density, because the systems were miscible. For such a system, the volume fraction of a polymer, such as PMMA-H and PC-H, determines  $\eta_0$  according to the Berry-Fox formula [17], which is denoted in eq. (3.2).

$$\eta_0(\phi) \propto \zeta_0 \phi^{3.6} \quad (3.2)$$

where  $\zeta_0$  is the monomeric frictional coefficient and  $\phi$  is the volume fraction of a polymer.

When we assume a specific volume of PMMA was identical to that of PC, the  $\eta_0$  of the blend must decrease by 32%. This was similar to the experimental results obtained for PC-H/PMMA-L (90/10) and PMMA-H/PC-L (90/10).

### 3.3.2 Segregation behavior at injection-molding

Injection-molding was used to prepare the sample bars for PC-H/PMMA-L (90/10) and PMMA-H/PC-L (90/10), respectively. Both products were transparent, as seen in Figure 3-11, indicating that the miscibility was not affected.

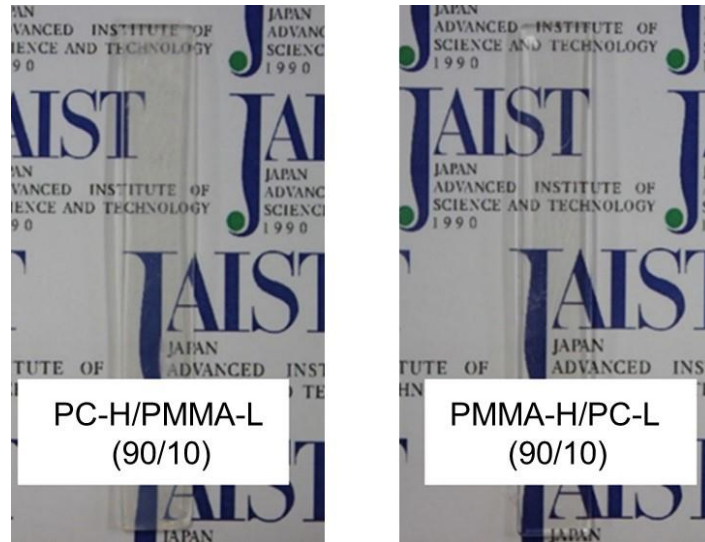


Figure 3-11 Injection-molded bars of PMMA-H/PC-L (90/10) and PC-H/PMMA-L (90/10).

As mentioned in the previous chapter, the blend compositions at surface were evaluated by ATR-IR spectra. For the measurements, the peak intensities of the stretching vibrations of carbonyl function, i.e.,  $1720 - 1730 \text{ cm}^{-1}$  for PMMA and  $1770 - 1780 \text{ cm}^{-1}$  for PC were employed. Before the measurements, the peak intensity ratios were evaluated using compression-molded films having various blend ratios to make the calibration curve. Since KRS-5 was employed as the ATR crystal, the penetration depth ( $d_p$ ), calculated by eq. (3.3), was around 1.4 mm.

$$d_p = \frac{\lambda/n_1}{2\pi\sqrt{\sin^2\theta - (n_2/n_1)^2}} \quad (3.3)$$

where  $\lambda$  is the wavelength of the infrared beam,  $n_1$  and  $n_2$  are the refractive indices of the sample and the ATR crystal, respectively, and  $\theta$  is the incident angle of IR.

The ATR-IR spectra of PMMA-H/PC-L (90/10) specimens produced by injection-molding and compression-molding are shown in Figure 3-12. The vertical axis was normalized by the absorbance  $A$  of PMMA, i.e.,  $A_{PC}/A_{PMMA}$ . The area at point 3 of the injection-molded bar was used to characterize the PC-L content. The IR spectra of PC at

1770 - 1780  $\text{cm}^{-1}$  was pronounced as seen in Figure 3-12. The content of PC-L at the surface of injection-molded bar was around 12%, whereas the compression-molded film had a PC-L content of 10%. The results revealed that injection-molding led to the PC-L surface segregation.

The ATR-IR spectra at point 3 for PC-H/PMMA-L (90/10) samples are shown in Figure 3-13. The absorbance  $A$  of PC, i.e.,  $A_{\text{PMMA}}/A_{\text{PC}}$ , was used to normalize the vertical axis. The peak intensity attributed to PMMA-L differed among them, as seen in the figure. The surface of the injection-molded product had more PMMA-L, which was calculated to be 14 wt%. The result supported that a low-molecular-weight fraction, irrespective of polymer species, shows surface segregation during injection-molding.

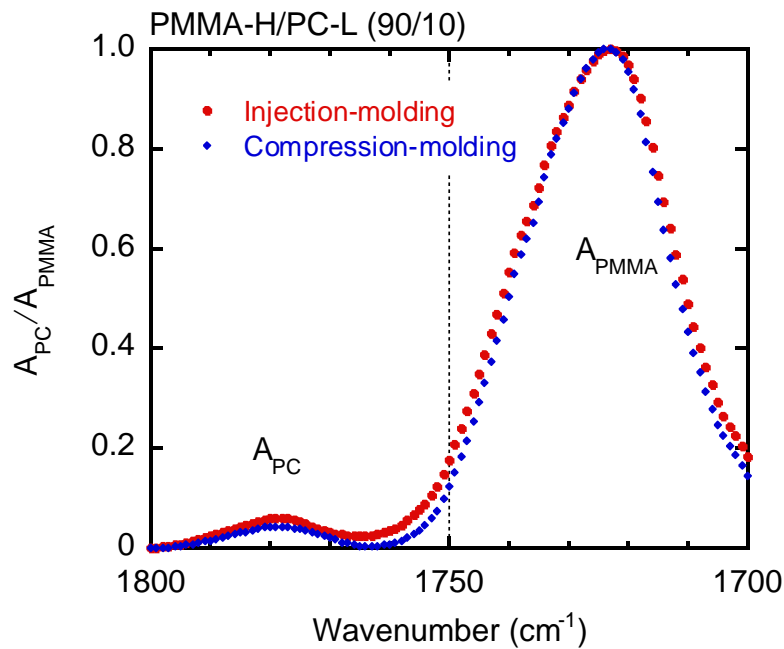


Figure 3-12 Normalized ATR-IR spectra of PMMA-H/PC-L (90/10) obtained by (circles) injection-molding and (diamonds) compression-molding.

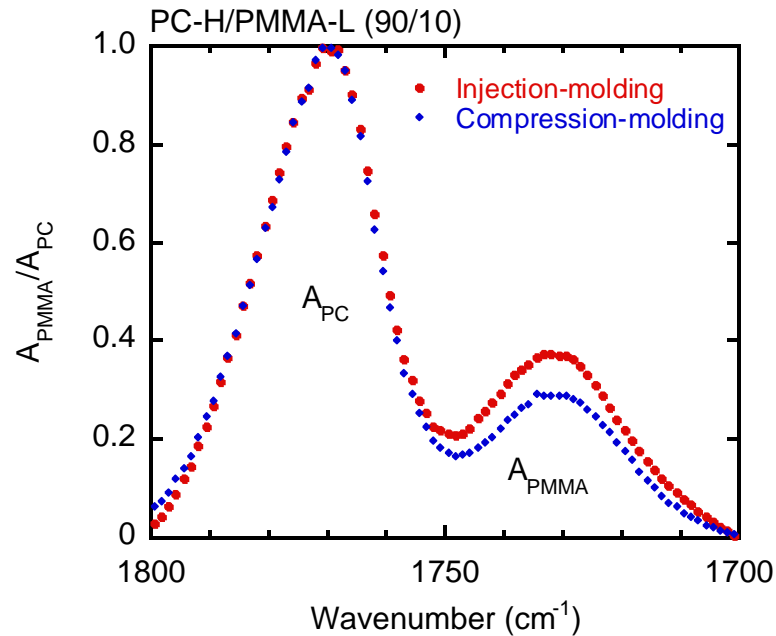


Figure 3-13 Normalized ATR-IR spectra of PC-H/PMMA-L (90/10) obtained by (circles) injection-molding and (diamonds) compression-molding.

Because the difference in peak intensities was noticeable for PC-H/PMMA-L (90/10), further ATR-IR measurements were done using this sample at various spots. Figure 3-14 shows that the PMMA-L concentration was high near the gate, indicating that the segregation was prominent in the high shear rate region. The PMMA-L concentration was determined to be around 17 wt% at point 1.

Increased PMMA content on the surface is highly appealing in industrial applications since it significantly improves the surface hardness and antiscratch properties. Moreover, the results in this chapter demonstrate the applicability of this phenomenon at injection-molding. Recently, several manipulated material designs have been proposed for injection-molding [18-20]. This will be also one novel method to provide a functionality of an injection-molded product.

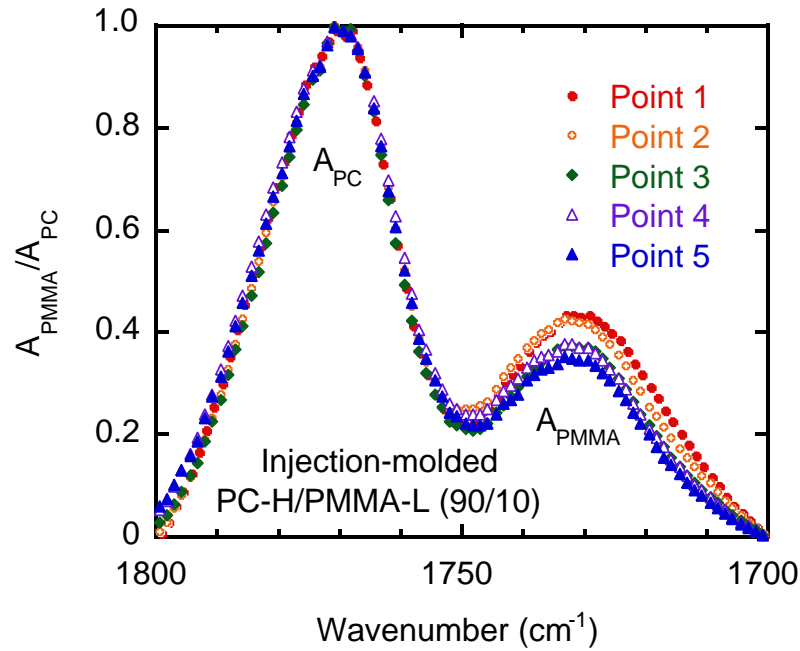


Figure 3-14 Normalized IR absorbances at each position for injection-molded PC-H/PMMA-L (90/10); (closed circles) point 1, (open circles) point 2, (closed diamonds) point 3, (open triangles) point 4, and (closed triangles) point 5.

The surface segregation of PMMA-L will provide another merit for PC. It is well known that PC shows poor flowability at injection-molding because of high  $T_g$  [21-25]. The molten PC injected into a mold shows a rapid increase in shear viscosity during cooling. Therefore, an extremely high pressure is often required for injection-molding. The enrichment of PMMA at surface decrease the  $T_g$  and shear viscosity, which must be responsible for improved flowability in a mold.

### 3.4 Conclusion

The segregation phenomenon was investigated using PC/PMMA blends with various molecular weights, including high and low molecular weights. In this experimental conditions, the blends having 20 wt% of PC-L and PMMA-L were miscible at 250°C with PMMA-H and PC-H, respectively. Based on the ATR-IR spectra, the surface composition of

the products produced by different processing methods was determined. When comparing the surface of the injection-molded product to that of the compression-molded film for PMMA-H/PC-L (90/10) blends, it was clarified that the PC-L content was higher at surface of the injection-molded bar. Furthermore, it was revealed that PMMA-L was abundant at surface of the injection-molded bar as compared to the compression-molded film for PC-H/PMMA-L (90/10) blends. Additionally, the segregation was evident near the gate position, i.e., the region with a high shear rate. These experimental results indicated that in the miscible blends a low-molecular-weight fraction was segregated in the high shear rate region at processing. This will be a revolutionary way for modifying the characteristics of the surface.

## Reference

1. Z. Tadmor and C. G. Gogos, *Principles of Polymer Processing*, 2<sup>nd</sup> ed., Wiley-Interscience, Hoboken, NJ, 2006.
2. <https://www.rnaautomation.com/robotics-in-injection-moulding>
3. M. M. Denn, *Polymer Melt Processing*, Cambridge university press, NY, 2008.
4. H. Arikata, *Injection Molding Daizen*, Nikkan Kogyo Shimbun, 2016.
5. P. C. Painter and M. M. Coleman, *Fundamentals of Polymer Science*, 2<sup>nd</sup> ed., CRC Press, Boca Raton, 1997.
6. H. Yoon, K. Okamoto, K. Umishita, and M. Yamaguchi, *Polym. Comp.* 2011, 32, 97.
7. A. Miyagawa, S. Korkiatithaweechai, S. Nobukawa, and M. Yamaguchi, *Ind. Eng. Chem. Res.* 2013, 52, 5048.
8. A. Miyagawa, V. Ayerdurai, S. Nobukawa, and M. Yamaguchi, *J. Polym. Sci., Part B, Polym. Phys. Ed.* 2016, 54, 2388.
9. S. Nobukawa, S. Hasunuma, T. Sako, S. Miyagawa, and M. Yamaguchi, *J. Polym. Sci.*,

- Part B, Polym. Phys. Ed.* 2017, 55, 1837.
10. S. Takahashi, H. Okada, S. Nobukawa, and M. Yamaguchi, *Eur. Polym. J.* 2012, 48, 974.
  11. G. D. Butzbach and J. H. Wendorff, *Polymer* 1991, 32, 1155.
  12. A. Miyagawa, S. Nobukawa, and M. Yamaguchi, *J. Soc. Rheol. Jpn.* 2014, 42, 255.
  13. M. Maeda, S. Nobukawa, K. Inomata, and M. Yamaguchi, *J. Soc. Rheol. Jpn.* 2019, 47, 111.
  14. T. Sako, A. Miyagawa, and M. Yamaguchi, *J. Appl. Polym. Sci.* 2017, 134, 44882.
  15. M. Miyashita and M. Yamaguchi, *Polymer* 2020, 202, 122713.
  16. T. G. Fox and P. J. Ferry, *J. Appl. Phys.* 1950, 21, 581.
  17. G. C. Berry and T. G. Fox, *Adv. Polym. Sci.* 1968, 5, 261.
  18. M. Yamaguchi, Y. Irie, P. Phulkerd, H. Hagihara, S. Hirayama, and S. Sasaki, *Polymer* 2010, 51, 5983.
  19. P. Phulkerd, S. Hirayama, S. Nobukawa, T. Inoue, and M. Yamaguchi, *Polym. J.* 2014, 46, 226.
  20. R. Hachisuka, R. Noda, and M. Yamaguchi, *Eng. Res. Express* 2021, 3, 015006.
  21. T. Sako, J. Date, M. Hagi, T. Hiraoka, S. Matsuoka, and M. Yamaguchi, *Polymer* 2019, 170, 135.
  22. Y. Tanaka, T. Sako, T. Hiraoka, and M. Yamaguchi, *J. Appl. Polym. Sci.* 2020, 137, 49516.
  23. M. Yamaguchi, K. Nakamura, T. Kimura, N. Moonprasith, T. Kida, K. Tsubouchi, T. Narita and T. Hiraoka, *Materials* 2022, 15, 2783.
  24. M. Fernandez, E. Munoz, and A. Santamaria, *Macromol. Chem. Phys.* 2008, 209, 1730.
  25. N. M. Rudolph, A. C. Agudelo, J. C. Granada, H. E. Park, and T. A. Osswald, *Rheol. Acta* 2016, 55, 673.

## Chapter 4 Viscosity drop in immiscible blends

### 4.1 Introduction

In this chapter, immiscible polymer blends in which one polymer has low molecular weight were focused. In many polymer blends with sea-island structure, rubbery dispersion exists to improve mechanical toughness. For such a blend, shape of the dispersion should be spherical to avoid anisotropic mechanical properties. Furthermore, the particle size should be small to decrease the ligament thickness, which accelerates the shear yielding, i.e., ductile deformation. Therefore, viscosity of dispersions must be almost similar to that of a continuous phase, as mentioned in Chapter 1. Once the dispersion has very low viscosity, the shape becomes fibrous under flow field, which enlarges the interfacial area.

Recently, Sako et al. [1] and Tanaka et al. [2] found that the shear viscosity of PC can be drastically reduced by blending polystyrene (PS) with low molecular weight. Figure 4-1 shows the shear viscosity for PC, PC/PS blends, and PC/PC-L blend, which were evaluated by a capillary rheometer.

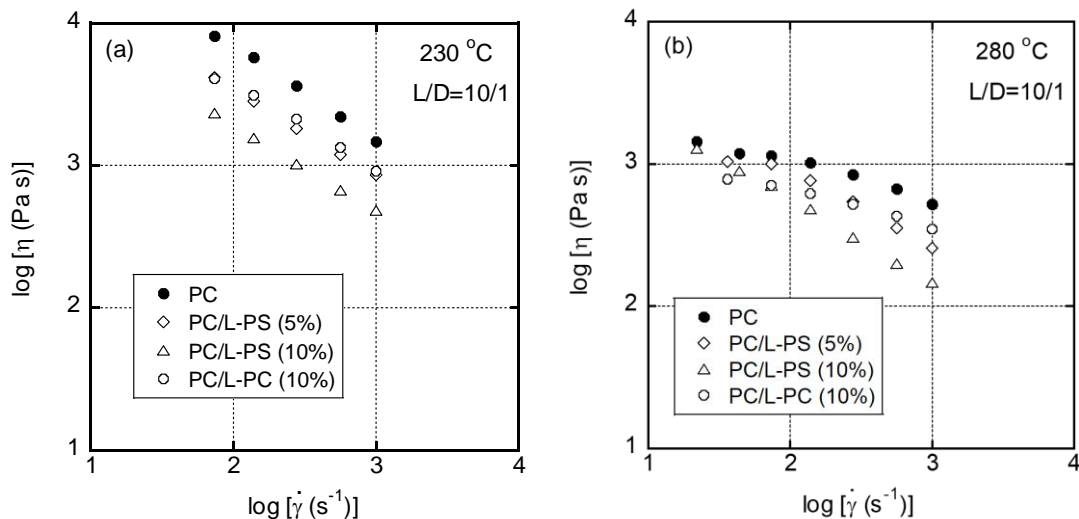


Figure 4-1 Flow curves at capillary extrusion for PC, PC/PS-L (5%), PC/PS-L (10%), and PC/PC-L (10%) at (a) 230 °C and (b) 280 °C [1]

In this experiment, the molecular weight of the PS sample was 51000 (Mw), which is slightly higher than  $M_c$  of PS. Although the blends were immiscible, the shear viscosity was much lower than that of the miscible system, i.e., PC/PC-L. Moreover, the viscosity drop was obvious at high shear rates and at low temperature, i.e., under high shear stress conditions. This phenomena was well confirmed by Tanaka et al. According to them, under shear flow, the PS droplets deform to the flow direction largely. Furthermore, they confirmed that the interfacial slippage between PC and PS occurs easily. Figure 4-2 shows the strain dependence of shear storage modulus.

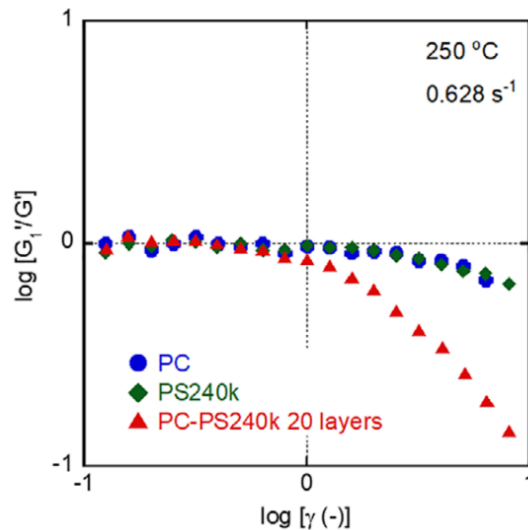


Figure 4-2 Strain dependences of  $G_1'/G'$  for PC, PS240k, and multilayered film. [2]

In this figure,  $G'$  is the primary value of  $G'$ , which is given by the Fourier expansion of shear stress  $\sigma$  as follows,

$$\begin{aligned} \sigma = & G_1' \gamma_0 \sin \omega t + G_1'' \gamma_0 \cos \omega t - G_3' \gamma_0^3 \sin 3\omega t - G_3'' \gamma_0^3 \cos 3\omega t \\ & + G_5' \gamma_0^5 \sin 5\omega t + G_5'' \gamma_0^5 \cos 5\omega t - L \end{aligned} \quad (4.1)$$

Where  $\omega$  is the angular frequency and  $\gamma_0$  is the applied strain. The samples were pure PC, pure PS, and the alternatively laminated films composed of 20 films of PC and PS. Obviously,

the laminated film shows the non-linearity, i.e., deviates from one, from a low strain, which is originated from the slippage between PC and PS. As similar to the laminated films, the viscosity drop at capillary extrusion was attributed to the interfacial slippage between PC and PS. Therefore, the viscosity decreased greatly at high shear stress conditions. If their assumption is correct, this technique should be applicable for all polymer species.

In this part, therefore, the flowability of isotactic polypropylene (PP) and PS is studied by the addition of another polymer with low viscosity. At present, injection-molding is employed for more than 40% of PP products [3]. Also for PS, a large amount of general-purpose PS (GPPS), high-impact PS (HIPS), and acrylonitrile-butadiene-styrene terpolymer (ABS) are processed by injection-molding [4]. It is always desired to reduce the shear viscosity at injection-molding without changing the molecular weight which affects the mechanical properties in the solid state.

The phenomenon of interfacial slippage at the boundary between immiscible polymers at multilayered-films processing was reported by Macosko et al. [5-9]. Furthermore, numerical simulations were used to investigate the phenomena [10,11]. When interfacial thickness is thin, entanglement couplings are not expected so much in the interface. The interfacial thickness  $\lambda$  is given by eq. (4.2): [11,12]

$$\lambda = \frac{2l_K}{(6\chi)^{1/2}} \quad (4.2)$$

where  $l_K$  is the Kuhn step length and  $\chi$  is the Flory-Huggins interaction parameter. Figure 4-3 shows the illustration of interface between immiscible polymers.

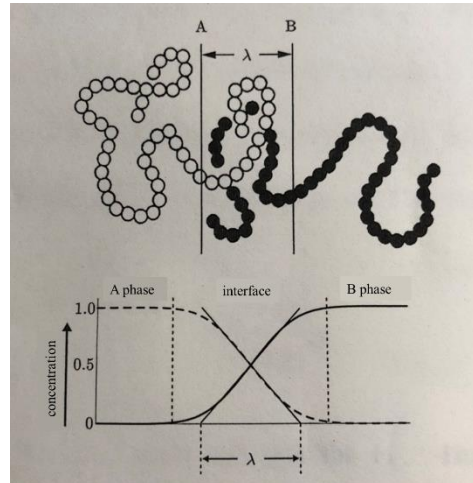


Figure 4-3 Polymer chain and concentration profile at interface [13]

The interfacial tension  $\Gamma$  is expressed in terms of the Flory-Huggins interaction parameter by eq. (4.3) [12,14]. Hence, the interfacial thickness  $\lambda$  is calculated from the interfacial tension by eq. (4.4) [15]:

$$\Gamma = \frac{k_B T}{l_K^2} \left( \frac{\chi}{6} \right)^{1/2} \quad (4.3)$$

$$\lambda = \frac{k_B T}{3l_K \Gamma} \quad (4.4)$$

where  $k_B$  is the Boltzmann constant.

According to eq. (4.4), the interfacial thickness is significantly thin even both polymers are different polyolefins such as isotactic polypropylene (PP) and high-density polyethylene (HDPE). It was reported that interfacial tension between PP and HDPE is approximately 2 mN/m [16,17]. Since the Kuhn's segment length is 0.57 nm for PP [18], the interfacial thickness is predicted to be 1.9 nm. The distance between neighboring entanglement space is calculated by the following relation.

$$\langle R^2 \rangle = C_\infty n l_0^2 \quad (4.5)$$

The characteristics ratio  $C_\infty$  of PP is known to be 4.2 and the entanglement molecular

weight is 4650. Therefore, the special distance is about 3.3 nm [19], which is longer than the interfacial thickness. As a result, adhesive strength between PP and HDPE is low [20]. As increasing the short-chain branches in polyethylene, however, adhesive strength becomes high because the interfacial tension is low as exemplified in Figure 4-4, leading to more entanglement couplings between PP and polyethylene in their interface [15,17]. It is also known that ethylene-1-butene, ethylene-1-hexene, and ethylene-1-octene copolymers where  $\alpha$ -olefin content is beyond 50 mol% are miscible with PP in a molten state and amorphous region in solid state [21-23].

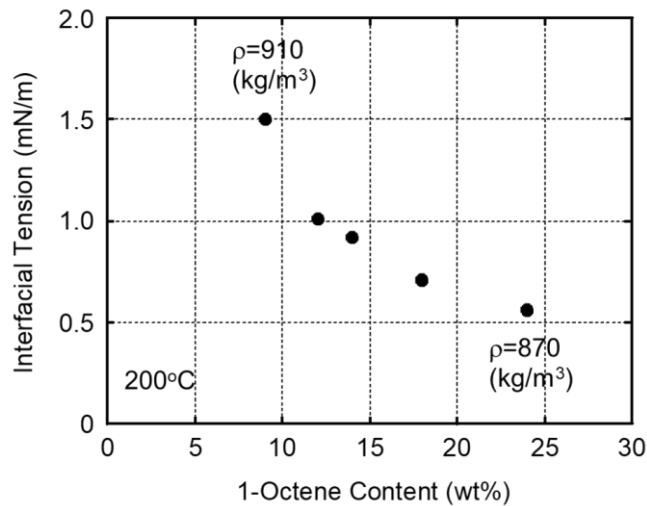


Figure 4-4 Relation between interfacial tension and 1-octene content for PP and ethylene-1-octene copolymers [17]

Cole et al. studied the delamination of multilayered films and found that the crazing mechanism overcomes the pullout mechanism when the molecular weight is beyond  $6M_e$  for miscible systems as illustrated in Figure 4-5 [24]. Even for immiscible pairs, the crazing mechanism is pronounced with increasing the interfacial thickness [25, 26]. Moreover, Cole et al showed that the number of entanglement couplings decides the strain energy release rate  $G_c$  by the following relation.

$$G_c \approx n_{ent}^2 \quad (4.6)$$

where  $n_{ent}$  is the number of entanglement.

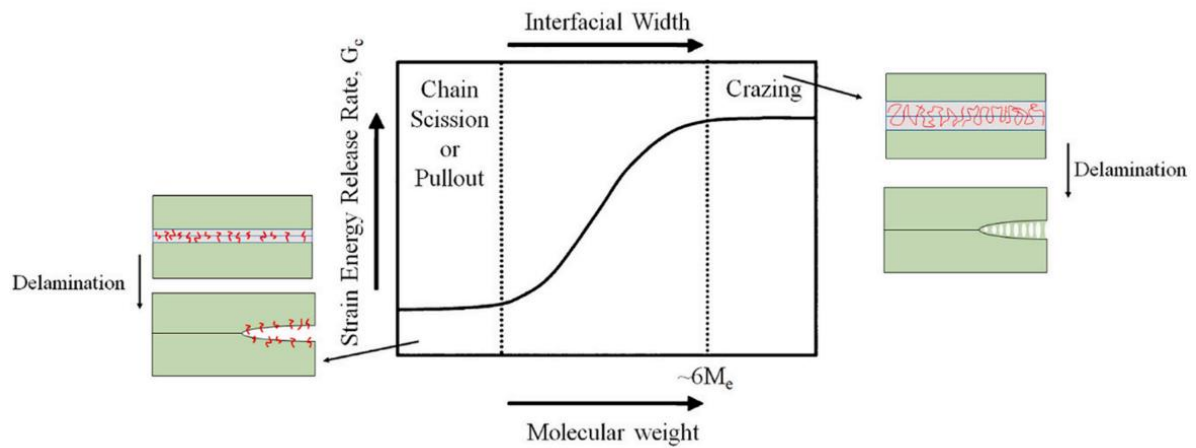


Figure 4-5 Schematic representation of the failure mechanism as a function of the molecular weight [24]

A similar result was reported by Eastwood et al. using a block copolymer that was located in the interface [27]

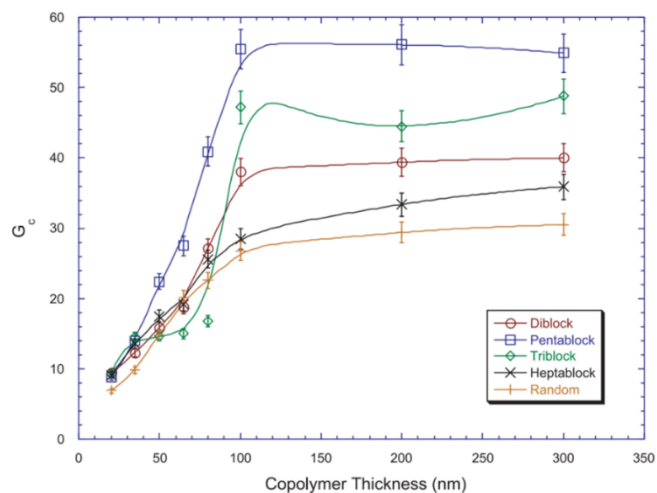


Figure 4-6 Fracture toughness of PS/PMMA copolymers modified with various copolymers as a function of copolymer thickness at the interface [27]

## 4.2 Experimental

### 4.2.1 Materials

Commercially available PP and PS samples with different molecular weights were employed. H and L in the sample names represent high and low molecular weights, respectively. PP-H is 3 g/10 min as the melt flow rate (MFR) [28], whereas PP-L has 200 g/10 min at 230°C under 2.16 kg. An ethylene 1-hexene copolymer, i.e., a linear low-density polyethylene, with 1.7 mol% of 1-hexene, having low molecular weight, was also employed as PE-L. The PE-L has 205 g/10 min as MFR at 190°C under 2.16 kg [29]. The number-average ( $M_n$ ) and weight-average ( $M_w$ ) molecular weights were evaluated by size exclusion chromatography (SEC). PP-H has  $M_n = 7.7 \times 10^4$  and  $M_w = 3.6 \times 10^5$  while PP-L has  $M_n = 2.3 \times 10^4$  and  $M_w = 1.0 \times 10^5$  as polypropylene standard [29]. PE-L has  $M_n = 1.0 \times 10^4$  and  $M_w = 2.4 \times 10^4$  as polyethylene standard [3]. Finally, PS-H has  $M_n = 9.9 \times 10^4$  and  $M_w = 2.4 \times 10^5$ , while PS-L has  $M_n = 3.3 \times 10^3$  and  $M_w = 4.0 \times 10^3$  [1.2].

The zero-shear viscosities at 190°C of the raw materials are listed in the table.

Table 4-1 Molecular weights and zero-shear viscosity of polymers

Sample code	$M_n$	$M_w$	Zero-shear viscosity (Pa s at 190 °C)
PP-H	$7.7 \times 10^4$	$3.6 \times 10^5$	$1.8 \times 10^4$
PP-L	$3.3 \times 10^4$	$5.3 \times 10^4$	$5.5 \times 10^1$
PE-L	$1.2 \times 10^4$	$7.5 \times 10^4$	$6.0 \times 10^1$
PS-H	$9.9 \times 10^4$	$2.4 \times 10^5$	$1.1 \times 10^4$
PS-L	$3.3 \times 10^3$	$4.0 \times 10^3$	$1.8 \times 10^{-1}$

### 4.2.2 Sample preparation

Melt-mixing was performed using a 30cc internal mixer (Labo Plastomill, 10M100, Toyo Seiki Seisakusho) at 30 rpm. The resin temperature was 190°C and the duration of

mixing was 3 min. Before mixing, the PS samples were dried under vacuum at 80°C for 4 h. Antioxidants such as tris(2,4-di-tert-butylphenyl)phosphate (Irgafos168, Ciba) and pentaerythritol tetrakis(3-(3,5-di-tert-butyl-4-hydroxyphenyl)propionate) (Irganox1010, Ciba) were added to prevent degradation during mixing. The content was 500 ppm. The weight contents of a minor polymer were 5 and 10 wt%. Then, the mixtures were compressed into flat films using a compression-molding machine under 10 MPa at 190°C for 3 min. The films with 500  $\mu\text{m}$  thick were cooled at 25°C by another compression-molding machine.

### 4.2.3 Measurements

Dynamic mechanical analysis of the blend films was performed to determine the tensile storage and loss moduli at 10 Hz as a function of temperature from 25 to 200°C at a heating rate of 2°C/min by a dynamic mechanical analyzer (DVE-E4000, UBM).

Angular frequency dependence of oscillatory shear moduli in the molten state was evaluated by a cone-and-plate rheometer (AR2000ex, TA Instruments) with  $\text{N}_2$  flow at 190°C. The cone angle was 4° and its diameter was 25 mm. The angular frequency was ranged from 0.1 to 628.3  $\text{s}^{-1}$ .

A capillary rheometer (140SAS, Yasuda Seiki Seisakusyo) was employed to measure the shear viscosity. Two circular dies with different diameters  $D$  and lengths  $L$  were used to evaluate the wall slippage. The entrance angle of both dies was  $2\pi$ . The barrel and die temperature was controlled at 190°C.

Blend morphology was observed using a scanning electron microscope (SEM, S-4100, Hitachi). An accelerating voltage was 10 kV. Samples were compression-molded films and extruded strands from the die with  $L=10$  (mm) and  $D=1$  (mm). After fracture, the PP-H/PS-L blends were dipped in cyclohexane at ambient temperature to remove PS-L dispersions,

i.e., etching process. For PS-H/PP-L and PP-H/PE-L, the fracture surface was observed without etching process. Before the observation, dried surface was coated by Pt/Pd using a sputtering machine to prevent charge-up.

### 4.3 Results and Discussion

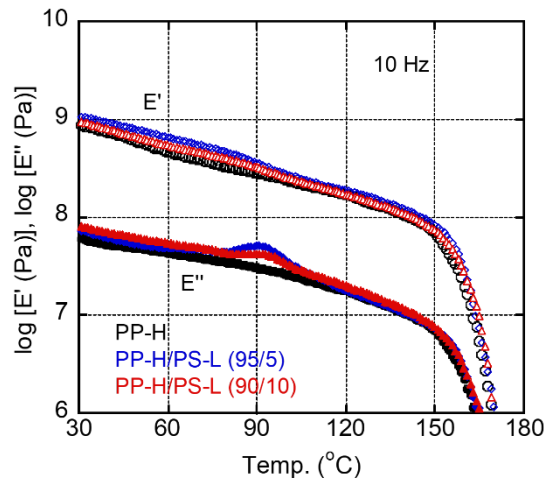


Figure 4-7 Temperature dependence of dynamic tensile modulus at 10 Hz for the PP-H/PS-L blends; 100/0, 95/5, and 90/10 (w/w).

Figure 4-7 shows the temperature dependence of tensile moduli such as storage modulus  $E'$  and loss modulus  $E''$  of PP-H/PS-L blends with PS-L contents of 0, 5, and 10 wt%. The blend samples exhibit a peak of  $E''$  around at 90°C which is ascribed to glass transition temperature  $T_g$  of PS-L, suggesting that PS-L is immiscible with PP-H. The location of the  $T_g$  peak is independent of the PS-L content. This is reasonable because PP chains are not dissolved in PS-L phase at all. The  $E'$  value decreased greatly at around 165°C, i.e., near the melting point of PP. In this temperature range, the PS-L addition did not affect the viscoelastic properties.

The shear storage modulus  $G'$  and loss modulus  $G''$  at 190°C for PP-H/PS-L and PP-

H/PS-H are plotted against the angular frequency in Figure 4-8. In this figure, the SEM pictures of the fractured surface of the films were shown below. The  $G'$  and  $G''$  curves for pure PP-H are denoted as solid lines. Dotted lines represent those of pure PS samples.

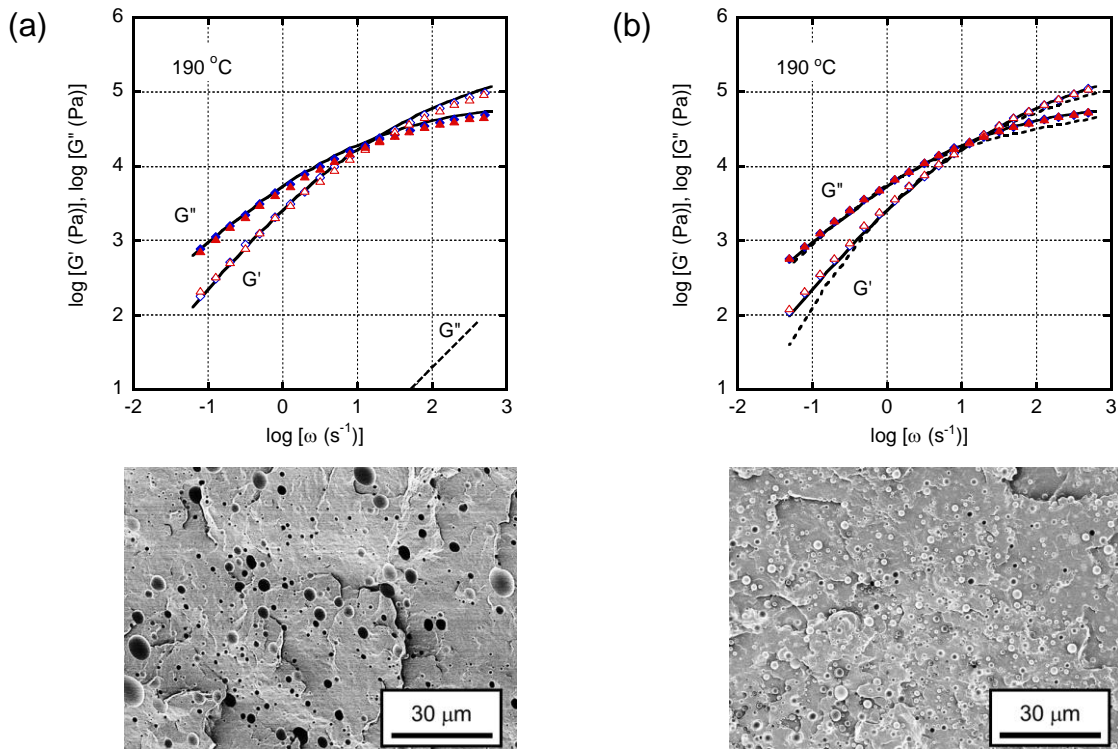


Figure 4-8 (closed symbols) shear storage modulus  $G'$  and (open symbols) loss modulus  $G''$  as a function of angular frequency at 190°C. (a) PP-H/PS-L and (b) PP-H/PS-H. The PS contents are (solid lines) 0 wt%, (diamonds) 5 wt%, and (triangles) 10 wt%.  $G'$  and  $G''$  for PS-L and PS-H are denoted as dotted lines. SEM pictures of the fractured surfaces of the films containing 10 wt% of PS samples are displayed below.

As seen in Figure 4-8 (a), loss modulus of PS-H was almost identical to that of PP-H at low frequencies. It indicated that both polymers showed a similar shear viscosity at this temperature, leading to fine dispersion. On the contrary, The loss modulus of PS-H was lower than that of PP-H at high frequencies. Since  $M_e$  of PS ( $\sim 1.3 \times 10^4$ ) is higher than that of PP ( $\sim 4.7 \times 10^3$ ), the rubbery plateau modulus of PS is low.

Furthermore, PP-H showed typical rheological behavior in the flow region, i.e.,  $G''$  is proportional to  $\omega$ . The slope of  $G'$  curve was slightly lower than 2. However, it increased with decreasing angular frequency. Both  $G'$  and  $G''$  values of PP-H/PS-L and PP-H/PS-H blends were also identical to those of pure PP-H. Strictly speaking,  $G'$  values at low frequencies must be slightly higher than those of pure PP-H, because of prolonged relaxation due to interfacial tension, although this was unclear in the figure. The long time relaxation can be expressed by the rheological emulsion model [22,30,31]. Presumably, the small volume fraction of the dispersed droplets will not give enough interfacial stress to be detected in this system.

SEM pictures of the fractured surfaces of films containing 10 wt% of PS were also illustrated in this figure. The phase separated morphology was obviously detected in both blends. The average droplet size and the standard deviation (denoted in the parenthesis) are  $2.39 \mu\text{m}$  ( $0.77 \mu\text{m}$ ) for PP-H/PS-L and  $1.56 \mu\text{m}$  ( $0.60 \mu\text{m}$ ) for PP-H/PS-H. Hence, PP-H/PS-H has smaller dispersions. The small size of the dispersed droplets must be attained by viscosity matching [32] as mentioned in Chapter 1.

The steady-state shear viscosity of PP-H and its blends with PS-L and PS-H was evaluated by using the capillary rheometer at  $190^\circ\text{C}$ . The samples were extruded through two circular dies with the identical  $L/D$  ratio, i.e.,  $L/D=10/1$  and  $20/2$ , to evaluate the slippage on the die wall by the Mooney method [33]. The apparent shear viscosity of the blends was compared without Bagley and Rabinowitsch corrections. The results were presented in Figure 4-9. The viscosity data obtained using both dies was plotted in the same figure. Since they were identical for all samples, it can be concluded that wall slippage did not occur for all blends even for the samples with PS-L. In the previous works, Tanaka et al. [2] and Sako

et al. [1] found the same results using PC blends with low-molecular-weight PS.

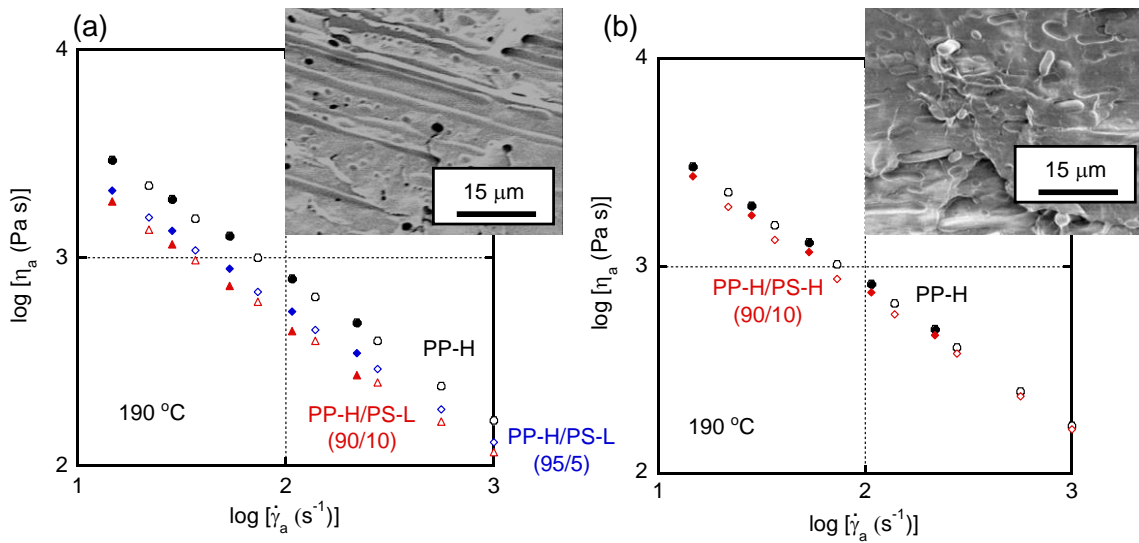


Figure 4-9 Relationship between apparent shear rate  $\dot{\gamma}_a$  and apparent shear viscosity  $\eta_a$  at 190°C. The extrusion was carried out through circular dies of (open symbols)  $L/D=10/1$  and (closed symbols)  $L/D=20/2$  for (a) PP-H/PS-L and (b) PP-H/PS-H. The PS amounts are (circles) 0 wt%, (diamonds) 5 wt%, and (triangles) 10 wt%. SEM pictures of the cut surfaces of the strands with 10 wt% of PS-H or PS-L are shown in the figure. The strands were obtained at  $73 \text{ s}^{-1}$  using the die having  $L/D=10/1$ .

As seen in Figure 4-9 (a), the shear viscosity of the blends decreased with increasing the PS-L content. The Cox-Merz rule, shown in eq. 4.7, is not applicable to PP-H/PS-L, because the complex shear viscosity of the blend is identical to that of pure PP-H as predicted from Figure 4-7.

$$\eta(\dot{\gamma}) = \eta^*(\omega)|_{\omega \rightarrow \dot{\gamma}} \quad (4.7)$$

$$\eta^*(\omega) = \frac{\sqrt{G'^2 + G''^2}}{\omega} \quad (4.8)$$

In contrast, as shown in Figure 4-9 (b), 10 wt% addition of PS-H barely affected the

shear viscosity. These results suggest that the shear viscosity in the steady-state of conventional polypropylene corresponds with the complex shear viscosity calculated by the oscillatory modulus. In other words, the Cox-Merz empirical rule is applicable.

Moreover, the morphology of cut surface of the strand extruded at  $73 \text{ s}^{-1}$  was observed. SEM images were shown in Figure 4-9. The dispersed droplets, i.e., PS-L phase, was found to be greatly deformed into fibrous shape along the flow direction. Although the critical capillary number is not revealed for the blend, pronounced deformation owing to hydrodynamic force provided by the deformation of the continuous PP-H occurs for PS-L. This will happen when the capillary number is significantly larger than the critical value for a sea-island blend with dispersion of low shear viscosity [34,35]. Thus, an enlarge interfacial area between PP-H and PS-L was given by the substantial deformation of droplets. PS-H deformation, on the other hand, was less visible due to its high shear viscosity.

In Figure 4-10, Bagley plots are produced for PP-H and PP-H/PS-L. Three different types of circular dies having the same diameter but with different die lengths were used, i.e.,  $L/D=10/1$ ,  $20/1$ , and  $40/1$ . As shown in the figure, straight lines were achieved for both PP-H and PP-H/PS-L ( $90/10$ ). The values of end pressure drop  $P_e$ , calculated from the intercept of y-axis, are depicted in Figure 4-11 as a function of shear rate. It should be noted that  $P_e$  decreased as increasing the shear rate for PP-H/PS-L, which is an extraordinary phenomenon. In general,  $P_e$  increases with shear viscosity and normal stress difference [36]. Although the mechanism of this behavior is unknown exactly, one possible explanation might be a non-linear pressure drop for PP-H/PS-L especially at high shear rates. In fact, as seen in Figure 4-10 (b), the pressure at  $L/D=40/1$  seemed to show an upper deviation from the straight line. The interfacial slippage could contribute this phenomenon.

According to the experimental data, interfacial slippage is the cause of the shear viscosity reduction in the capillary flow, as mentioned in the previous articles [1.2]. The difference between PS-L and PS-H indicates that the deformation of dispersed phase, which can be controlled by viscosity ratio, has a significant impact on the viscosity drop. However, the impact of interfacial tension is unknown. Therefore, linear low-density polyethylene, PE-L, was employed instead of PS-L, because interfacial tension between PE-L and PP is lower than that between PS-L and PP.

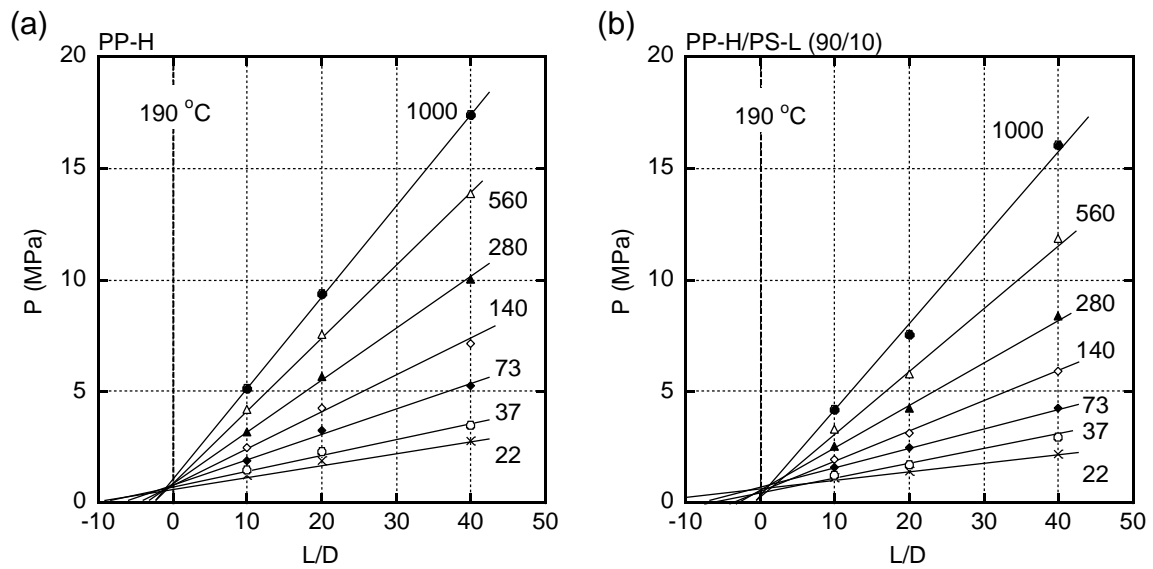


Figure 4-10 Pressure plotted by  $L/D$  (Bagley plots) for (a) PP-H and (b) PP-H/PS-L (90/10). The numerals denote shear rates ( $\text{s}^{-1}$ ).

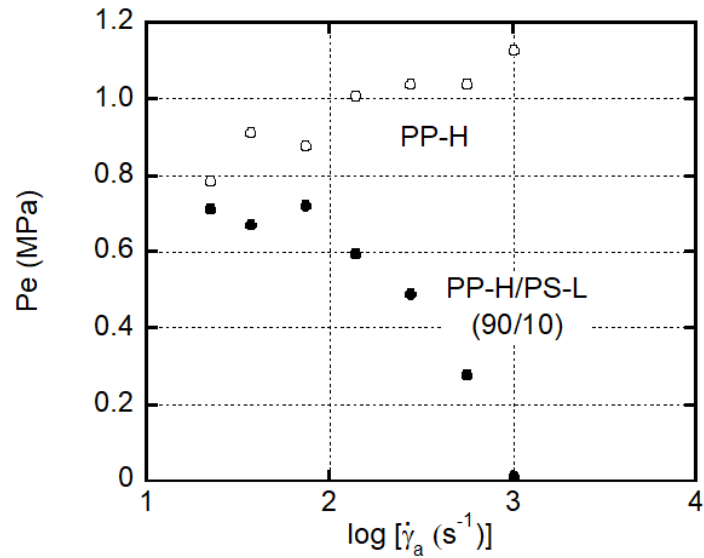


Figure 4-11 Relationship between apparent shear rate  $\dot{\gamma}_a$  and end pressure drop  $P_e$  for PP-H and PP-H/PS-L (90/10).

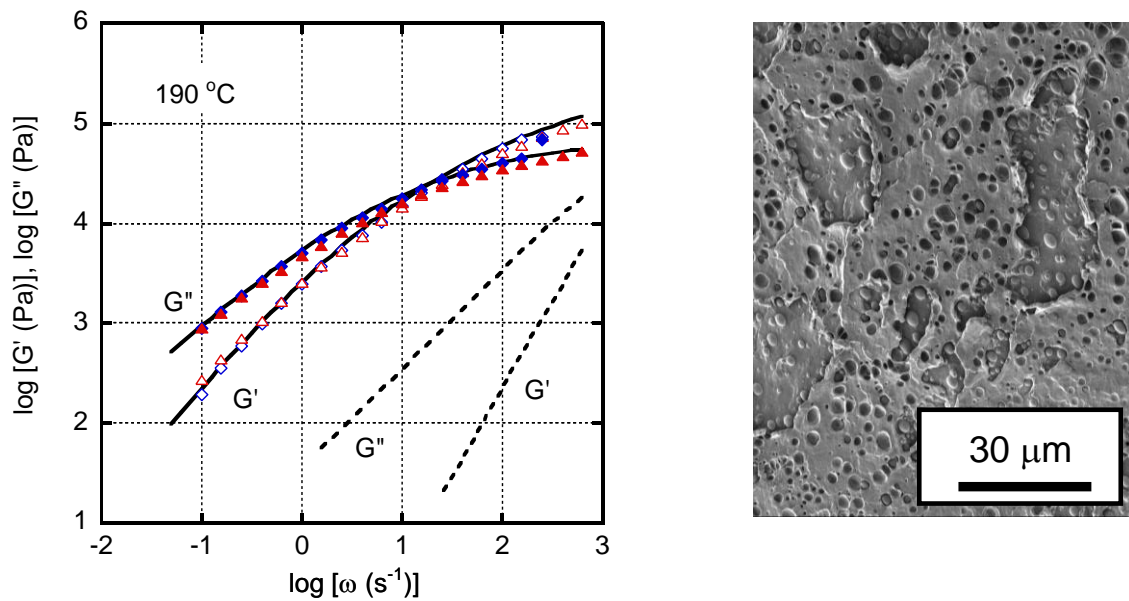


Figure 4-12 (closed symbols) shear storage modulus  $G'$  and (open symbols) loss modulus  $G''$  at 190°C as a function of angular frequency for (solid lines) PP-H, (diamonds) PP-H/PE-L (95/5), and (triangles) PP-H/PE-L (90/10). Dotted lines denote  $G''$  and  $G'$  for PE-L. An SEM picture of the fractured surface of PP-H/PE-L (90/10) film is also displayed.

Figure 4-12 shows an SEM picture and the linear viscoelasticity for PP-H/PE-L (90/10). Although ethylene-1-hexene copolymer containing more than 50 mol% of 1-hexene is miscible with PP in the amorphous region [37], PE-L with 1.7 mol% of 1-butene was not miscible with PP. Therefore, phase-separated structure was detected. The average droplet size of PE-L was 1.80  $\mu\text{m}$  and its standard deviation was 0.81  $\mu\text{m}$ . As seen in the figure, the viscoelastic characteristics of PP-H/PE-L were comparable to those of PP-H/PS-L in the experimental frequency range. Although the blend has phase-separated structure, a shoulder in  $G'$  attributed to a prolonged relaxation was not detected also for this blend.

Flow curves of PP-H and PP-H/PE-L, i.e., apparent shear viscosity plotted against the shear rate on wall, are denoted in Figure 4-13. Compared with Figure 4-8, the drop of shear viscosity was not significant, especially at high shear rates. This is quite different from the results obtained using PP-H/PS-L.

Chandavasud et al. [38], Funke et al. [39], and Kamal et al. [40] calculated the interfacial tension between PP and PS. They reported the value as 4.8 mN/m at 200°C [38] and 4.3 mN/m at 230°C [38]. Although it is well known that molecular weight slightly affects interfacial tension [40,41], it is clear that the interfacial thickness between PP and PS is less than the entanglement distance, implying that there are no/few entanglements between PP and PS. In opposite, the interfacial tension between PP and PE-L is low, that is, around 1.0 mN/m [15,17], leading to some entanglement couplings due to a thick interfacial area with short distance between neighboring entanglement points. Therefore, slippage at interface barely takes place between PP-H and PE-L due to a strong adhesion as compared with that between PP-H and PS-L.

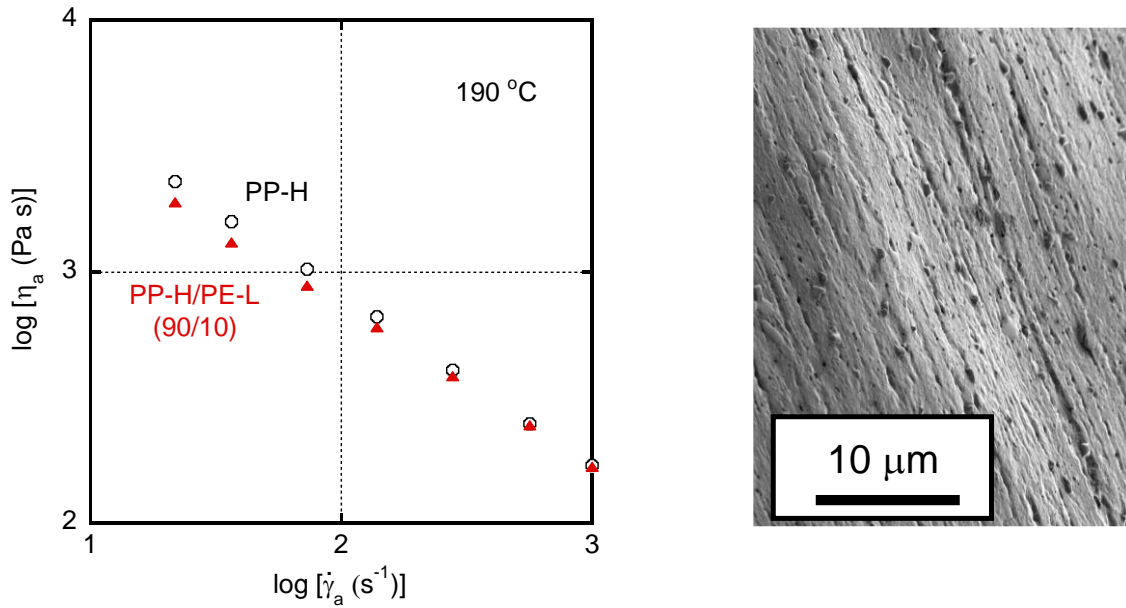


Figure 4-13 Relationship between apparent shear rate  $\dot{\gamma}_a$  and apparent shear viscosity  $\eta_a$  at 190°C. The extrusion was carried out through the circular die with  $L/D=10/1$ . The PP-L amount are (circles) 0 wt% and (triangles) 10 wt%. An SEM picture of the cut surface of the strand with 10 wt% of PE-L was shown in the figure. The strand was obtained at  $73 \text{ s}^{-1}$ .

The effect of the addition of a low viscosity dispersion was investigated to confirm the results of PP-H/PS-L system. Here, the blends with PS-H as a continuous phase and PP-L as a dispersion were employed. The rheological properties such as oscillatory shear modulus and steady-state shear viscosity were measured. The results of the oscillatory shear modulus and an SEM picture of the film were shown in Figure 4-14. The  $G''$  curves were identical to those of PP-H/PS-L blends, while the  $G'$  increase at low frequencies was more apparent than that for PP-H/PS-L. Base on the emulsion model of phase-separated polymer blends, the relaxation time of the deformation of droplets  $\tau_D$  owing to interfacial tension is given by the following equation [30,31];

$$\tau_D = \frac{\eta_c R}{4\Gamma} \frac{(19K + 16)(2K + 3 - 2\phi(K - 1))}{10(K + 1) - 2\phi(5K + 2)} \quad (4.9)$$

$$K = \eta_c / \eta_d \quad (4.10)$$

where  $\eta_c$  is the viscosity of continuous phase and  $\eta_d$  is that of dispersed phases.  $R$  is the radius,  $\phi$  is the volume fraction of dispersed phase, and  $\Gamma$  is the interfacial tension.

As seen in the figure, the SEM image shows a large droplet of PP-L. The average droplet size was  $3.04 \mu\text{m}$  and its standard deviation was  $1.57 \mu\text{m}$ . The large difference in the viscosity must be responsible for the coarse morphology.

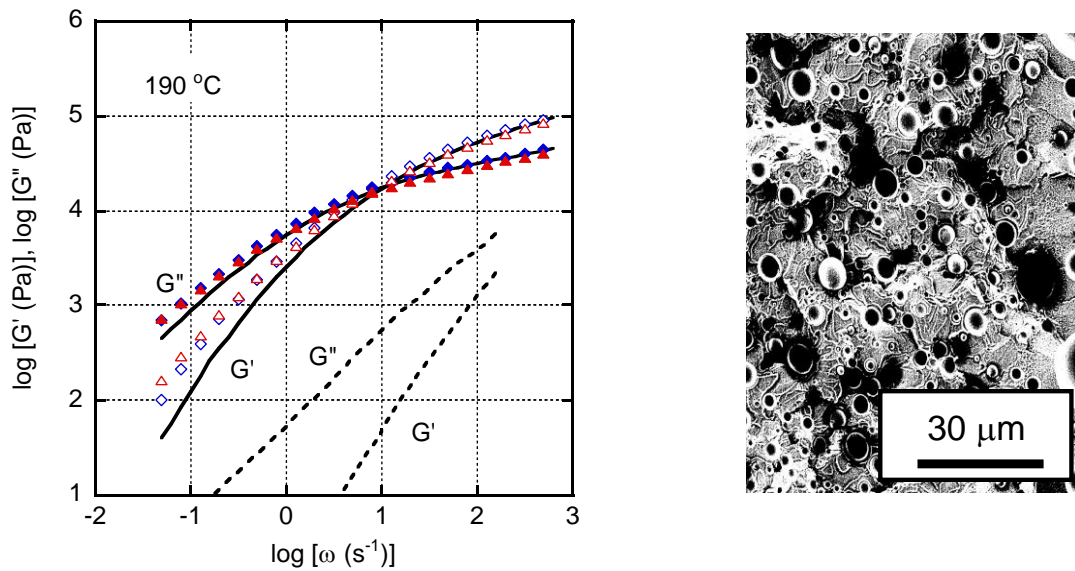


Figure 4-14 (closed symbols) shear storage modulus  $G'$  and (open symbols) loss modulus  $G''$  at  $190^\circ\text{C}$  as a function of angular frequency for: (solid lines) PS-H, (diamonds) PS-H/PP-L (95/5), and (triangles) PS-H/PP-L (90/10). Dotted lines denote  $G'$  and  $G''$  for PP-L. An SEM picture of the fractured surface of PS-H/PP-L (90/10) film is also displayed.

The shear viscosity was evaluated by the capillary rheometer for PS-H/PP-L blends as shown in Figure 4-15. It was found that the viscosity was dropped greatly. The SEM image of extruded strand was also attached in the figure. The PP-L dispersion deformed into the flow direction was clearly observed in the SEM picture. Conventional PS blends such as acrylonitrile-butadiene-styrene terpolymer (ABS) and high-impact polystyrene (HIPS) are

often processed by high-shear-rate processing operations such as injection-molding. Therefore, this behavior must be noted from the viewpoints of industrial application.

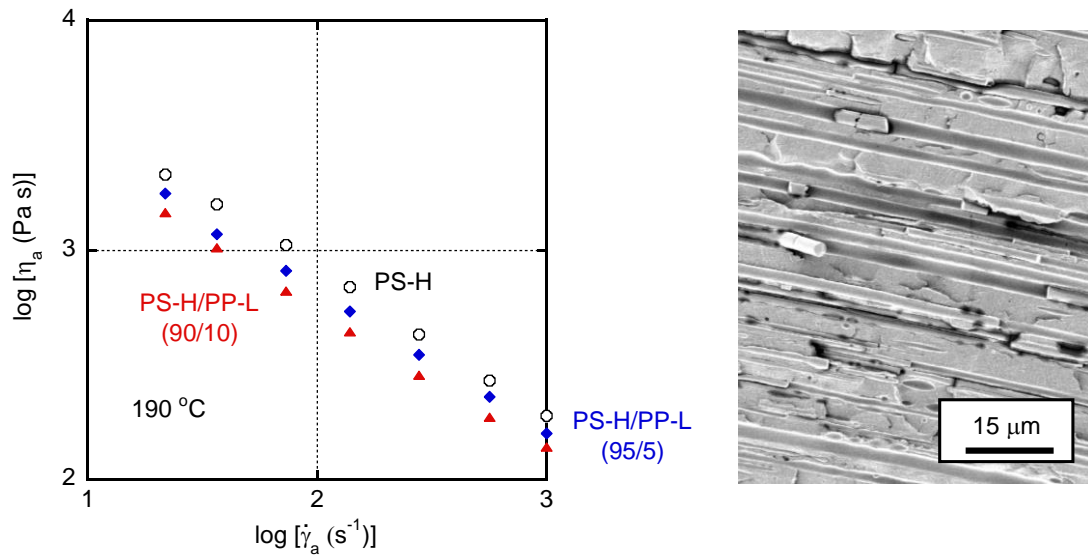


Figure 4-15 Relationship between apparent shear rate  $\dot{\gamma}_a$  and apparent shear viscosity  $\eta_a$  at 190 °C. The extrusion was carried out through circular die with  $L/D=10/1$ . The PP-L amount are (circles) 0 wt%, (diamonds) 5 wt%, and (triangles) 10 wt%. An SEM picture of the cut surface of the strand of the PS-H/PP-L (90/10) was shown in the figure. The strand was obtained at  $73 \text{ s}^{-1}$ .

From these results, it could be summarized that the shear viscosity drop is originated from interfacial slippage which occurred at enlarged interface. Therefore, droplets have to show low viscosity with a high interfacial tension with a continuous phase.

#### 4.4 Conclusions

The rheological properties of immiscible polymer blends, in which one component has significantly low viscosity, were studied. In this chapter, PP-H, PS-H, PP-L, PS-L and PE-L were employed. All blends were found to be immiscible including PP-H/PE-L.

Although PP-H/PS-L and PP-H/PS-H showed similar linear viscosities properties in the molten state, steady-state shear viscosity of the former blend was much lower than that of the latter especially in the high shear rate region. The same phenomena were detected also for PS-H/PP-L and PS-H/PP-H blends. However, the addition of PE-L did not decrease the shear viscosity of PP-H so much. It was confirmed that a large deformation occurs in the dispersion when the dispersion has much lower viscosity than the continuous phase. These experimental results showed that the viscosity decrease occurs when the dispersion has low shear viscosity and high interfacial tension with the continuous phase.

This indicates that the slippage at interface between a continuous phase and dispersion is responsible for the marked viscosity decrease. Because the viscosity drop becomes obvious at high shear rates, this technique can be used for injection-molding to increase the flow length, i.e., one of the most important processing operations in industry.

## References

1. T. Sako, J. Date, M. Hagi, T. Hiraoka, S. Matsuoka, and M. Yamaguchi, *Polymer* 2019, 170, 135.
2. Y. Tanaka, T. Sako, T. Hiraoka, M. Yamaguchi, and M. Yamaguchi, *J. Appl. Polym. Sci.* 2020, 137, 49516.
3. J. Seemork, T. Itoh, T. Sako, R. Wiwattananukul, S. Nobukawa, H. Sasaki, Y. Satoh, and M. Yamaguchi, *Adv. Polym. Technol.* 2018, 37, 1153.
4. Do. V. Rosato and Do. V. Rosato, *Reinforced Plastics Handbook*, 3<sup>rd</sup> ed, Elsevier Oxford UK 2004
5. R. Zhao and C. W. Macosko, *J. Rheol.* 2002, 46, 145.
6. J. Zhang, T. P. Lodge, and C. W. Macosko, *J. Rheol.* 2006, 50, 41.

7. P. C. Lee, H. E. Park, D. C. Morse, and C. W. Macosko, *J. Rheol.* 2009, 53, 893.
8. H. E. Park, P. C. Lee, and C. W. Macosko, *J. Rheol.* 2010, 54, 1207.
9. A. M. Jordan, B. Lee, K. Kim, E. Ludtke, O. Lhost, S. A. Jaffer, F. S. Bates, and C. W. Macosko, *J. Rheol.* 2019, 63, 751.
10. F. Brochard-Wyart, C. Gay, and P. G. de Gennes, *Macromolecules* 1996, 29, 377.
11. A. Ramachandran, K. Tsigklifis, A. Roy, and G. Leal, *J. Rheol.* 2012, 56, 45.
12. E. Helfand and Y. Tagami, *J. Polym. Sci., B, Polym. Phys. Ed.* 1971, 9, 741.
13. T. Ougisawa, *Polymer Alloy*, Kyoritsu, 2014
14. E. Helfand and Y. Tagami, *J. Chem. Phys.* 1971, 56, 3592.
15. M. Yamaguchi, *J. Appl. Polym. Sci.* 1998, 70, 457.
16. A. M. C. Souza and N. R. Demarquette, *Polymer* 2002, 43, 1313.
17. C. J. Carriere and H. C. Silvis, *J. Appl. Polym. Sci.* 1997, 66, 1175.
18. F. S. Bates and G. H. Fredrickson, *Macromolecules* 1994, 27, 1065.
19. P. Phulkerd, S. Arayachukeat, T. Huang, T. Inoue, S. Nobukawa, and M. Yamaguchi, *J. Macromol. Sci., Part B, Phys.* 2014, 53, 1222.
20. R. P. Wool, *Polymer Interfaces*, Hanser, Munich 1995.
21. M. Yamaguchi, H. Miyata, and K. Nitta, *J. Appl. Polym. Sci.* 1996, 62, 87.
22. M. Yamaguchi, H. Miyata, K. Nitta, and T. Masuda, *J. Appl. Polym. Sci.* 1997, 63, 467.
23. M. Yamaguchi and H. Miyata, *Macromolecules* 1999, 32, 5911.
24. F. Gholami, L. Pakzad, and E. Behzadfar, *Polymer* 2020, 208, 122950.
25. H. R. Brown, *J. Mater. Sci. Lett.* 1979, 14, 237.
26. H. R. Brown, *Macromolecules* 2001, 34, 3720.
27. E. Eastwood, S. Viswanathan, C. P. O'Brien, D. Kumar, and M. D. Dadmunal, *Polymer* 2005, 46, 3957.

28. Y. Fujii, R. Nishikawa, P. Phulkerd, and M. Yamaguchi, *J. Rheol.* 2019, 63, 11.
29. M. Siriprumpoonthum, S. Nobukawa, Y. Satoh, H. Sasaki, and M. Yamaguchi, *J. Rheol.* 2014, 58, 449.
30. D. Graebbling, R. Muller, and J. F. Palierne, *Macromolecules* 1993, 26, 320.
31. J. F. Palierne, *Rheol. Acta* 1990, 29, 204.
32. S. Wu, *Polym. Eng. Sci.* 1987, 27, 335.
33. C. W. Macosko, *Rheology: Principles, Measurements, and Applications*, Wiley, New York 1994.
34. H. E. H. Meijer, J. M. H. Janssen, and P. D. Anderson, *Mixing of Immiscible Liquids, in Mixing and Compounding of Polymers*, 2<sup>nd</sup> ed., Ed. I. Manas-Zloczower, Hanser, Munich 2009.
35. T. Yokohara, K. Okamoto, and M. Yamaguchi, *J. Appl. Polym. Sci.* 2010, 117, 2226.
36. M. Yamaguchi and M. Takahashi, *Polymer* 2001, 42, 8663.
37. M. Yamaguchi, H. Miyata, and K. Nitta, *J. Polym. Sci., B, Polym. Phys. Ed.* 1997, 35, 953.
38. C. Chandavasu, M. Xanthos, K. K. Sirkar, and C. G. Gogos, *Polymer* 2002, 43, 781.
39. Z. Funke, C. Schwinger, R. Adhikari, and J. Kressler, *Macromol. Mater. Eng.* 2001, 286, 744.
40. M. R. Kamal, R. Lai-Fook, and N. R. Demarquette, *Polym. Eng. Sci.* 1994, 34, 1834.
41. D. G. Legrand and G. L. Gaines, *J. Colloid Interf. Sci.* 1975, 50, 272.

## Chapter 5: General conclusion

Molecular weight and its distribution are significantly important characteristics to describe properties of a polymeric material. Although various properties such as chain stiffness and solubility parameter are insensitive to molecular weight beyond the critical molecular weight, viscosity and mixing entropy at polymer blending are drastically affected by molecular weight. In this thesis, a role of a low-molecular-weight polymer in polymer blends for both miscible and immiscible systems is focused.

When a contribution of mixing entropy is dominated in a blend containing a low-molecular-weight polymer, the system becomes miscible in an equilibrium state. Binary blends of PC and PMMA, in which one of them has low molecular weight, are one of the examples. In this system, flow-induced segregation behavior without phase separation, i.e., concentration gradient, was recently discovered. However, the driving force of segregation was unknown with poor experimental results. Therefore, the segregation behavior was studied in detail.

First, the effect of processing factors such as shear rate, residence time, and temperature on the segregation behavior was studied using a miscible blend of PC and a low-molecular-weight PMMA. A capillary rheometer equipped with a rectangular die was employed for extrusion, and ATR-IR was used to quantify the PMMA content at surface of extrudates. It was found that the segregation of the low-molecular-weight component, i.e., PMMA, occurred, which provided the PMMA-rich surface compared with the blend sample prepared by compression-molding. The PMMA content at surface increased at high shear rates and at high temperature. However, the residence time in the die barely affected the extent of segregation.

Second, the effect of molecular weight of PMMA on the segregation was evaluated. The experimental results demonstrated that the PMMA with low molecular weight showed marked segregation compared with that with high molecular weight. In the case of polycarbonate with low molecular weight, i.e., PC-L, there was no evidence of segregation in the extrudate of PC/PC-L, i.e., the blend system containing the same polymer species. The segregation phenomena appear in a miscible blend with a positive Flory-Huggins parameter, according to these findings.

In Chapter 3, the surface segregation behavior was studied using injection-molded products composed of PC and PMMA, in which one of them has low molecular weight. Prior to injection-molding, it was confirmed that blends containing less than 20 wt% of PC-L and PMMA-L were miscible with PMMA-H and PC-H, respectively, at 250°C. The surface composition of injection- and compression-molded products was evaluated using ATR-IR spectra. It was discovered that the PC-L content at the PMMA-H/PC-L (90/10) surface was greater on the injection-molded bar than that at the compression-molded film. Furthermore, the PMMA-L content was found to be more at the PC-H/PMMA-L (90/10) surface of the injection-molded bar than that of the compression-molded film. Moreover, the surface PMMA-L content of an injection-molded bar depended on the location. It was high near the gate, i.e., the region with a high shear rate. This corresponded with the results obtained by the capillary extrusion in Chapter 2. The experimental results demonstrated that the segregation behavior can be applicable in industry immediately.

In Chapter 4, my interest was focused on immiscible blends in which one component has low molecular weight. The blends showed phase separation with dispersions having extremely low shear viscosity. In this study, PP-H, PS-H, PP-L, PS-L, and PE-L were used. All blends, including PP-H/PE-L, were found to be immiscible in this study.

Although PP-H/PS-L and PP-H/PS-H had similar linear viscoelastic properties in the molten state, the former showed a significantly lower steady-state shear viscosity than the latter, particularly in the high shear rate region. The viscosity drop was observed also for PS-H/PP-L. However, the addition of PE-L did not significantly reduce the steady-state shear viscosity of PP-H. It is well known that affine deformation occurs at  $Ca \gg Ca_{crit}$  when the dispersion has much lower viscosity than the continuous. Also in this experiment, a large deformation of a low-molecular-weight polymer was detected, leading to a large interface. This implies that the marked viscosity drop is caused by interfacial slippage between a continuous phase and dispersions. In the case of PP-H/PE-L having a low interfacial tension, the interface was presumably strong enough not to show slippage. This approach may be utilized for injection-molding to improve the flow length, which is strongly required in industry.

Although the experimental results performed in this thesis contain the detailed rheological behaviors under shear flow for polymer blends containing a low-molecular-weight polymer, the mechanical properties in the solid state of these samples should be verified in the next step. For miscible blends of PC/PMMA, the amount of a low-molecular-weight component, i.e., PMMA-L in PC-H/PMMA-L or PC-L in PMMA-H/PC-L, should be compared to clarify the appropriate condition to show segregation to a great extent. As mentioned earlier, PMMA has a high potential to give the antiscratch nature with rigidity for PC. Therefore, the surface hardness and scratch resistance should be investigated using an injection-molded product. In the meantime, tensile/bending strength and impact strength should be characterized as compared with those of pure PC. Such type of materials would be employed in automobile parts and so on. In the case of PMMA-H blends with PC-L, the refractive index gradient should be checked, because the refractive

index of PC is much higher than that of PMMA. An optical fiber having a high refractive index at outer area can reduce the light loss. When such a high-performance optical fiber can be processed only by the extrusion process, there must be a huge industrial advantage.

In the case of immiscible blends, such as PP-H/PS-L and PS-H/PP-L, their mechanical properties such as tensile/bending strength and impact toughness should be examined, because the dispersion of rigid materials may increase the stress concentration, leading to brittle fracture. Furthermore, a similar trial should be performed using a rubbery material having low viscosity. For the blend system, the rubbery dispersion, which enhances the flow length at injection-molding, may also contribute to enhance the mechanical toughness. This will be an ideal polymeric material.

## Achievements

### Publications

1. N. Moonprasith, M. S. Nasri, R. A. Saari, P. Phulkerd, and M. Yamaguchi  
Viscosity decrease by interfacial slippage between immiscible polymers  
*Polymer Engineering and Science*, 2021, 61, 1096–1103.  
<https://doi.org/10.1002/pen.25642>
2. N. Moonprasith, J. Date, T. Sako, T. Kida, T. Hiraoka, and M. Yamaguchi  
Segregation behavior of miscible PC/PMMA blends during injection molding  
*Materials* 2022, 15, 2994-3006. <https://doi.org/10.3390/ma15092994>
3. N. Moonprasith, M. Tatsumichi, K. Nakamura, T. Kida, K. Tsubouchi, T. Hiraoka, and M. Yamaguchi  
Preparation of graded materials for miscible PC/PMMA blends by segregation under shear flow  
To be submitted.

### Other publication

1. M. Yamaguchi, K. Nakamura, T. Kimura, N. Moonprasith, T. Kida, K. Tsubouchi, T. Narita, and T. Hiraoka  
Complicated structure change during capillary extrusion of binary blends of polycarbonate and poly(methyl methacrylate)  
*Materials* 2022, 15, 2783-2794. <https://doi.org/10.3390/ma15082783>

**Presentations****International Conferences:**

1. N. Moonprasith, M. S. Nasri, R. A. Saari, P. Phulkerd, and M. Yamaguchi  
“Study on rheological properties on immiscible binary blends of polypropylene and polystyrene”  
37<sup>th</sup> International Conference of the Polymer Processing Society (PPS-37), Fukuoka, Japan, April 2022
2. N. Moonprasith, M. S. Nasri, R. A. Saari, T. Kida, M. Yamaguchi  
“Viscosity at pressure-driven shear flow for immiscible blends containing a low-viscous polymer”  
International Chemistry Conference (CHEMEET 2022), (on-line) June 2022

**Domestic Conferences:**

1. N. Moonprasith, M. S. Nasri, R. A. Saari, P. Phulkerd, and M. Yamaguchi  
“Effect of low-molecular-weight polystyrene on shear viscosity of polypropylene”  
71<sup>st</sup> Annual Meeting of the Society of Polymer Science (SPSJ-71), Kyoto (on-line), Japan, May 2022
2. N. Moonprasith, T. Kida, M. Yamaguchi  
“Blend composition at surface of injection-molded products comprising miscible blends of polycarbonate and poly(methyl methacrylate)”  
71<sup>st</sup> Symposium on Macromolecules (SPSJ), Hokkaido, Japan, September 2022

## **Acknowledgments**

Foremost, I would like to express my greatest gratitude to my supervisor, Professor Masayuki Yamaguchi for his continuous encouragement of my Ph.D. research and study, as well as for his patience, inspiration, excitement, and immense knowledge. His advice was invaluable during the research and writing of this thesis. Without his professional coaching and encouraging guidance, I would never have completed my study. This is one of the greatest chapters of my life.

Besides my advisor, I would like to convey my appreciation to Associate Professor, Eijirou Miyako, and Senior Lecturer Patchanee Chammingkwan, who provided me with a lot of valuable support. I also deeply appreciate my thesis committee members: Professor Toshiaki Taniike, Professor Kazuaki Matsumura, Professor Tatsuo Kaneko Tatsuo, and Associate Professor Yusuke Hiejima for their encouragement, insightful comments, and challenging questions.

In addition, I am profoundly grateful to my supervisor at Thammasat University Associate Professor Pisanu Toochinda for his help and advice during my completion sub-theme research. Appreciation is also extended to my co-supervisors, Dr. Surapich Loykulant for his kind suggestion and discussion in this work.

Furthermore, I am particularly very grateful to the Doctoral Dual Degree Program (JAIST-SIIT) for financial support during my doctoral study. Moreover, I am also grateful gratitude to the MTEC-NSTDA for the great opportunity in the doctoral study program. Without these facilities and sponsorship, I would not have been able to achieve and complete my study.

Sincere thanks are also extended to Assistant professor Takumitsu Kida and Assistant professor Panita Phulkerd who always provided me valuable support for both academics and lifestyle. Especially for Mrs. Masami Matsumoto who help me deal with Japanese documents. I could not forget to thank all present and former members of Yamaguchi lab including all internship members for their warm support, company, and friendship which make my living life became colorful and memorable.

Finally, I would like to extend my deepest gratitude to my beloved mother and family members. Without their constant love, assistance, and encouragement, I would not have had enough cheerfulness to finish this thesis. Moreover, appreciate and thank you to all Thai members in JAIST and everyone else for fulfilling my loneliness.

Nantina Moonprasith

September 2022

JAIST